National Library of Canada
Canadian Theses Service
Ottawa, Canada
K1A 0N4

Bibliothèque nationale du Canada
Services des thèses canadiennes

CANADIAN THESES

THÈSES CANADIENNES

NOTICE

The quality of this microfiche is heavily dependent upon the quality of the original thesis submitted for microfilming. Every effort has been made to ensure the highest quality of reproduction possible.

If pages are missing, contact the university which granted the degree.

Some pages may have indistinct print especially if the original pages were typed with a poor typewriter ribbon or if the university sent us an inferior photocopy.

Previously copyrighted materials (journal articles, published tests, etc.) are not filmed.

Reproduction in full or in part of this film is governed by the Canadian Copyright Act, R.S.C. 1970, c. C-30. Please read the authorization forms which accompany this thesis.

AVIS

La qualité de cette microfiche dépend grandement de la qualité de la thèse soumise au microfilmage. Nous avons tout fait pour assurer une qualité supérieure de reproduction.

S'il manque des pages, veuillez communiquer avec l'université qui a conféré le grade.

La qualité d'impression de certaines pages peut laisser à désirer, surtout si les pages originales ont été dactylographiées à l'aide d'un ruban usé ou si l'université nous a fait parvenir une photocopie de qualité inférieure.

Les documents qui font déjà l'objet d'un droit d'auteur (articles de revue, examens publiés, etc.) ne sont pas microfilmés.

La reproduction, même partielle, de ce microfilm est soumise à la Loi canadienne sur le droit d'auteur, SRC 1970, c. C-30. Veuillez prendre connaissance des formules d'autorisation qui accompagnent cette thèse.

THIS DISSERTATION HAS BEEN MICROFILMED EXACTLY AS RECEIVED

LA THÈSE A ÉTÉ MICROFILMÉE TELLE QUE NOUS L'AVONS REÇUE

NL 339 (r. 86/01)

Canada

National Library of Canada
Bibliothèque nationale du Canada

Canadian Theses Division
Division des thèses canadiennes

Ottawa, Canada
K1A 0N4

0-315-24833-5

95

PERMISSION TO MICROFILM — AUTORISATION DE MICROFILMER

• Please print or type — Écrire en lettres moulées ou dactylographier

Full Name of Author — Nom complet de l'auteur

RICHARD WITZKE

Date of Birth — Date de naissance

APRIL 30, 1959

Country of Birth — Lieu de naissance

CANADA.

Permanent Address — Résidence fixe

11928 - 128 ST.
EDMONTON, ALTA. T5L-1C1
CANADA.

Title of Thesis — Titre de la thèse

LOW-FREQUENCY EDDY CURRENT TESTING OF WELD BEADS.

University — Université

UNIVERSITY OF ALBERTA.

Degree for which thesis was presented — Grade pour lequel cette thèse fut présentée

M.Sc. IN METALLURGICAL ENGINEERING

Year this degree conferred — Année d'obtention de ce grade

1984

Name of Supervisor — Nom du directeur de thèse

B.M. PATCHETT.

Permission is hereby granted to the NATIONAL LIBRARY OF CANADA to microfilm this thesis and to lend or sell copies of the film.

The author reserves other publication rights, and neither the thesis nor extensive extracts from it may be printed or otherwise reproduced without the author's written permission.

L'autorisation est, par la présente, accordée à la BIBLIOTHÈQUE NATIONALE DU CANADA de microfilmer cette thèse et de prêter ou de vendre des exemplaires du film.

L'auteur se réserve les autres droits de publication; ni la thèse ni de longs extraits de celle-ci ne doivent être imprimés ou autrement reproduits sans l'autorisation écrite de l'auteur.

Date

SEPT. 18, 1984

Signature

R Witzke

THE UNIVERSITY OF ALBERTA

Low-Frequency Eddy Current Testing of Weld Beads

by

(C) Richard Witzke

A THESIS

SUBMITTED TO THE FACULTY OF GRADUATE STUDIES AND RESEARCH

IN PARTIAL FULFILMENT OF THE REQUIREMENTS FOR THE DEGREE

OF Master of Science in Metallurgical Engineering

Department of Mineral Engineering

EDMONTON, ALBERTA

Fall 1984

THE UNIVERSITY OF ALBERTA

RELEASE FORM

NAME OF AUTHOR Richard Witzke

TITLE OF THESIS Low-Frequency Eddy Current Testing of Weld Beads

DEGREE FOR WHICH THESIS WAS PRESENTED Master of Science in Metallurgical Engineering

YEAR THIS DEGREE GRANTED Fall 1984

Permission is hereby granted to THE UNIVERSITY OF ALBERTA LIBRARY to reproduce single copies of this thesis and to lend or sell such copies for private, scholarly or scientific research purposes only.

The author reserves other publication rights, and neither the thesis nor extensive extracts from it may be printed or otherwise reproduced without the author's written permission.

(SIGNED) R. Witzke

PERMANENT ADDRESS:

11928 - 128 ST.
EDMONTON, ALBERTA
T5L - 1C1

DATED SEPTEMBER 18, 1984

THE UNIVERSITY OF ALBERTA

FACULTY OF GRADUATE STUDIES AND RESEARCH

The undersigned certify that they have read, and recommend to the Faculty of Graduate Studies and Research, for acceptance, a thesis entitled Low-Frequency Eddy Current Testing of Weld Beads submitted by Richard Witzke in partial fulfilment of the requirements for the degree of Master of Science in Metallurgical Engineering.

.....

Supervisor

.....

.....

Date. SEPTEMBER 6, 1984

Abstract

The eddy current nondestructive testing method has traditionally been used for the detection of surface and subsurface flaws in conducting materials. The basic problem with inspection to greater depths is shallow skin depth or lack of penetration at realistic operating frequencies. To overcome this problem and the effect of lift-off, specially designed through-transmission probes were used which operate in the frequency range of 100 to 2000 Hz. By using a conventional single-frequency impedance-plane analysis technique, phase detector circuitry and filters, welds in 1/2" (12.7 mm) thick aluminum alloy plate were inspected to detect flaws within the welds.

Different operating and material conditions, such as electrical conductivity, magnetic permeability, lift-off, dimensional changes and cracks produce their own unique impedance-plane plots. This thesis describes and illustrates how the "signatures" of various test object conditions may be used to characterize the flaws present within the welds. By using an X-Y storage oscilloscope to record the signatures, flaws such as incomplete penetration, cluster porosity and large isolated pores were easily identified. Future considerations extend to the inspection of other metals, including steel, using a conventional differential probe configuration.

Acknowledgements

I would like to thank my supervisor, Dr. B.M. Patchett, for his encouragement and guidance throughout my research. My appreciation is also extended to the technical staff in the Department for their assistance, in particular, Mr. C. Bicknell and Mr. T. Forman.

I would also like to thank Mr. S. DeWalle of *ANDEC* for supplying the through-transmission eddy current probes used in this project.

Table of Contents

Chapter — Page

1. General Introduction 1
2. Literature Survey 5
   - 2.1 Survey Introduction 5
   - 2.2 Basic Electromagnetic Principles 6
     - 2.2.1 Early Discoveries 6
     - 2.2.2 Induced Emf 17
     - 2.2.3 Maxwell's Contributions 20
     - 2.2.4 Modern Developments 23
   - 2.3 Basic Eddy Current Principles 25
     - 2.3.1 Electromagnetic Induction 25
     - 2.3.2 Operating Variables 31
       - 2.3.2.1 Coil Impedance 31
       - 2.3.2.2 Electrical Conductivity 36
       - 2.3.2.3 Magnetic Permeability 39
       - 2.3.2.4 Skin Effect 42
       - 2.3.2.5 Lift-off and Fill Factors 47
       - 2.3.2.6 Edge Effect 50
     - 2.3.3 Impedance Concepts 50
   - 2.4 Survey Summary and Conclusions 58
3. Experimental Procedure 61
   - 3.1 Materials 61
   - 3.2 Specimen Preparation 61
   - 3.3 Verification Tests 66
     - 3.3.1 Radiographic Nondestructive Tests 66
     - 3.3.2 Ultrasonic Nondestructive Tests 67

3.4 The Eddy Current Test System 68

3.4.1 Basic Test System Configuration 68

3.4.2 Amplitude-Phase Detector System 71

3.4.3 Test Coil Assembly Handling/C-scan Equipment 76

3.4.4 Test Coil Configurations 80

3.5 Test System Operation 90

3.5.1 Initial Probe Studies 90

3.5.2 Impedance-Plane Analyses 92

4. Test Results and Discussion 93

4.1 Verification Test Results 93

4.2 Initial Probe Studies 99

4.2.1 Penetration Characteristics 99

4.2.2 Probe Sensitivity 108

4.2.3 Lift-off Effects 112

4.3 Impedance-Plane Analyses 114

4.3.1 Flaw Detection 114

4.3.2 Characterization of Flaws 120

4.4 Industrial Applications 127

5. Conclusions 131

6. Recommendations for Future Work 135

6.1 General Recommendations 135

6.2 Thermal Stability 136

6.3 Standards 136

References 138

List of Figures

Figure		Page
1.	Magnetic field around a wire: a)direction of the magnetic field; b)contribution to the magnetic field at point *P*.	7
2.	Magnetic field of a current loop.	11
3.	Coil with widely spaced turns.	11
4.	Lines of magnetizing force for a real coil.	13
5.	Faraday's circuit, used to illustrate electromagnetic induction.	15
6.	Illustration of Lenz's law.	15
7.	Oblique magnetic flux lines.	18
8.	Faraday's induced emf law.	18
9.	Induced currents: a)simple two loop case; b)spatial flow of currents in a test object.	27
10.	Current and magnetic field phase angles: a)without test object; b)with test object.	29
11.	Impedance-plane diagram.	33
12.	Coupled circuit (simple conducting loop).	33
13.	Coupled circuit (test coil encircling a bar).	38
14.	Conductivity locus.	38
15.	Magnetic permeability effects on test coil impedance.	41
16.	The skin effect: a)variation of eddy current density as a function of depth; b)variation of eddy current phase angle as a function of depth.	45
17.	Typical material thickness loci.	48
18.	Lift-off loci on the impedance plane.	48
19.	Frequency effects on the impedance plane.	52

Figure Page

20. Metal thinning on the impedance plane. 52

21. Coating thickness on the impedance plane:
a)aluminum coating on thick copper plate;
b)copper coating on thick aluminum plate. 54

22. Cracks on the impedance plane. 56

23. Direction of surface and subsurface cracks
on the impedance plane. 56

24. Specimen 1 - Artificially produced
incomplete penetration flaw. 63

25. Specimen 2 - Artificially produced
porosity flaws. 64

26. Specimen 3 - Artificially produced
incomplete penetration flaw. 65

27. General line diagram for an eddy current
test system. 69

28. Operational functions of the eddy current
test system. 69

29. Block diagram for the Defectomat system. 72

30. Evaluating monitors: a)Y-component
evaluation; b)amplitude evaluation;
c)sector-amplitude evaluation. 77

31. Prototype eddy current coils: a)encircling
coil; b)inside coil; c)probe coil. 83

32. Double coil configuration. 83

33. Differential eddy current coils:
a)standard-comparison arrangement;
b)self-comparison arrangement. 84

34. Through-transmission sensing coil. 86

35. Probe *A* - excitation coil. 87

36. Probe *B* - excitation coil. 88

37. Probe *C* - excitation coil. 89

Figure Page

38. Magnetic field produced by probe *A* (contour plot). 102

39. Magnetic field produced by probe *A* (perspective block diagrams). 103

40. Magnetic field produced by probe *B* (contour plot). 104

41. Magnetic field produced by probe *B* (perspective block diagrams). 105

42. Magnetic field produced by probe *C* (contour plot). 106

43. Magnetic field produced by probe *C* (perspective block diagrams). 107

List of Plates

Plate		Page
1.	The Defectomat (Model F2.825.03).	73
2.	Test coil assembly handling/C-scan equipment.	79
3.	Probe assembly mount.	81
4.	Horizontal scanning of a weld bead.	81
5.	Radiograph of specimen 1 - IP flaw (reduced size).	94
6.	Radiograph of specimen 2 - CP and LIP flaws (reduced size).	95
7.	Radiograph of specimen 2 - CP flaw (true size).	96
8.	Radiograph of specimen 2 - LIP flaw (true size).	96
9.	Radiograph of specimen 3 - IP flaw (reduced size).	97
10.	Radiograph of specimen 3 - IP flaw (true size).	98
11.	Probe *A* - sensitivity to IP flaw (specimen 1).	109
12.	Probe *B* - sensitivity to IP flaw (specimen 1).	111
13.	Probe *C* - sensitivity to IP flaw (specimen 1).	111
14.	Probe *A* - lift-off effects (specimen 1).	113
15.	Probe *B* - lift-off effects (specimen 1).	113
16.	Detection of cluster porosity - probe *A*.	116
17.	Detection of large isolated pores - probe *A*.	116
18.	Detection of incomplete penetration - probe *A*.	118
19.	Detection of cluster porosity - probe *B*.	118

Plate Page

20. Detection of large isolated pores - probe *B*. 119

21. Detection of incomplete penetration - probe *B*. 119

22. Flaw signatures - probe *A* (300 Hz). 121

23. Flaw signatures - probe *B* (300 Hz). 121

24. Flaw signatures - probe *A* (500 Hz). 123

25. Flaw signatures - probe *B* (500 Hz). 123

26. Flaw signatures - probe *A* (700 Hz). 125

27. Flaw signatures - probe *B* (700 Hz). 125

1. General Introduction

Electromagnetic nondestructive test methods are widely used in the metals industry to inspect and evaluate metals for quality control. Because the tests are nondestructive, they can be used to inspect an entire production output if desired. The basic principle of the electromagnetic test is that electromagnetic field perturbations caused by the presence of a test object in the field are measured and used indirectly to evaluate conditions of interest in the test object. The correlation between the instrument readings and the structural characteristics and serviceability of the test object must be carefully and repeatedly established for these methods to be reliable.

Electromagnetic nondestructive test methods use the effects of electromagnetic induction, electromagnetic fields, or varying currents for probing, measuring, or inspecting. The most commonly used electromagnetic nondestructive test is the eddy current test, and is the subject of this thesis. It will be shown that eddy current testing is based on the principles of electromagnetic induction and that the main operational functions common to the eddy current test are: 1)the excitation of one or more test coils to produce an electromagnetic field within the test object, 2)the modulation of the electromagnetic field quantities by the test object, 3)the conversion of test coil output signals for analysis, 4)the detection or demodulation of the test coil output signals, 5)the analysis of the test

coil output signals, 6)the display or indication of results, and 7)the handling of the test object being inspected.

A number of eddy current testing methods are available, but the most common eddy current test method is the vector-point or impedance-plane analysis method, where impedance changes in the test coil representing changes in the test object are monitored using an X-Y storage oscilloscope. This eddy current testing method may be used to identify and differentiate between a wide variety of physical, structural and metallurgical conditions in electrically conductive ferromagnetic and nonferromagnetic metal parts. This testing method may be used to: 1)measure or identify such properties and conditions as electrical conductivity, magnetic permeability, physical dimensions, grain size, hardness and heat treatment, 2)detect seams, laps, cracks, voids and inclusions, 3)sort dissimilar metals by detecting differences in their composition, microstructure and other properties and 4)measure the thickness of a nonconductive coating on a conductive metal, or the thickness of a conductive coating on a dissimilar conductive metal. Because of its versatility, the impedance-plane analysis technique was used for this study.

Eddy current testing may be used to inspect and evaluate a wide variety of metal materials and products. This is true, provided that the physical requirements of the material are compatible with the inspection method. In many cases, however, the method may be sensitive to a number of

unimportant properties and/or characteristics inherent within a material which may result in misleading instrument signals or instrument signals that mask critical variables. This may occur if both a conductivity change and flaw are detected at the same time. This may also occur if the coil-to-object distance or lift-off varies during the test, as would occur during the inspection of a weld bead.

The purpose of this thesis project was to develop a suitable test coil capable of producing a magnetic field which would penetrate weld beads in thick plates of aluminum alloy, yet still maintain a suitable degree of sensitivity to flaws within the weld. To achieve the required penetration, testing equipment capable of operating at low frequencies (eg. 100 to 2000 Hz) was used. The equipment was also phase selective to provide a means of discriminating against any undesirable variables associated with the eddy current test. Another requirement of this project was the development of a suitable system to overcome the effects of lift-off associated with the crown of a weld bead.

A suitable choice of testing equipment and probe design allowed a variety of flaws to be detected and characterized using the impedance-plane analysis method of eddy current inspection. Incomplete penetration, cluster porosity and large isolated pores present within welds made in aluminum alloy plate were identified using this method. The results were verified using both ultrasonic and radiographic nondestructive tests.

The theory of eddy current nondestructive testing is presented in the literature survey. The development of the eddy current test system and testing technique, conclusions and recommendations for future work, including practical applications of this system, are presented in the experimental section of this thesis.

2. Literature Survey

2.1 Survey Introduction

Development of the eddy current method of inspection was based on early discoveries in the field of electromagnetism and technological advances in the areas of metallurgy, metals fabrication and instrumentation. It will be shown that electromagnetic induction is one of the key principles of the eddy current test and that electromagnetic effects are caused within a conductive test object as a result of varying electromagnetc fields. These fields result in eddy current flow within a conductive material. A secondary electromagnetic field is set up as a result of this eddy current flow, which creates electrical signals within the test coil that are related to the electrical conditions of the test object. The basic principles of electromagnetism will be presented as a historical development.

With the basic electromagnetic principles realized, the two major functions of the eddy current test method will be studied. These functions include the excitation of the test coil with a sinusoidal signal and the modulation of the test coil output signals, as represented by changes in the impedance-plane diagram. The principle operating variables of the eddy current inspection method will be investigated, as well as impedance concepts and the phase discrimination technique.

2.2 Basic Electromagnetic Principles

2.2.1 Early Discoveries

The principles of the eddy current method of inspection are founded on early discoveries in the field of electromagnetism. In 1820 Oersted[1,2] discovered the magnetic effect of electric current. He showed that a magnetic needle, when placed under a current-carrying wire, takes up a direction perpendicular to that of the current. He also found that the effect was passed from the wire to the needle through materials such as brass, glass, wood and water. These were simple, yet important observations, since they illustrated the presence of a magnetic field and initiated the subject of electromagnetism.

Figure 1a illustrates the magnetic field around a wire. Oersted's examination of the field at any point *P*, at the end of radius vector **r**, showed that the direction of the magnetizing force was always at right angles to both the direction of current flow and the direction of the radius vector. The result is a circular magnetic field around the wire.

Oersted's observations were soon confirmed by Ampère[2,3] who took the experiment one step further, examining the reaction of the magnet upon the current. He showed that the direction of the force exerted upon a current by the earth's magnetic field was consistent with Newton's third law, which

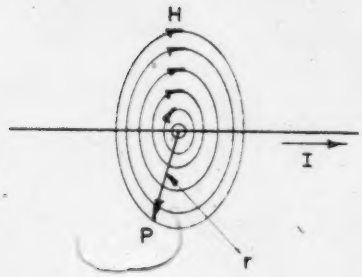

(a)

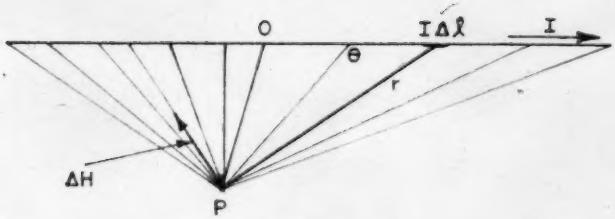

(b)

Figure 1. Magnetic field around a wire: a)direction of the magnetic field; b)contribution to the magnetic field at point *P*.

states that, *for every action there is always an opposed equal reaction.* Ampère then studied the action of one electric current upon another. He discovered that two parallel wires carrying currents were mutually attractive when the currents flowed in the same direction and repulsive when the currents flowed in the opposite directions.

Two of Ampère's contemporaries, Biot and Savart', repeated Oersted's experiment and discovered a law describing the magnetic effect. They found that the direction of force on the magnetic pole was perpendicular to the wire and circumferential with respect to the wire. They also found that the force was proportional to the reciprocal of the distance from the pole to the wire. With their findings, Biot developed an equation which states that the field, of any point, is the integrated sum of the field effects of the individual contributions of all differential current elements in the system. Although credited to Biot, this equation is commonly known as Ampère's law.

To illustrate Ampère's law, the origin of the field at point P is considered, as in Figure 1a. The field at point P is actually made up of the combined contributions of the field effect from the current-carrying wire. This is illustrated in Figure 1b. In this case, the current flow I through the wire is made up of a series of elemental currents $I\Delta\ell$. Ampère's law states that the contribution of the field, at point P, by the elemental current $I\Delta\ell$, is directly proportional to the strength of the current element

and to the sine of the angle θ between the direction of the elemental current flow and the line connecting the elemental current with point P, where the direction of the field contribution at point P is perpendicular to both the direction of the current element flow and the line connecting the current element flow with point P. The law also states that the contribution of the field, at point P, by the elemental current, is inversely proportional to the square of the distance from the current element to point P; thus, the equation reads:

$$\Delta H \simeq I\Delta\ell \sin\theta / r^2 \qquad (1)$$

This is the field contribution from a single current element (N.B.: bold-face type indicates a vector quantity). The quantity $I\Delta\ell$ should remain constant, while the angle θ and distance r have different values for each current element. All the contributions may be summed to give the total value of the magnetizing force **H** at point P.

In this example, it was assumed that the current had the same value along the wire. If the current varies with time or distance along the wire, the contributions to **H** will also vary. In addition, all of the lines from P to the current elements lie in a single plane (i.e., the straight current path or wire); therefore, all of the elemental **ΔH** values lie in the same direction. If the wire were curved,

the elemental values would not have the same directions; therefore, all of the contributions would have to be added as vectors. Further complications result if many wires are present and oriented in different directions. As simple as the equation might appear, these complications may still be handled by applying Ampère's law.

The effect of using a loop of wire is illustrated in Figure 2. The lines of magnetic force, B, tend to be straight near the center of the loop and gradually approach a circular pattern near the wire. For points close to the wire, a length of wire that is very short compared to the radius will closely approximate a straight line; therefore, the wire behaves magnetically like a long straight wire, resulting in concentric circles of magnetic force. In this case, the amplitude varies inversely with the square of the distance from the current element and directly as a function of the angle between the direction of the current element and the radius vector between the current element at point *P*. Each contribution to the field is at right angles to the plane containing both the radius vector and the direction of the current element. Reversing the direction of the current will result in the reversal of the direction of the magnetic field.

Going one step further, a multi-turn coil or solenoid may be analyzed in a similar fashion. The coil's field is the vector sum of the fields set up by all of the turns that make up the coil. Figure 3, which illustrates a coil with

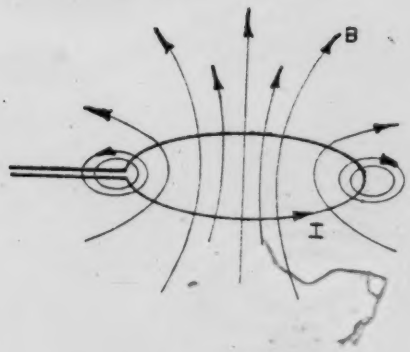

Figure 2. Magnetic field of a current loop.

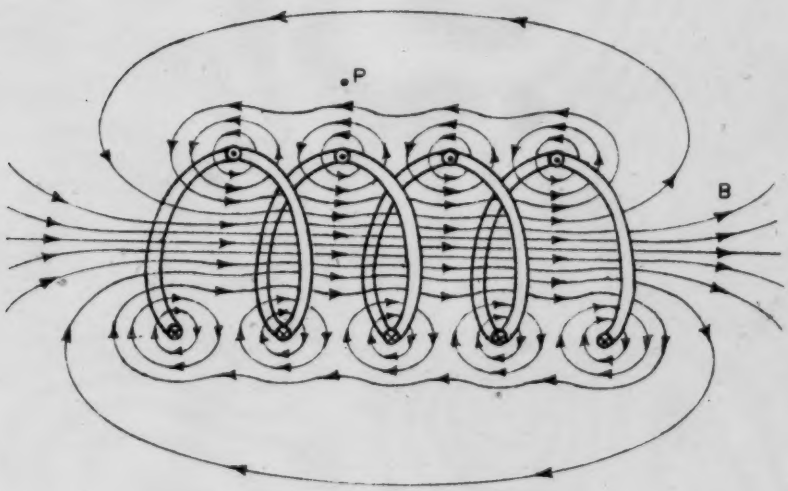

Figure 3. Coil with widely spaced turns.

widely spaced turns, suggests that the fields tend to cancel between the wires. It also suggests that, at points inside the coil and reasonably far from the wires, B is parallel to the coil's axis. In the limiting case of adjacent tightly packed square wires, the coil becomes essentially a cylindrical sheet and the requirements of symmetry confirm the previous statement.

For a point *P* outside the coil, such as in Figure 3, the field set up by the upper part of the coil turns tends to cancel the field set up by the lower part of the coil turns. As the coil approaches the limiting case, the magnetic field at points outside the coil approach zero. Taking the external field to be zero is not a bad assumption for a practical coil, if its length is much greater than its diameter and if only external points near the central region of the coil are considered. Figure 4 shows the lines of magnetizing force for a real coil. Although this coil is far from ideal, the spacing of the lines of *B* in the central plane illustrate how the external field is much weaker than the internal field.

Oersted's discovery of the magnetic field associated with an electric current suggested to several other investigators the possibility that magnetism could in some way give rise to electricity. This opposite effect was not demonstrated until 1831 when Faraday[3,4] discovered electromagnetic induction, one of the key principles of the electromagnetic test. Joseph Henry, in 1830, was the first

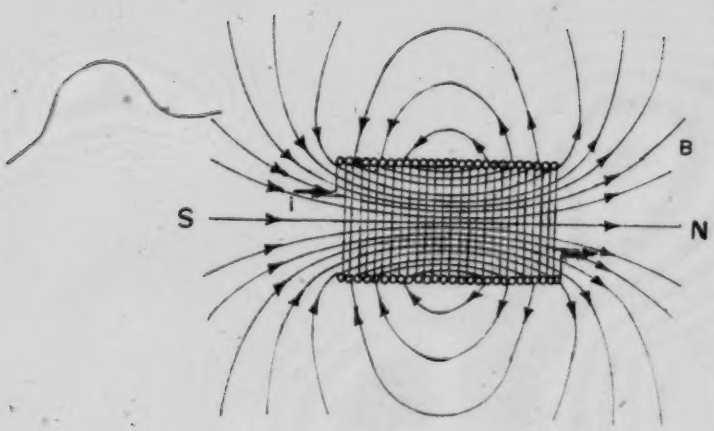

Figure 4. Lines of magnetizing force for a real coil.

to observe such a phenomenon, but Faraday published his independent discovery first and is therefore credited with the discovery.

In these early studies, coils were wound on a soft iron ring, as illustrated in Figure 5. In this arrangement, one of the coils was connected through a switch to a battery. The circuit of the other coil W_2 included a wire which passed over a magnetic needle three feet from the iron ring. Faraday discovered that by connecting the battery to winding W_1 the magnetic needle moved, oscillated and returned to its original position, and then by disconnecting the battery, oscillations were again produced. These results showed that a current was generated in coil W_2, given a change in current through coil W_1. By adding a coil in the W_2 circuit, adjacent to the magnetic needle, Faraday was able to make some additional observations. He observed that the needle moved initially in one direction when the battery was connected and initially in the opposite direction when disconnected. In both cases, after the initial movement, the magnetic needle oscillated and returned to its original position.

Faraday repeated this experiment using a wooden core instead of an iron core. He obtained results similar to those with the soft iron ring core, but the current was lower. A galvanometer was required to measure this low current. In later experiments, Faraday discovered that the mere approach or removal of a current-carrying conductor

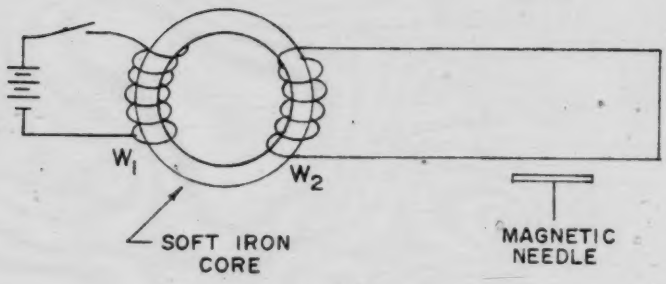

Figure 5. Faraday's circuit, used to illustrate electromagnetic induction.

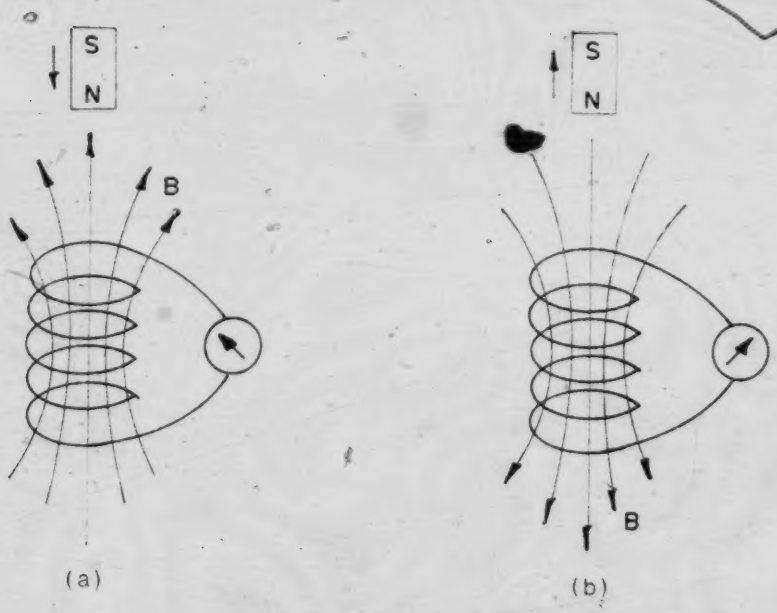

Figure 6. Illustration of Lenz's law.

induced a current in a neighbouring coil and that the motion of magnets produced similar effects.

Although Faraday was able to predict the direction of an induced current, he did not state his principle as succinctly as Lenz'. In 1834, Lenz conducted a series of experiments which led him to his rule for predicting the direction of an induced current:

"the direction of the induced current is always such that its electromagnetic action tends to oppose the change which produces it."

Lenz's law is illustrated in Figure 6. As a bar magnet approaches the top of the coil, as in Figure 6a, the current induced in the coil gives rise to an induction that opposes the approach of the magnet. Likewise, as the magnet is withdrawn, as in Figure 6b, its motion is again opposed by the magnetic field arising from the current induced in the coil.

An important concept to be learned from Faraday's experiment is that of magnetic flux or magnetic induction. The magnetic field intensity **H** produces a magnetic flux **B** in the direction of **H** and its value is proportional to the product of the permeability and the magnetic force (i.e., $B=\mu H$). This leads to the concept of total flux. The total flux ϕ is obtained by summing up the flux over a given area. As an example, the total flux for a given coil, such as Figure 2, would be equivalent to

$$\phi = B_{av} \times A \qquad (2)$$

where B_{av} is the average magnetic flux and A is the cross-sectional area of the coil. The flux ϕ is given in units of webers, named in honor of W.E. Weber, German physicist. The magnetic flux density is the total flux per unit area (ϕ/A). If **B** is oblique to the plane of area, then

$$\phi = B_{av} A \cos\theta \qquad (3)$$

where θ is the angle between **B** and the normal to the area, as illustrated in Figure 7.

2.2.2 Induced Emf

Although induced current has been mentioned, it should be realized that the primary effect is the induced emf. This gives rise to a current, provided the circuit is complete. Figure 8 shows a single-turn loop placed in a magnetic field having a flux density **B** and a total flux ϕ threading the loop. Faraday found experimentally that the magnitude of the induced emf in a single loop was directly proportional to the time rate of change of the total magnetic flux enclosed by the loop:

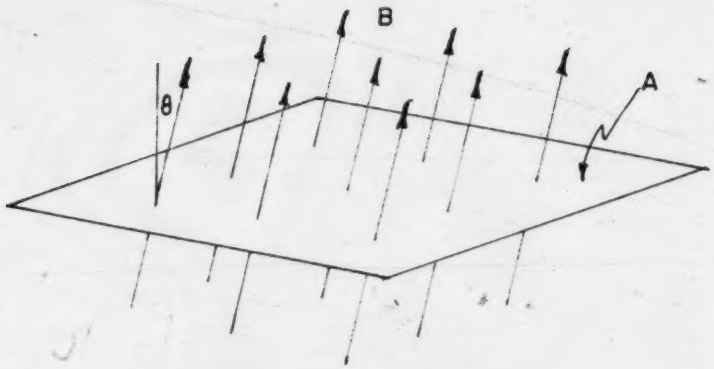

Figure 7. Oblique magnetic flux lines.

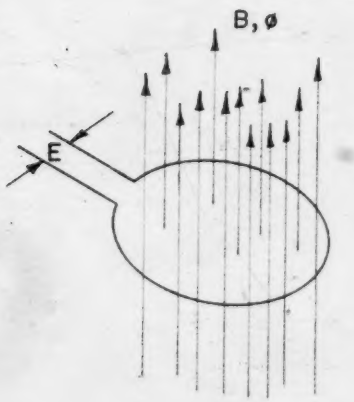

Figure 8. Faraday's induced emf law.

$$E = -\Delta\phi/\Delta t \qquad (4)$$

where $\Delta\phi$ is the change in flux and Δt is the change in time. E is given in volts when $\Delta\phi/\Delta t$ is given in webers per second.

An emf ($\Delta\phi/\Delta t$) is induced in each turn of a coil; therefore, if *N* turns are connected in series, the total emf in the coil is *N* times that induced in a single loop:

$$E = -N\Delta\phi/\Delta t \qquad (5)$$

If the flux varies at a sinusoidal rate (i.e., if alternating current is used), the induced voltage at the terminals of the loop would vary as the cosine function, because the time rate of change of a sine function is a cosine function. Application of the negative sign results in a 90° shift between the output voltage and the total magnetic flux threading the loop, where the output voltage leads the total magnetic flux.

The induced voltage, by Ohm's law[4], will cause a current to flow around the loop. The amount of current which flows in the loop depends on the electrical resistance of the loop and, in accordance with Ampère's law, the current will make new contributions to the existing field which, in turn, will affect the induced voltage around the loop. These

contributions will be discussed in section 2.3.

2.2.3 Maxwell's Contributions

The years from 1831 to 1931 were a time for development of basic mathematical and electrical analyses, as well as electrical techniques. The most important contributions to the development were made by Maxwell'. Maxwell was greatly influenced by Faraday's experimental results and ideas about magnetic lines of force. In 1864, he presented his classical dissertation on a dynamic theory of the electromagnetic field. Maxwell skillfully modified the existing equations developed through the contributions of Oersted, Coulomb'°, Ampère, Biot, Savart, Gauss'' and Faraday to develop his four renowned equations''.

The scope of Maxwell's equations is remarkable, including as it does the principles of all large scale electromagnetic and optical devices such as motors, cyclotrons, electronic computers, radio, television, radar and optical instruments. These principles include the generation and flow of eddy currents in conductors and the associated electromagnetic fields; thus, all the electromagnetic induction effects that are basic to the eddy current inspection method are described, in principle, by Maxwell's equations for the appropriate boundary values for practical applications.

Maxwell's first equation, derived by applying the divergence theorem to Gauss' theorem for electricity, takes

the differential form:

$$\nabla \cdot \mathbf{D} = \rho \qquad (6)$$

where ∇ is the vector differential operator, $\mathbf{D}$ is the electrical displacement and ρ is the volume density of free charge. This equation relates the electric field to the charge enclosed within a surface.

Maxwell's second equation, an extension of Ampère's law, relates the magnetic effect to a change in the electric field or current by:

$$\nabla \times \mathbf{H} = \mathbf{J} + \delta \mathbf{D}/\delta t \qquad (7)$$

where $\mathbf{H}$ is the magnetic intensity, $\mathbf{J}$ is the current density and $\delta \mathbf{D}/\delta t$ is the density of displacement current. The displacement current may exist if the electric field is changing. In a conductor, the $\delta \mathbf{D}/\delta t$ term vanishes, while in a dielectric it is the $\mathbf{J}$ term which vanishes.

Maxwell's third equation, derived from Faraday's law of electromagnetic induction, relates the rate of change of magnetic induction to the resulting electric field. The differential form of Maxwell's third equation may be

written as:

$$\nabla \times \mathbf{E} = -\delta \mathbf{B}/\delta t \qquad (8)$$

where **E** is the intensity of the field associated with the induced emf (force per unit charge) and $\delta \mathbf{B}/\delta t$ is the rate of change of magnetic induction.

Finally, Maxwell's fourth equation, derived by applying the divergence theorem to Gauss' theorem for magnetism, shows that the total flux of magnetic induction through any closed surface is equal to zero. His fourth equation may be written as:

$$\nabla \cdot \mathbf{B} = 0 \qquad (9)$$

where **B** is the magnetic flux density. Maxwell's fourth equation is a direct consequence of the fact that the induction is the curl of a vector.

The recognition to include a displacement current to account for electromagnetic events in space where no conduction currents exist, as in the space between the plates of a capacitor, was one of Maxwell's major contributions to physics. This single discovery led to his conclusions that electromagnetic waves could be propagated

in free space and that visible light was such an electromagnetic radiation. Maxwell also predicted the presence of lower frequency waves, called Hertzian or radio waves. His work was also an important foundation for the works of Lorentz and Einstein in the development of the theory of special relativity.

2.2.4 Modern Developments

In 1879, Hughes detected differences in electrical conductivity, magnetic permeability and temperature in metal using an eddy current method. Further development of the electromagnetic theory was necessary before eddy current methods could be used in practical applications. Since nondestructive testing techniques were not common in the 1800's, much of the analytical work and measurements were accomplished in connection with other electrical problems and were later applied to nondestructive testing. Calculation of the flow of induced current in metals was later possible by the solution of Maxwell's equations for symmetrical configurations using specific boundary conditions. These mathematical techniques were important in the electric power generation and transmission industry, as well as in the methods of induction heating and eddy current inspection.

With the advent of World War II came a rapid growth in the metals industry and a need for improved nondestructive testing techniques to meet the new requirements of the

metals industry. The earliest advances in the development of a practical eddy current technique were made by Vigness, Pinger and Gunn[12] in 1942. An early, well documented work was presented by Farrow[13] in 1943. He pioneered the development and application of an eddy current system for the inspection of welded steel tubing. His system included a separate primary excitation coil, differential secondary detector coils and a direct current magnetic saturating coil. The inspection system also included a balancing network, high frequency amplifier, frequency discriminator-demodulator, low frequency pulse amplifier and filter. These are the same basic elements present in a modern eddy current inspection system. In the same year, Zuschlag[14] also made some major contributions in the design, development and application of eddy current nondestructive testing equipment.

Probably the most thorough work done on the theory and application of eddy current testing methods was made by Förster and his associates[15-17]. During the past 25 years they applied all of the basic principles of eddy currents and a combination of the results of detailed analytical studies and measurements made with models representing various test objects (i.e., mercury models with artificial flaws and specimens with varying conductivities and diameters) to develop their eddy current testing systems.

An excellent survey of electromagnetic nondestructive tests, prior to 1950, was presented by McMaster and Wenk[18]

in 1950. Their publication gives a list of related patents and operational features common to each of the methods listed. Another excellent contribution to the field was made by Libby[19-25]. He presented many papers on the topic of multifrequency eddy current testing and has given an excellent introduction to the eddy current nondestructive test method in his book entitled "Introduction to Electromagnetic Nondestructive Test Methods"[25]. In this book, Libby describes the basic principles, techniques and applications of eddy current testing in great depth, with the principles emphasized, making this book an excellent reference source for this thesis. Some other general purpose reference sources include papers by Förster[17], Libby[24] and Hochschild[26].

The remainder of this literature survey will be devoted to detailed studies of the basic eddy current principles. The electromagnetic field, flow of currents and formation of signals will be investigated.

2.3 Basic Eddy Current Principles

2.3.1 Electromagnetic Induction

It has already been shown that the main principle of the eddy current test method is electromagnetic induction. The principle of electromagnetic induction will now be discussed in greater detail.

By placing an electrically conductive test object adjacent to a test coil, varying currents may be induced into the object by the varying magnetic field created as a result of current flow through the test coil. In the same manner, the induced currents produce a varying magnetic field. The field associated with the test coil is commonly called the primary field, while the field associated with the test object is called the secondary field. In the case of nonmagentic test objects, this secondary field opposes the primary field to an extent that depends on the conductivity, size of the object and the operating test frequency. The electrical phase angle of the induced eddy currents vary according to the test object parameters and the test frequency. The phase angle of the secondary field varies in the same manner.

In practice, the secondary field is monitored by observing its effects on the current or voltage of the primary test coil, or upon currents or voltages induced in secondary test coils placed near the primary test coil. The primary and secondary coils are commonly wound as a pair, as illustrated in Figure 9a for a simple two loop case. An alternating current I_p is applied to the primary loop, producing a primary magnetic field which induces an alternating emf in the secondary loop. This emf causes a current to flow in the secondary loop (I_s). This current may be determined using Ohm's law, which states that the current is equal to the ratio of the final induced emf to the

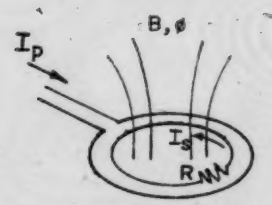

(a)

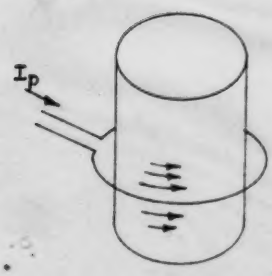

(b)

Figure 9. Induced currents: a)simple two loop case; b)spatial flow of currents in a test object.

resistance R_s of the secondary loop (i.e., $I_s = E_s/R_s$). As indicated earlier, the secondary field opposes the primary field, thus the final induced emf will be consistent with the final existing magnetic field and secondary resistance.

Given the situation in Figure 9b, where the secondary coil is replaced with a solid test object, the same basic events occur, but the currents flow over a larger volume. This large amount of current flow interacts, by electromagnetic induction, with its various parts, as well as with the current in the primary coil. As with the situation in Figure 9a, the final induced emf will be consistent with the final existing magnetic field. Given a fixed excitation current, the total effect of the field conditions may be monitored by measuring the final voltage existing across the excitation coil. Variations in the test object (i.e., voids, cracks, inclusions, etc.) which affect the flow of eddy currents within the test object may be detected by observing their effect upon the voltage.

To illustrate the amplitude and phase relationships of a.c. signals with the same test frequency, phasor diagrams are commonly used. Figures 10a and 10b illustrate the relationship between the excitation current, magnetic flux and coil voltage in a single test coil, with and without a test object present. Without a test object present, as in Figure 10a, the primary magnetic flux ϕ_p is in phase with the excitation current. No secondary magnetic flux is shown, since only a single coil is used and no test object is

(a)

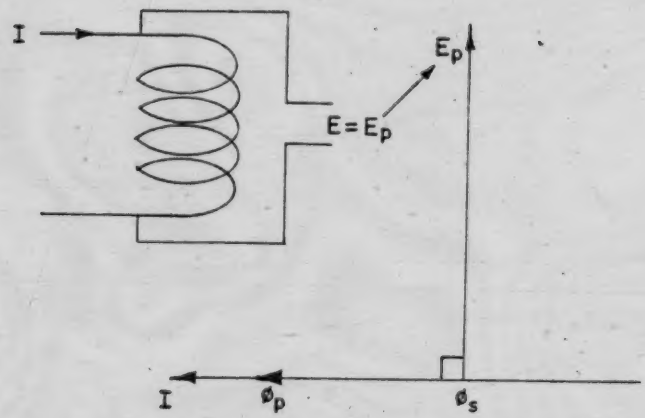

(b)

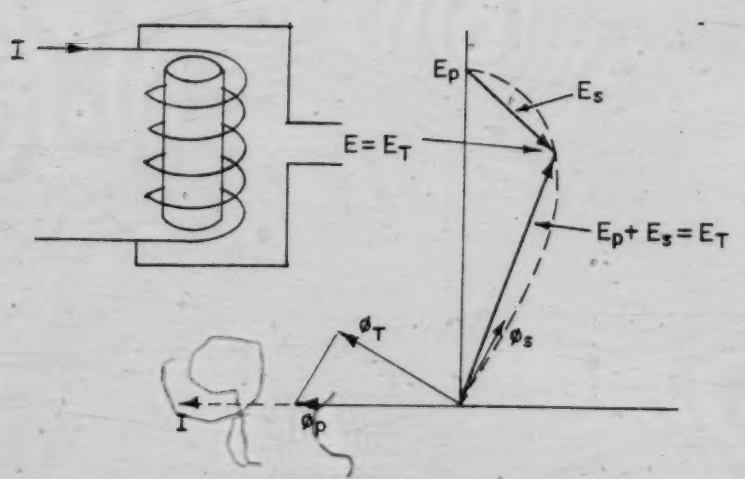

Figure 10. Current and magnetic field phase angles: a)without test object; b)with test object.

present within the field of the coil. A very small secondary magnetic flux is present due to eddy current flow through the wire itself; however, the magnitude of this flux shall be considered negligible. With a fixed alternating current I applied to the test coil, a voltage is developed across the test coil which lags the excitation current by an angle of 90 electrical degrees.

When a test object is placed within the test coil, as in Figure 10b, eddy currents are set up within the test object and a secondary magnetic flux ϕ_s is established. Vector addition of the secondary flux to the primary flux gives a new total flux ϕ_T. This total flux produces a new test coil voltage E_T which lags ϕ_T by 90°. The same result may be obtained by considering the fluxes separately, producing their own induced voltages. The actual test coil signal voltage is E_s; however, this voltage is not directly available. E_s may only be obtained by subtracting a fixed voltage, equivalent in phase and amplitude to the primary voltage E_p.

With the principle of electromagnetic induction more fully understood, the principle operating variables of the eddy current inspection method may be examined. These variables include: a)coil impedance, b)electrical conductivity, c)magnetic permeability, d)skin effect, e)lift-off factor, f)fill factor and g)edge effect. Each of these variables will be considered in the following section.

2.3.2 Operating Variables

2.3.2.1 Coil Impedance

When alternating current is flowing in a test coil, two limitations are imposed to the flow of current. These limitations include the alternating current resistance R of the wire and the inductive reactance X_L of the coil. The alternating current resistance of an empty coil at low frequencies or having a small wire diameter is very nearly the same as the direct current resistance of the wire used for the coil. As either the frequency or the wire diameter increases, the ratio of the alternating current resistance to direct current resistance increases. The resistance component is proportional to the energy dissipated in the magnetic field of the coil. Inductive reactance, on the other hand, is the combined effect of inductance and frequency. The inductive reactance component is proportional to the energy stored in the magnetic field.

Both the resistance and inductive reactance make up the total resistance to flow of alternating current in a coil. The total resistance may be represented by the following equation:

$$Z = R + jX_L \qquad (10)$$

where $X_L = \omega L = 2\pi f L$ (ω is the angular frequency, f is the

frequency in Hz and L is the inductance of the coil). The total resistance Z is commonly referred to as the impedance and is expressed in ohms. The complex term, jX_L, indicates that the alternating current and voltage in the system do not have the same phase angle. The complex operator j is replaced with j to avoid possible confusion with the symbol i sometimes used to represent electric current. Equation (10) may be represented by a phasor diagram, as described in the following paragraph.

The voltage drop across a coil is directly proportional to the impedance of the coil, in accordance with Ohm's law ($E=IZ$); thus, a phasor diagram representing the voltage drop across the circuit also represents the impedance of the circuit, where the horizontal axis represents the resistive or energy loss axis, and the vertical axis represents the energy storage or reactance axis, as shown in Figure 11. Such a phasor diagram is called an impedance-plane diagram. Because each specific condition in the test object may result in a specific coil impedance, each condition may correspond to a particular point on the impedance-plane diagram. Impedance-plane diagrams have been studied extensively by such investigators as Förster and Stambke[16], Hochschild[27] and Hagemaier[28].

Consider a circuit described by Libby[25], consisting of a primary excitation circuit and a secondary detection circuit, as shown in Figure 12. An impedance-plane diagram may be constructed which closely represents the condition

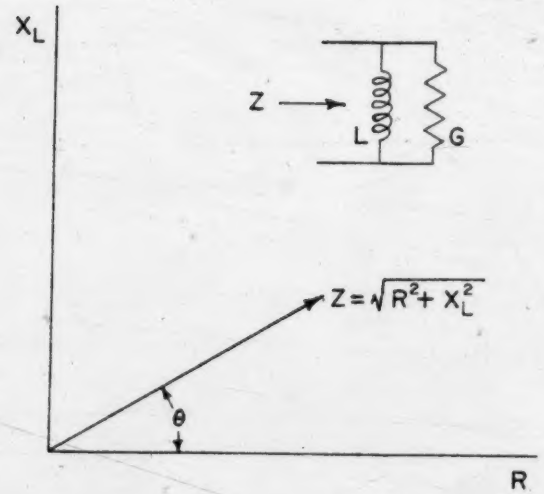

Figure 11. Impedance-plane diagram.

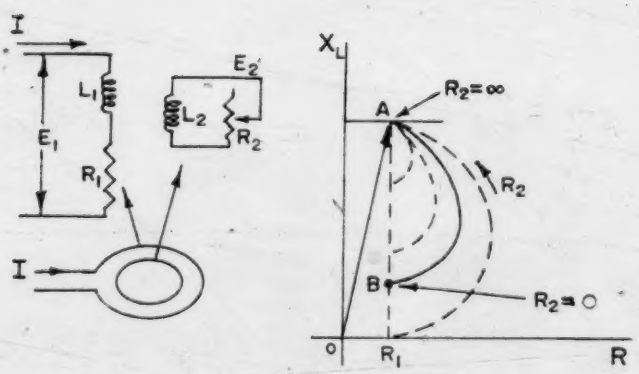

Figure 12. Coupled circuit (simple conducting loop).

existing in a practical eddy current test. Both the primary and secondary circuits have an inductance and resistance component. The resistance in the secondary loop is variable. With $R_2=\infty$ (i.e., the loop is open) the voltage drop across the primary loop is equal to the product of the current and impedance ($E=IZ$); thus, the phasor OA represents the input impedance of the circuit for the open loop condition.

If R_2 is varied from its infinite position toward zero, the input impedance will also vary until point B is reached (see Figure 12). The resistance component of the input impedance will then be the same as it was when R_2 was set at its infinite position. The reactance component, however, is greatly decreased as a result of the secondary magnetic field. The current flowing in the secondary loop sets up a secondary field which opposes the primary field, resulting in a net decrease in the flux of the primary loop, thus lowering the apparent inductive reactance of the circuit. This example illustrates what might happen to the test coil input impedance if the test object resistivity is varied.

Impedance-plane diagrams have been investigated quantitatively as a conducting cylindrical model by Förester and Stambke[1] and Hochschild[2]. These authors presented the solutions for the total flux within a solenoid in a concise manner using Maxwell's equations. By applying Faraday's law, they then obtained the induced coil voltage, which represents the coil impedance. The final equation for the total flux threading the loop was derived as:

$$\phi_i = 2\pi\mu H_0 r/k[(\text{bei}'kr - j\text{ber}'kr)/(\text{ber}ka + j\text{bei}ka)] + \pi\mu H_0(b^2 - a^2) \quad (11)$$

where,

μ=magnetic permeability
H_0=magnetic field intensity within a long empty coil
a=radius of cylindrical specimen
b=radius of coil
k=propagation constant
r=radial distance from centerline of coil
ber=Kelvin Bessel real function
ber'=Kelvin Bessel real first derivative
bei=Kelvin Bessel imaginary function
bei'=Kelvin Bessel imaginary first derivative

Faraday's law for the induced voltage around any circular loop at radius r is:

$$e_i = -d\phi/dt = -d/dt \int \mathbf{B} \cdot ds \quad (12)$$

Substituting (11) into (12) gives the equation for the induced coil voltage:

$$e_i = -\omega\pi\mu H_0 2r^2/kr[(\text{ber}'kr + j\text{bei}'kr)/(\text{ber}ka + j\text{bei}ka] - j\omega\pi\mu H_0(b^2 - a^2) \quad (13)$$

By application of Ampère's circuital law, the magnetic field intensity within a long empty coil was found to be equal to the current sheath strength I_s (i.e., $H_0 = I_s$). Rearranging

the terms in (13) and placing $H_o=I_s$ and $r=a$ gives:

$$e_i = -\omega\pi\mu I_s[2a^2/ka((\text{ber}'ka+j\text{bei}'ka)/(\text{ber}ka+j\text{bei}ka)) + j(b^2-a^2)] \quad (14)$$

This voltage represents the impedance by the following equation (neglecting coil resistance and capacitance):

$$Z = -e_i/I_s \quad (15)$$

Substituting (14) into (15) gives the impedance of a one meter length section of an infinitely long, single-layer coil encircling a conducting cylinder:

$$Z = \omega\pi\mu a^2 2/ka\ [(\text{ber}'ka+j\text{bei}'ka)/(\text{ber}ka+j\text{bei}ka)] + j\omega\pi\mu(b^2-a^2) \quad (16)$$

where ω represents the angular frequency ($\omega=2\pi f$). Impedance concepts will be discussed in more detail at the end of this chapter.

2.3.2.2 Electrical Conductivity

The effect of conductivity, σ, on the impedance-plane diagram may be illustrated by replacing the secondary coil

of Figure 12 with a solid test object, as in Figure 13. Given the same primary coil, a specimen with zero conductivity results in the same impedance as for the infinite resistance case in Figure 12, since conductivity is merely the reciprocal of resistivity. As the conductivity is increased, the impedance begins to change in the same manner as Figure 12, although at the higher conductivities the locus departs sharply from the circular path and approaches the limiting resistance R_1 at a 45° angle. The locus approaches R_1 at a 45° angle because the effective conductance and susceptance (i.e., the imaginary or complex term associated with conductance) of the metal vary due to the skin effect and the effective coupling between the exciting coil and the metal varies due to the redistribution of eddy currents.

Several common nonmagnetic materials have been plotted on a conductivity locus in Figure 14. Point *A* represents the reactance of an empty coil and the impedance points for the various materials appear as a series of dots along a smooth curve, according to their respective conductivities. The lower conductivity materials typically have higher reactance values than the higher conductivity materials. As the conductivity is increased the test coil resistance appears to pass through a maximum, which is normally not as great as the corresponding maximum of an idealized curve. The reason for this is that the test coil, for an ideal case, is assumed to have infinite length, while a practical test coil

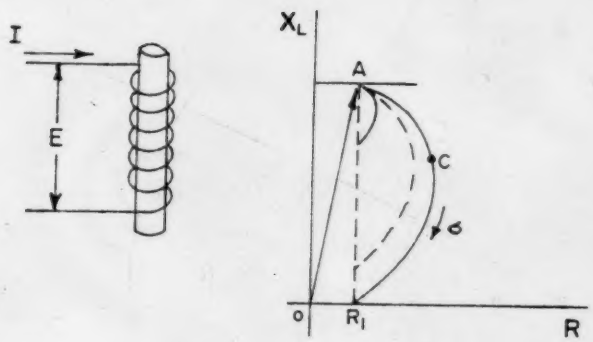

Figure 13. Coupled circuit (test coil encircling a bar).

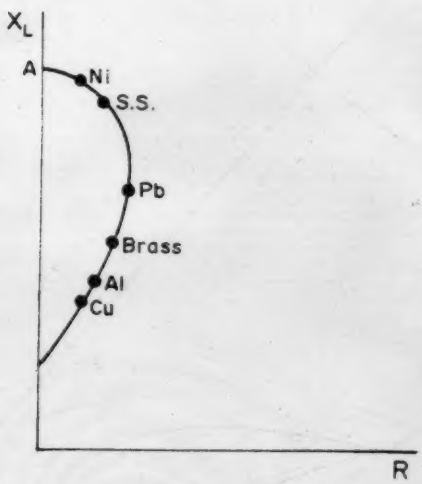

Figure 14. Conductivity locus.

is typically very short.

For a given metal, many factors influence the conductivity, notably temperature, composition, heat treatment and resulting microstructure, grain size, hardness and residual stresses. Since the test coil impedance changes with a change in conductivity, eddy currents may be used to monitor the composition and metallurgical characteristics of a metal. The use of eddy currents in this capacity will be discussed in greater detail in section 2.3.3.

2.3.2.3 Magnetic Permeability

The basic theory of magnetism and the modern theory of magnetism may be found in a number of sources[29-31]. The basic principles of magnetism were first introduced by Faraday[32] who, in 1845, discovered differences in the magnetization of materials, which later led to the classification of magnetic materials into three groups called diamagnetic, paramagnetic and ferromagnetic. Two additional classifications have been added since this discovery and are designated ferrimagnetic and antiferrimagnetic.

Maxwell also contributed to the study of magnetism and has supplied an equation relating magnetic flux density **B** and magnetic field intensity or magnetizing force **H**:

$$B = \mu H \qquad (17)$$

where μ is the magnetic permeability of the material. In free space the value of the magnetic permeability μ_o is $4\pi x10^{-7}$ H/m. In ferromagnetic metals μ varies as a function of the degree of magnetization; thus, the relationship between **B** and **H** differs from linearity.

Ferromagnetic metals and alloys, including iron, nickel, cobalt and some of their alloys, act to concentrate the flux of a magnetic field. The presence of a magnetizing force causes atomic magnetic elements of the magnetic material to become aligned with the field, increasing the magnetic flux density. Maxwell's relationship describes this effect on a macroscopic scale. An increase in flux density gives a greater induced voltage in the test coil, thus raising its impedance. The increase in impedance is primarily in the reactance direction, except for the effect of a small amount of energy loss resulting from magnetic hysteresis and conduction losses.

The increase in reactance obtained by placing a magnetic material in a previously empty coil, as illustrated in Figure 15, is the distance between point *O* and point *A*. A material with a relative permeability or permeability factor of 2 would double the length of the reactance component *OA*. Permeability factors of 100 or more are not uncommon; thus, the impedance of the test coil may be greatly increased. Impedance plots for relative permeability values of 1, 5 and 10 are illustrated in Figure 15. Test objects also have an associated conductivity that makes the impedance change

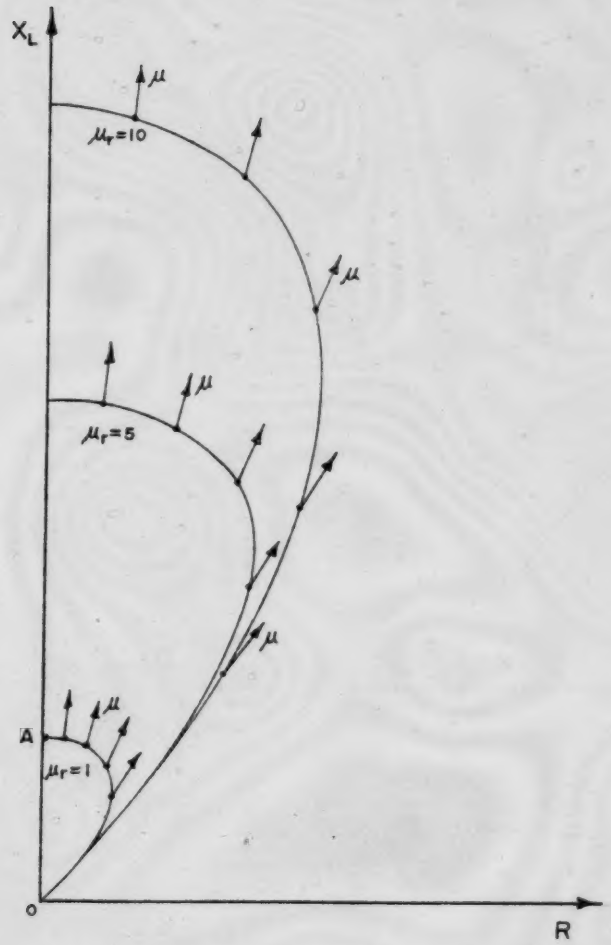

Figure 15. Magnetic permeability effects on test coil impedance.

resulting from permeability occur in a different direction, as shown by the small arrows in Figure 15.

The eddy current test is very sensitive to test object magnetic permeability variations. This often results in misleading test signals; however, the magnetic effects may be reduced by use of a magnetic saturation technique, discussed later in this thesis.

2.3.2.4 Skin Effect

Another phenomenon of the flow of eddy currents in a test object is the "skin effect", perhaps one of the most outstanding characteristics of eddy current flow. As eddy currents flow in a conducting material, the currents become concentrated near the surface of the material adjacent to the excitation coil. This effect increases with an increase in either the test operating frequency, test object conductivity, or magnetic permeability. As the depth below the surface is increased, the current amplitude decreases exponentially and the phase angle of the current becomes increasingly lagging.

The skin effect phenomenon may be explained in a number of ways. In one explanation, eddy currents flowing in a test object at a given depth are shown to produce magnetic fields at a greater depth which oppose the primary field, thus reducing its effect and causing a decrease in eddy current flow as depth increases. In another explanation, the skin effect is caused by the absorption of energy from an electromagnetic wave as it progresses into the test object.

The change of current density with depth, or skin effect, has also been described quantitatively by use of Maxwell's second equation, which relates current density to magnetic field intensity:

$$\nabla \times \mathbf{H} = \mathbf{J} \tag{18}$$

or

$$dH_z/dx = -J_y \tag{19}$$

Libby[25] derived the equation for H_z:

$$H_z = H_0 \exp[-((1+j)/\sqrt{2})\sqrt{\omega\mu\sigma}x] \tag{20}$$

Now substituting (20) into (19) gives:

$$J_y = -d/dx[H_0 \exp[-((1+j)/\sqrt{2})\sqrt{\omega\mu\sigma}x]] \tag{21}$$

$$J_y = (1+j)(\omega\mu\sigma/2)^{1/2} H_0 \exp[-(1+j)(\omega\mu\sigma/2)^{1/2}x] \tag{22}$$

The surface current density J_0 may be found by placing $x=0$ in (22):

$$J_0 = (1+j)(\omega\mu\sigma/2)^{1/2} H_0 \tag{23}$$

Combining (22) and (23) gives:

$$J_y = J_0 \exp[-(1+j)(\omega\mu\sigma/2)^{1/2}x] \qquad (24)$$

With this equation, the current density may be determined for any depth x from the surface of a test object. The value of x for which the exponential component is equal to unity is called the skin depth, standard depth of penetration, or depth of eddy current penetration under plane wave conditions. The standard depth or penetration is usually represented by the symbol δ, so that

$$(\omega\mu\sigma/2)^{1/2}\,\delta = 1 \qquad (25)$$

for the above statement.

The standard depth of penetration may also be defined as the depth at which the density of eddy currents is reduced to 1/e times its value at the surface. Equation (24) may be illustrated graphically, as in Figure 16a.

Solving for δ in (25), the standard depth of penetration equation may be found:

$$\delta = (2/\omega\mu\sigma)^{1/2} = (1/\pi f\mu\sigma)^{1/2} \qquad (26)$$

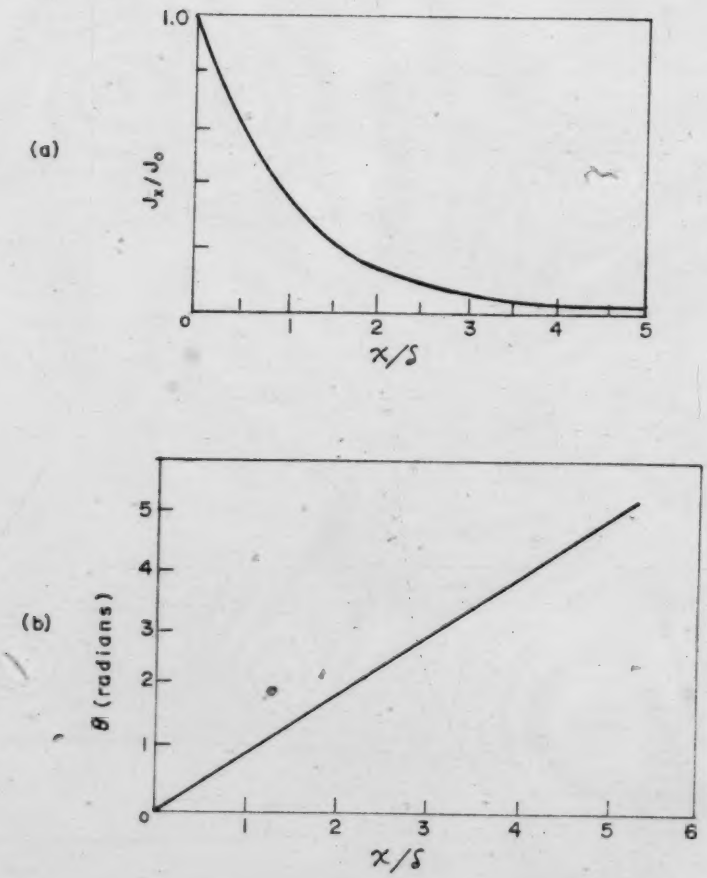

Figure 16. The skin effect: a)variation of eddy current density as a function of depth; b)variation of eddy current phase angle as a function of depth.

where, f= frequency
μ= magnetic permeability ($=4\pi x10^{-7}$ H/m for nonmagnetic materials)

For magnetic materials:

$$\mu=\mu_r\cdot\mu_o$$

where, μ_r= relative permeability
μ_o= $4\pi x10^{-7}$ H/m, the magnetic permeability of free space

The phase angle lag, using the phase angle of the current density at the surface as a reference angle, is given by:

$$\theta= x(\pi f\mu\sigma)^{1/2}= x/\delta \qquad (27)$$

where θ is the phase angle lag, in radians. Equation (27) is illustrated graphically in Figure 16b.

The standard depth of penetration is normally used if it is desired that eddy currents are to penetrate an upper layer, through a faying surface for example, to detect anomalies in a second layer. If, however, thickness variations of the part are not to influence the test, the effective depth of penetration is used. The effective depth is defined as the depth at which the eddy current density is reduced to 5% of its value at the surface and, hence, thickness effects are no longer noticed. The effective depth

is calculated as follows:

$$\delta_E = 2.6/(\pi f \mu \sigma)^{1/2}$$

or $$\delta_E = 2.6\delta \qquad (28)$$

The skin effect may be troublesome in applications where a large amount of penetration is desired. The skin effect may also be useful. By properly calibrating an eddy current instrument, it is possible to measure material thickness because of the varying reponse to thickness. Figure 17 illustrates the effect of changing material thickness on the impedance-plane diagram. As indicated by the curves, measurements of thickness by the eddy current method are more accurate on thin materials than on thick materials. The opposite is true of thickness measurements made by the ultrasonic nondestructive testing method; thus, the two methods complement each other here.

2.3.2.5 Lift-off and Fill Factors

When alternating current is applied to a probe inspection coil the inspection instrument will give some indication even if there is no conductive material in the vicinity of the coil, as shown in Figure 18. As the coil is moved closer to the material, the impedance will change until the probe makes contact with the material, as shown by the lift-off loci in Figure 18. At this point, the impedance

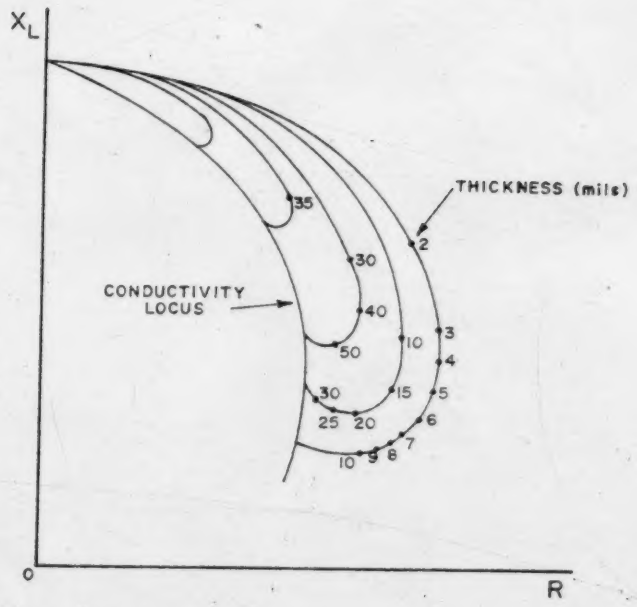

Figure 17. Typical material thickness loci.

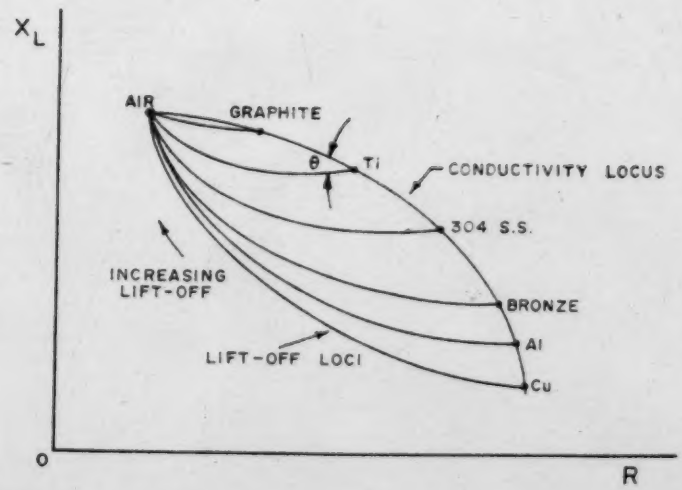

Figure 18. Lift-off loci on the impedance plane.

corresponds to the conductivity of the specimen. The change in indication with changes in the spacing between the coil and test object is known as "lift-off". Normally the changes along the lift-off loci are logarithmic, where the largest change in impedance occurs when the probe is near the test object.

The lift-off effect is so pronounced that small variations in spacing may mask the indications resulting from the conditions of primary interest (i.e., cracks, inclusions, etc.); consequently, it is usually necessary to maintain a constant spacing between the test object and inspection coil. The lift-off effect also causes difficulties when inspecting a complex shape. Although lift-off may be troublesome in many applications, it may also be useful. By utilizing the lift-off effect, the thickness of nonconductive coatings on metals, such as paint or anodized coatings, may be measured.

When an encircling inspection coil is used for eddy current testing, a condition comparable to lift-off exists and is known as "fill factor". Fill factor is the measure of how well the part being inspected fills the coil (i.e., the ratio of coil diameter to specimen diameter). As with lift-off, the fill factor is pronounced, making it necessary to maintain a constant fill factor to avoid masking of signals. Impedance changes which occur due to a change in fill factor are very similar to those which occur due to lift-off. Fill factor may be used as a rapid method for

monitoring variations in the outside diameter of rods and tubes.

2.3.2.6 Edge Effect

When a test coil is moved near the edge of a test object, the eddy currents become distorted, as they are unable to flow beyond the edge of the object. The distortion of eddy currents results in an indication known as "edge effect". This effect produces a response similar to the lift-off response, but unlike lift-off, little can be done to eliminate edge effect. The magnitude of the effect is very large, thus limiting inspection near the edges of a test object. A reduction in coil diameter may lessen the effect somewhat, but there are practical limits to the size of coil which may be used for a given application.

2.3.3 Impedance Concepts

It is immediately recognized, from the previous section, that the impedance-plane diagram is a useful tool in eddy current testing. The impedance-plane diagram may be used to monitor a number of test and test object conditions, including: electrical conductivity, magnetic permeability, specimen thickness, coating thickness and the presence of inclusions, voids or cracks. By utilizing the phase relations and amplitudes of the test responses obtained from such conditions, two or more of these conditions may be separated from one another or characterized. Hagemaier[24] presented a good overview of impedance-plane analyses, while

Förster[15,16] described, in detail, the effect of conductivity changes, thickness changes, lift-off and edge effect on the impedance-plane diagram in sections one, two and three of his articles. Hochschild[27] also presented a summary of eddy current testing by impedance analysis.

Figure 18 may be used as a simple illustration of lift-off versus conductivity on the impedance-plane diagram. This figure shows the change in separation angle θ between the conductivity locus and lift-off locus with a change in conductivity. High conductivity materials, such as copper, have a larger separation angle than lower conductivity materials, such as titanium. As a result, the lift-off and conductivity variables may be separated with greater ease when inspecting materials of high conductivity.

In all cases, it should be realized that frequency affects the impedance-plane diagram. Figure 19 illustrates the effect of test frequency on the conductivity and lift-off curves for nonmagnetic alloys. A change in frequency results in a nonlinear shift of the points along the conductivity locus. This phenomenon may be used advantageously, since it allows the conductivity points to be located for either optimum response or suppression. In a specific application, a frequency is chosen that causes the conductivity points for the variable to be measured to move in a substantially different direction from those points to be suppressed. Figures 19a, 19b and 19c show how the angle of separation between conductivity and lift-off may be

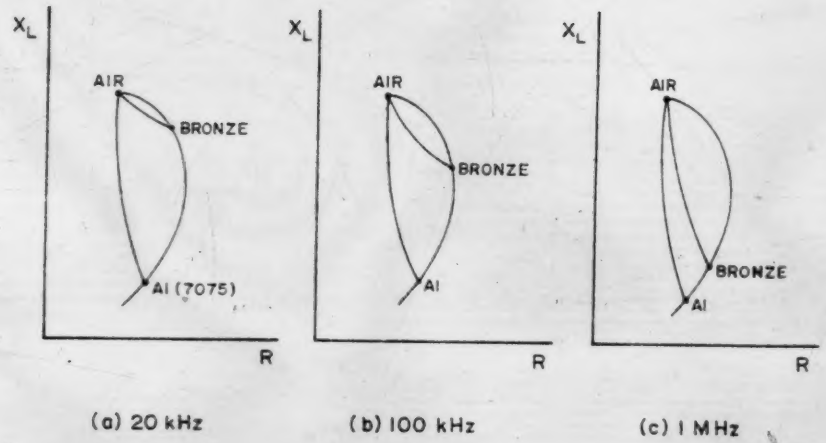

Figure 19. Frequency effects on the impedance plane.

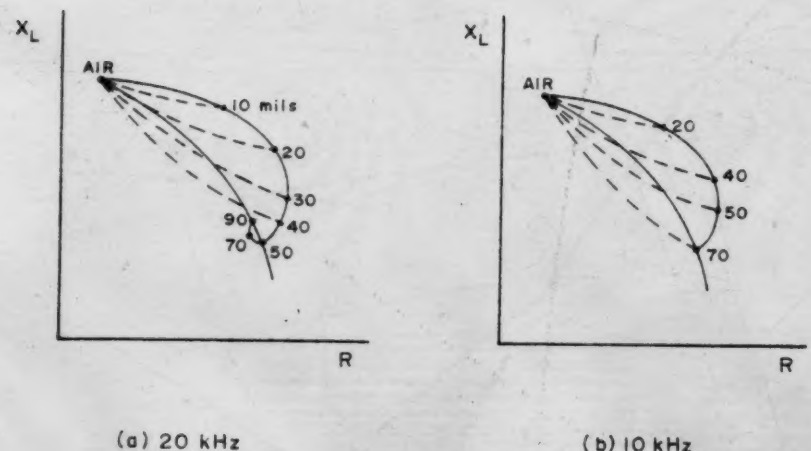

Figure 20. Metal thinning on the impedance plane.

increased by increasing the frequency. In general, for conductivity measurements and surface crack detection a frequency is chosen which places the material or conductivity point just below the knee on the conductivity curve. At this point a large separation angle exists between the lift-off and conductivity curves.

Metal thinning may also be analyzed using an impedance-plane diagram. Figure 20 illustrates the thickness curve for aluminum relative to the conductivity locus and lift-off loci. Using an operating frequency of 20 kHz or higher, the thickness locus cuts across the conductivity locus in two places. This occurs because the eddy currents are penetrating the specimen at a value of δ. At lower frequencies (10 kHz or lower) the loop in the thickness loci is less pronounced, since the depth of penetration (δ) is greater than at the higher frequencies. Because of the nonlinearity of the thickness points on the locus, measurements of thickness by the eddy current method are more accurate on thin materials than thick materials. Although more accurate measurements are obtained with thin materials, the angle of separation between the lift-off loci and thickness locus is less with thin materials; therefore, the lift-off should be maintained constant when testing thin materials to avoid misinterpretation of the results.

Figure 18 illustrates the lift-off effect when a conductive material is coated with a nonconductive material. Conductive coatings, on the other hand, result in a

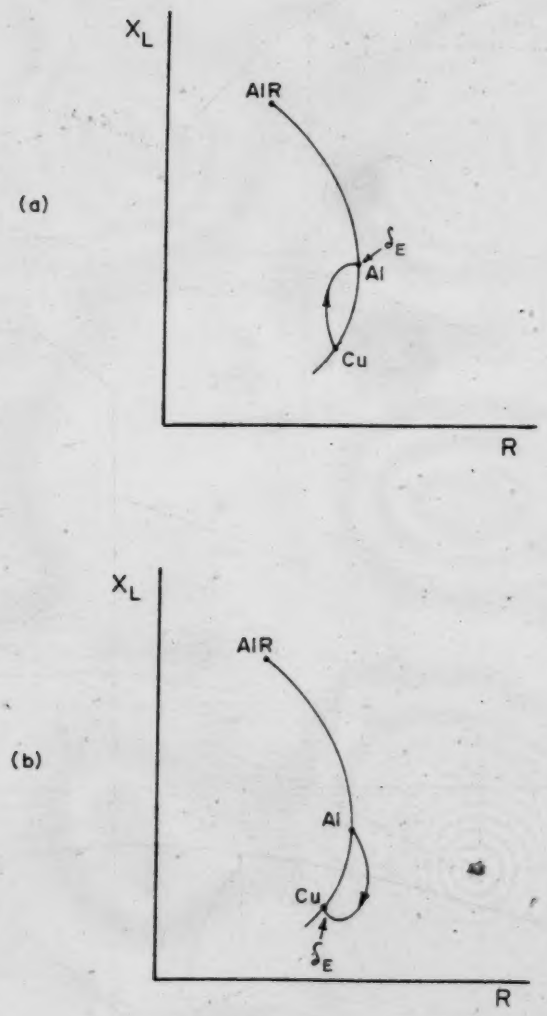

Figure 21. Coating thickness on the impedance plane: a)aluminum coating on thick copper plate; b)copper coating on thick aluminum plate.

different impedance-plane diagram. Figure 21a shows the impedance locus for a low conductivity coating on a high conductivity material. The movement of the test coil impedance is clockwise and approaches the point δ_ε on the conductivity locus corresponding to thick aluminum. The opposite is true when a low conductivity material is coated with a high conductivity material (Figure 21b). The movement of impedance with increasing thickness is not linear, rather the deflections for subsequent equal thickness changes become less as the thickness increases; thus, the measurement of plating thickness by the eddy current method is more accurate on thin materials. In general, the thickness loci of Figures 21a and 21b spiral with increasing curvature in a clockwise direction. The start of the spiral approximates a straight line, but as the thickness increases the spiral becomes more pronounced. The degree of spiraling and shape of the curve varies as the operating frequency is changed, therefore an operating frequency is selected to obtain the maximum response to thickness changes.

Perhaps the most frequent use of the eddy current inspection method is finding surface cracks in aircraft structures. The impedance-plane analysis technique is a useful tool in such testing. It allows for the separation of variables on the impedance plane. Figure 22 shows the crack response relative to the lift-off and conductivity loci for aluminum alloys. Such a test response allows for quick detection of cracks in aircraft parts.

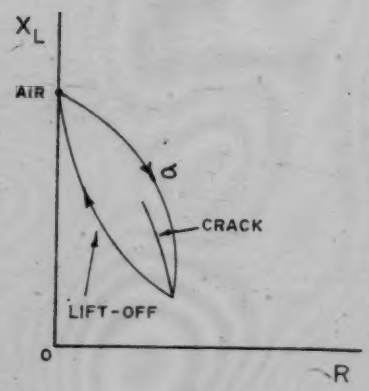

Figure 22. Cracks on the impedance plane.

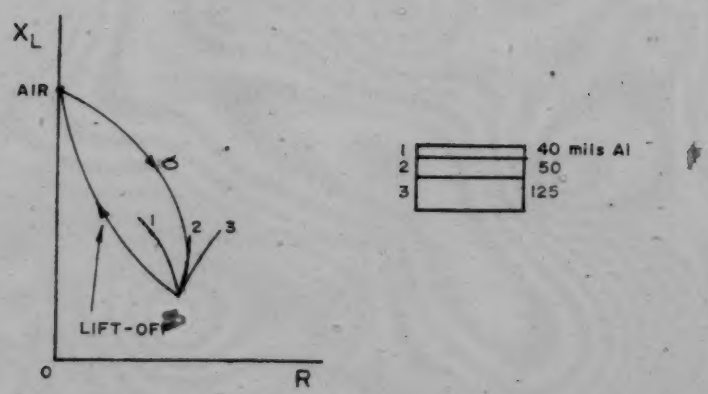

Figure 23. Direction of surface and subsurface cracks on the impedance plane.

Eddy current testing has also been used to detect subsurface cracks in aircraft structures using low-frequency techniques[33]. Hagemaier and Steinberg showed that subsurface cracks in aluminum up to 0.35" (8.9 mm) in thickness could be detected at 100 Hz and showed methods of determining the length of these cracks. No reports of using conventional eddy current techniques for inspection to greater depths have been published.

Figure 23 shows how through-thickness cracks in second- and third-layer aluminum structures appear on the impedance-plane diagram. The surface crack response runs approximately parallel to the lift-off locus, the second-layer crack response parallel to the conductivity locus and the third-layer crack response to the right of the conductivity locus. The shift in phase of the crack signals is associated with the skin effect and is to some degree dependent on the probe design, as will be shown in the experimental section of this thesis.

In each example, it was observed that linear material values did not necessarily produce linear responses on the impedance-plane diagram. Lift-off, edge effect and plating thickness changes produce logarithmic changes; metal thinning and material spacing or separation produce exponential changes; conductivity and permeability changes vary with test frequency in a nonlinear fashion.

In general, test responses may be improved by selecting the optimum operating frequency[24], by rotating the results

on the impedance plane and by increasing or decreasing the vertical and/or horizontal gains on the cathode ray tube used to display the test signal responses. The optimization of test coil responses is also dependent on the physical characteristics of the test coil. Smith and Dodd[34] describe a method of maximizing the lift-off effect by adjusting the physical dimensions of the test coil. Dodd, Deeds and Spoeri[35] describe some methods for optimizing flaw detection by changing the coil configuration and dimensions, as well as the operating frequency. Dodd, Deeds, et al.[36-38] have also presented some solutions for the test impedance functions for various test object conditions. They have also produced computer programs for the calculations used in these solutions.

The impedance-plane analysis technique is clearly a useful tool in eddy current nondestructive testing. It clearly delineates many of the test and test object conditions typical to the eddy current test, thus providing for better interpretation of test coil responses.

2.4 Survey Summary and Conclusions

The basic principles discussed in this section of the thesis provide the foundation for development in the field of eddy current nondestructive testing. It was shown that electromagnetic induction is one of the key principles of the eddy current test method and that the fundamental system variables which affect the induced emf include: 1)the test

object conductivity, 2)the test object permeability, 3)the skin effect, 4)lift-off and fill factors, 5)the edge effect and 6)the presence of test object flaws, such as cracks. It was also shown that the test coil operating frequency, test coil configuration and test coil size affect the induced emf and ultimately the test coil impedance.

Although it has been shown that eddy current impedance-plane analysis is a powerful means of evaluating a wide variety of material conditions, the separation of variables is not always simple. Unusual test object geometry or test system requirements may limit the ability to separate the test object variables using phase relations. As a result, special electronic circuitry and coil designs are used for special applications to maximize the response to, and separation of, test object variables. Regardless of the complexities involved, eddy current testing has become a common nondestructive testing technique. In particular, the eddy current testing method is used extensively in aircraft maintenance inspection and tubular goods inspection, particularly for the detection of surface and subsurface cracks.

To date, no work has been published on the use of conventional eddy current nondestructive testing techniques for the through-transmission inspection of thick sections. The subject of this project is the inspection of weld beads in 1/2" (12.7 mm) thick aluminum alloy plate using a low-frequency eddy current through-transmission testing

technique. Several limitations of conventional eddy current testing are encountered. The skin effect limits inspection at high frequencies, thus limiting the sensitivity of the test coil and separation of the test coil responses. The effect of lift-off is also a problem, as the crown profile of a weld bead varies along its length. Edge effects, a problem in most eddy current applications, are also prevalent.

The major goal of the following experimental studies was to overcome the adverse nature of these effects by coil design and/or optimization of the coil's response using electronic phase discrimination circuitry and filters. Characterization of the test coil responses using impedance-plane analyses was another goal in this project. The design, construction and operation of the eddy current system (including the test coils) will be explored in the remainder of this thesis.

3. Experimental Procedure

3.1 Materials

Aluminum alloys were chosen as the test object material for this project. Aluminum was chosen, since the depth of penetration of eddy currents is high in aluminum and magnetic permeability effects are not present. As a result, it was possible to keep the number of operating variables to a minimum. For example, if steels were used then the penetration of eddy currents would be low, limiting the inspection to thin sheets, rather than plates. In addition, the effects of magnetic permeability would complicate impedance-plane analyses.

Two types of aluminum alloys were used: type 5083 in the as-received (cold-rolled) condition and 6061 with a T6 temper. Two alloys were chosen so that conductivity changes on the impedance plane could be analyzed. In all cases, 1/2"Tx3"Wx12"L (12.7mm x76.2mm x305mm) plates of aluminum were used to produce the test objects. The final dimensions of the test object were governed by the size of the probe, since edge effects were undesirable. The filler wire used for all the welds was type 5356.

3.2 Specimen Preparation

To provide sufficient clearance between the probe and edge of the test object two plates of aluminum were welded together, resulting in the final dimensions of

1/2"Tx6"Wx12"L (12.7mm x152mm x305mm) for each test object. In all, three test objects were constructed. In each case, the plates were restrained to provide minimal distortion of the weldment.

In the first case, two 5083 plates were welded together using the gas metal-arc welding process (GMAW). A square groove butt joint preparation with no root opening was used. By running a single partially penetrating weld bead over the groove on each side of the plate, a test object containing an incomplete penetration flaw (IP) was produced. To complete the preparation, the crown of the weld bead was removed from both sides of the plate for half the length of the weld by milling. The weld specimen is illustrated in Figure 24 (specimen 1).

In the second case, two 5083 plates were welded together using the gas tungsten-arc welding process (GTAW) and a double-V-groove butt joint preparation with no root opening. The groove angle was 90° and the weld was made using a multi-pass technique. With one side of the plate welded, holes of varying diameters were drilled into the weld metal and covered by subsequent welds on the opposite side of the plate. In this manner, voids resembling porosity were left near the center of the weld bead. To simulate large isolated pores (LIP) a 0.22" (5.6 mm) diameter drill bit was used. To simulate cluster porosity (CP) both a 1/16" (1.6 mm) diameter and 5/64" (2.0 mm) diameter drill bit were used. The depths of all the holes were approximately 1/4"

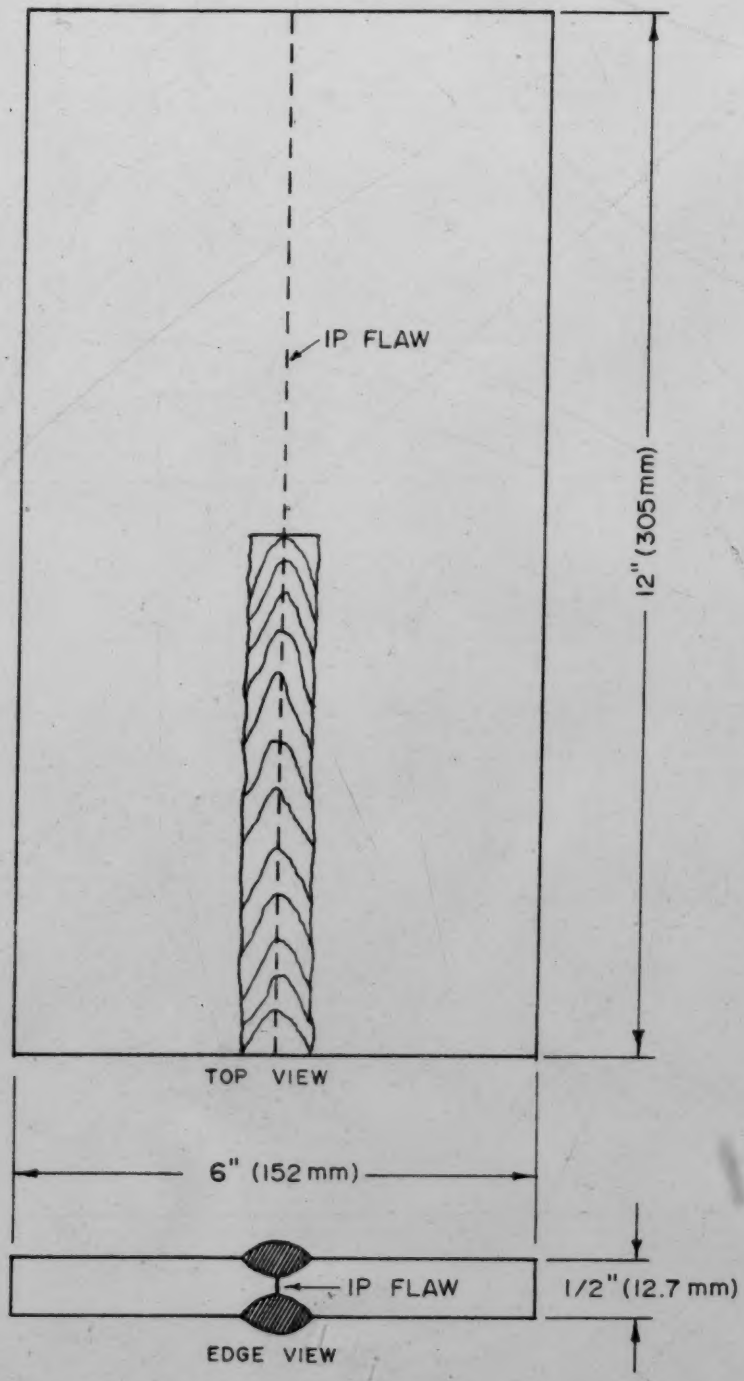

Figure 24. Specimen 1 - Artificially produced incomplete penetration flaw.

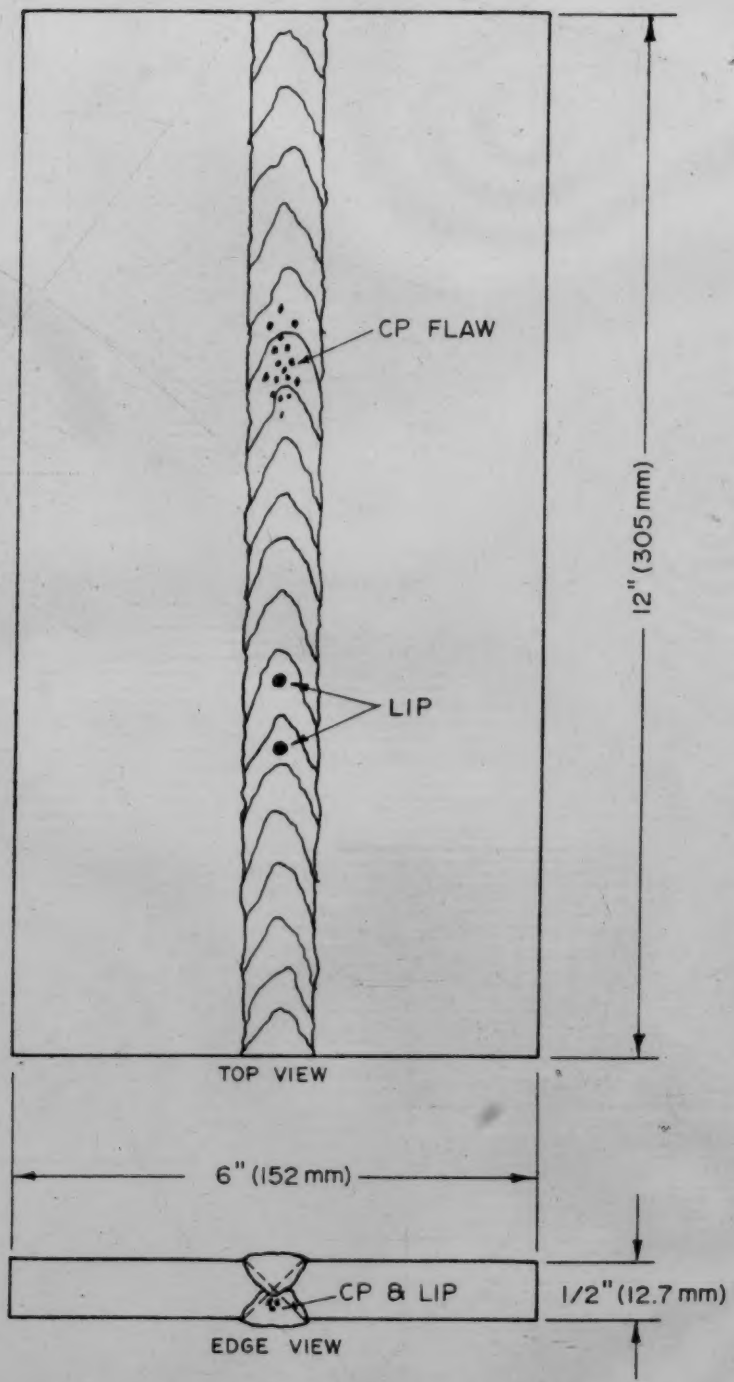

Figure 25. Specimen 2 - Artificially produced porosity flaws.

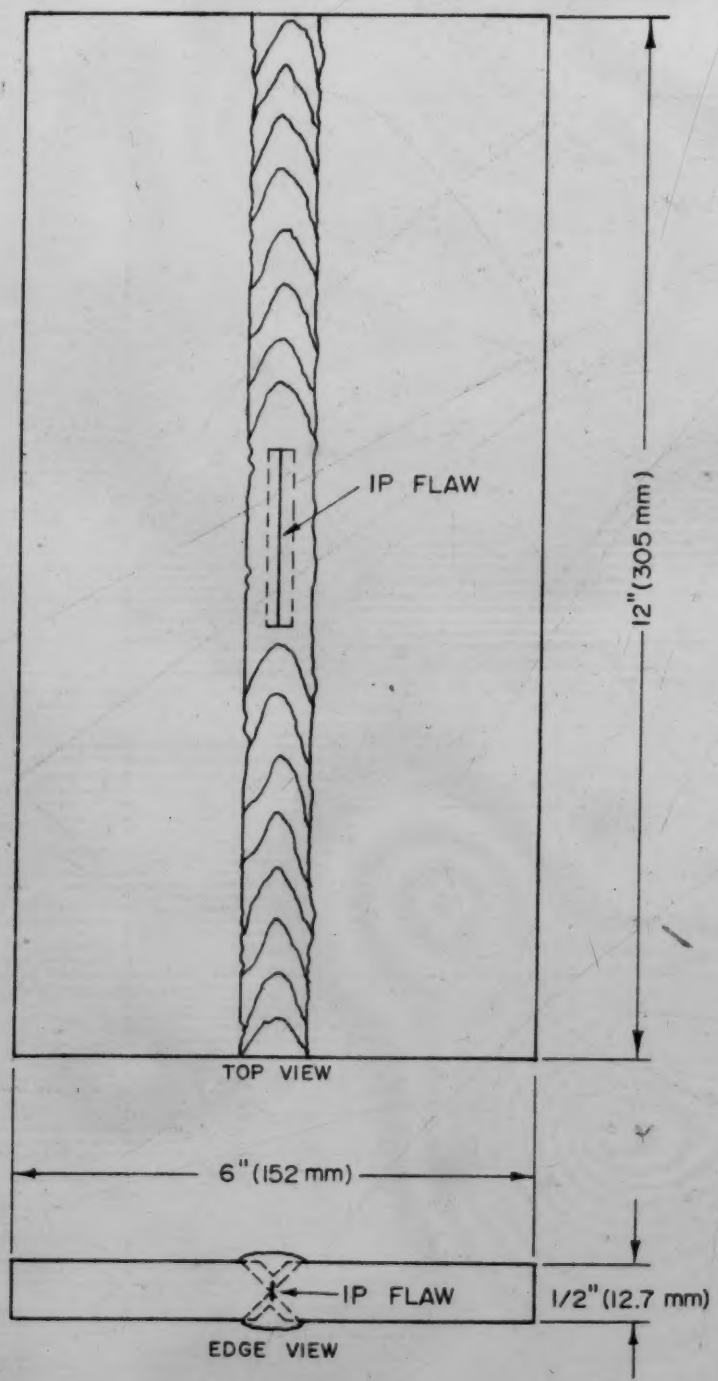

Figure 26. Specimen 3 - Artificially produced incomplete penetration flaw.

(6.35 mm). The weld specimen is illustrated in Figure 25 (specimen 2).

In the third case, two 6061 plates were welded together in a manner similar to that described for specimen 2, except that the central portion of the plate did not have a 1/4" (6.35 mm) V-preparation. In this case, a 1/8" (3.2 mm) V-preparation was used for the central 2" (50.8 mm) of the weldment. In this manner, a narrow gap, approximately 1/4" (6.35 mm) deep, was obtained in the central portion of the weldment, simulating an incomplete penetration flaw. The weld specimen is illustrated in Figure 26 (specimen 3).

3.3 Verification Tests

3.3.1 Radiographic Nondestructive Tests

To support the results obtained by these studies, an alternate means of examining the test specimens was necessary. The first and most ideal verification test for this project was the radiographic nondestructive inspection technique. It was most ideal, since the actual image of the flaw is recorded on photographic film, thus resulting in less disputable flaw indications.

To obtain the film records, a conventional X-ray tube was used as the source of radiation. X-rays were chosen over gamma rays, since they provide greater resolution when examining 1/2" (12.7 mm) thick aluminum plates. The resolution obtained from gamma ray sources is poor, since

the intensity of gamma radiation is far too great for radiographing such thin sections of aluminum. X-ray sources also provide more flexibility, since the penetration of X-rays can be varied by adjusting the tube voltage.

Test specimen 1 was radiographed to an image quality level of 2-4T, specimen 2 to a level of 2-4T and specimen 3 to a level of 5-1T. These image quality levels correspond to an equivalent sensitivity of approximately 3%. Equivalent sensitivity is based on the visibility of the 2T hole in an ASTM or ASME plaque-type penetrameter. Positive prints were made from the film records.

3.3.2 Ultrasonic Nondestructive Tests

The second verification test used in this project was the ultrasonic nondestructive inspection technique. Ultrasonic tests were performed to determine the depth of the incomplete penetration flaws in specimens 1 and 3. To perform the tests, a Sonatest (Model UFD.1) ultrasonic flaw detector was used in conjunction with a 60° aluminum angle probe. The sensitivity of the instrument was adjusted by monitoring reflections off a 0.060" (1.5 mm) diameter hole drilled in each plate. Scanning was done manually, using methods prescribed for scanning weld beads in flat plate.

3.4 The Eddy Current Test System

3.4.1 Basic Test System Configuration

The basic eddy current test system, as illustrated by the general line diagram in Figure 27, consists of : 1)an inspection coil or set of coils, 2)a test object placed within or adjacent to the test coil, 3)an a.c. function generator, 4)amplification circuitry, 5)detector or demodulation circuitry, 6)filtering circuitry, 7)an output display in the form of an oscilloscope, chart recorder or meter and 8)material handling equipment. The test system is generally divided into seven main operational functions which include: 1)coil excitation, 2)signal modulation, 3)signal preparation, 4)signal demodulation, 5)signal analysis, 6)signal display and 7)test object handling. The functions are related to one another, as illustrated in Figure 28.

The signal generator supplies the excitation current to the test coils. The test coils are labeled "test coil assembly" since a wide variety of test coil configurations are available for eddy current testing. The signal generator may be a single-frequency sinusoidal (a.c.) generator with power amplifier, a multiple sinusoidal waveform generator with power amplifiers, or a pulse generator with power amplifier. Normally a variable frequency a.c. generator with power amplifier is used for general purpose eddy current testing. Signal modulation occurs as a result of the

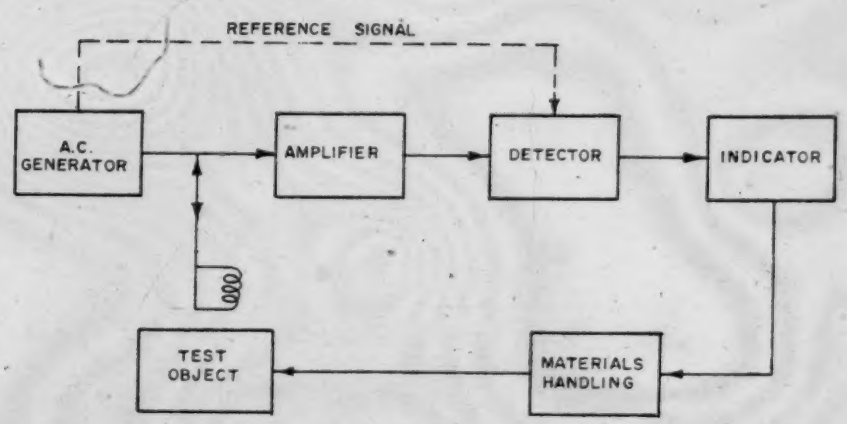

Figure 27. General line diagram for an eddy current test system.

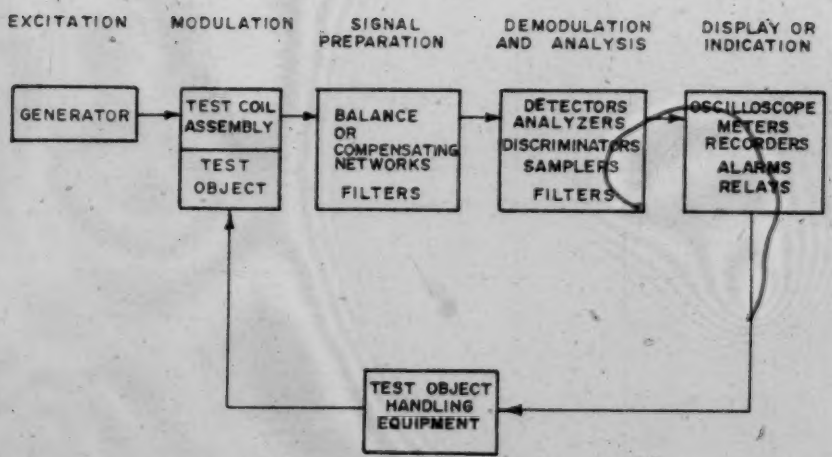

Figure 28. Operational functions of the eddy current test system.

interaction between the electromagnetic field of the test coil assembly and the test object.

The signal preparation portion of the test system consists of circuits which alter the signal output of the test coil assembly before applying the signal to the demodulation and analysis functions. These circuits consist of a.c. compensating or balancing networks which subtract a steady a.c. component from the input signal so that the amplifiers do not need as large a dynamic range as otherwise would be necessary. Filters are included at this stage to improve the signal-to-noise ratio. Amplifiers are used in this stage to raise the signal to the desired level for the demodulation and analysis process.

The demodulation and analysis stage comprises of a detector and an analyzer. The detector is usually either a simple amplitude detector or an amplitude-phase detector. If an amplitude-phase detector (often termed phase selective detector) is used, a reference signal must be furnished by the generator, as shown by the dashed line in Figure 27. Sampling circuits and discriminators may be included at this stage, as well as various types of summing and comparison circuits. Filters may also be included at this stage for filtering the demodulated signal to accentuate or discriminate against certain characteristics of the signal.

The final display of results is obtained at the display or indication stage. The signal may be displayed by use of meters, recorders, cathode-ray tubes, light alarms, audible

alarms, relay outputs, or automatic reject equipment.

Test object handling demands may vary depending on the nature of the test. The equipment required for test object handling may be either very simple or very complicated in mechanical design. In some tests, the test coil assembly is designed so that it is positioned and held manually. In this case the test object handling demands are minimal. In other cases, mechanical devices are used to feed the test object past the test coil assembly so that the tests can be made rapidly under uniform conditions. Such tests normally require complete automation, thus require a more complicated mechanical design.

3.4.2 Amplitude-Phase Detector System

The single most common detector system used in eddy current testing equipment is the amplitude-phase type, which provides both amplitude discrimination and phase discrimination of the test coil output signals. Since both amplitude and phase are monitored, the output display is in the form of an impedance-plane diagram making this type of system a logical choice for multipurpose use. Such a detector system was used in this research project.

The eddy current test instrument used for this project is shown in Plate 1. The instrument used, manufactured by the Dr. Förster Institute, was the Defectomat (Model F2.825.03). A block diagram for this system is shown in Figure 29.

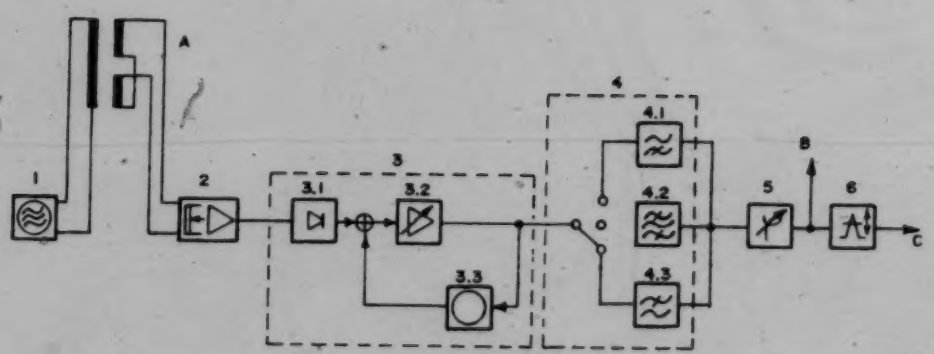

1 SIGNAL GENERATION
2 INPUT STAGE
3 DEMODULATOR
3.1 PHASE SELECTIVE RECTIFIER
3.2 SENSITIVITY CHANGEOVER
3.3 COMPENSATION
4 SPEED MATCHING
4.1 HIGH-PASS FILTER
4.2 BAND-PASS FILTER
4.3 LOW-PASS FILTER
5 PHASE ADJUSTER
6 ANALYSIS
A SIGNAL TRANSMITTER
B DATA OUTPUT
C EQUIPMENT CONTROL

Figure 29. Block diagram for the Defectomat system.

Plate 1. The Defectomat (Model F2.825.03).

The signal generator, referred to as the transmitter in Förster literature, supplies the connected test coil assembly with the excitation current which may be preselected over a wide range of frequencies. The frequency changeover switch permits reproducible frequency settings between 100 Hz and 1 MHz in 1% steps of the adjusted exponent.

The voltage produced in the coil assembly is called the carrier voltage. The amplitude and phase of the carrier voltage is modulated by the data of the signal produced by an inhomogeneity in the test object, as described in the theoretical section of this thesis. The input stage or receiver section accepts the carrier voltage and amplifies it. Amplification is adjustable by means of a test coil level control. This control permits adjustment of the level between 0 and -24 dB in 6 dB increments.

The heart of the eddy current testing instrument is the demodulation and analysis stage. The amplitude-phase detector used in the Defectomat allows for use of the impedance-plane or phase discrimination technique to discriminate against unwanted test variables. Demodulation is accomplished by phase-selective rectification. A sensitivity changeover and compensation control is also included at this stage. The sensitivity changeover control permits changes in the amplification level between 0 and 69.5 dB in 0.5 dB increments. A compensating or nulling circuit is provided to compensate for excessively high input

signals which would normally exceed the dynamic range of the display instrument. In this case, the voltage components representing the inductive reactance and resistance are automatically nulled or zeroed by this device. The circuitry used for the nulling is essentially an advanced a.c. bridge design.

After demodulating and amplifying the carrier voltage, the X and Y components of the signal are fed into a series of filters. Three filter modes are available for testing. A low pass filter is selected for purely static signal displays, a band pass filter is selected for scanning at constant speeds and a high pass filter is selected for scanning at variable speeds. In each case, a filter frequency control is used to select the relevant limit and center frequencies.

Before passing to the output display the conditioned signal is routed through a phase rotating device where the position of the complex output signal may be rotated through 360° in 10° steps. This device enables the phase position of any desired signal to be rotated to the most favourable direction for evaluation. At this stage, the signal is also prepared for display and recording.

At this point, the signal is ready to be displayed. The test system is equipped with an X-Y storage oscilloscope, digital voltmeter, strip chart recorder for slow changing test signals and analog outputs for connecting external signal recording and processing devices. The full scale

output of all these devices is ±1V. The oscilloscope enables the operator to evaluate the data using impedance-plane analyses, while the chart recorder allows for modulation analyses. During modulation analysis the X,Y or vector sum voltage output is recorded on a strip chart which is synchronized to the speed of the mechanism handling the probe assembly or test object.

In addition to the above, the test signals may be analyzed using two adjustable trigger thresholds equipped with signal lamps. Three methods of evaluating the test signals exist. These methods are illustrated in Figure 30. The low flaw threshold *A* can be adjusted between 10 and 100% of the full CRT screen, which represents ±1V, in 10% steps. The flaw threshold *B* can be adjusted in the same manner. If the signal exceeds the preset trigger thresholds (i.e., the cross-hatched area in each illustration) a signal is given on the indicating lamp. In the case of the sector-amplitude method, the evaluation sector can be varied from ±10° to ±80° in 10° steps. Using any of these methods, two test variables may be monitored at the same time, although the sector-amplitude method provides more flexibility than the other two methods.

3.4.3 Test Coil Assembly Handling/C-scan Equipment

The test object handling demands for this project were minimal. The aluminum plates remained stationary while the probe assembly was moved along the length of the weld bead.

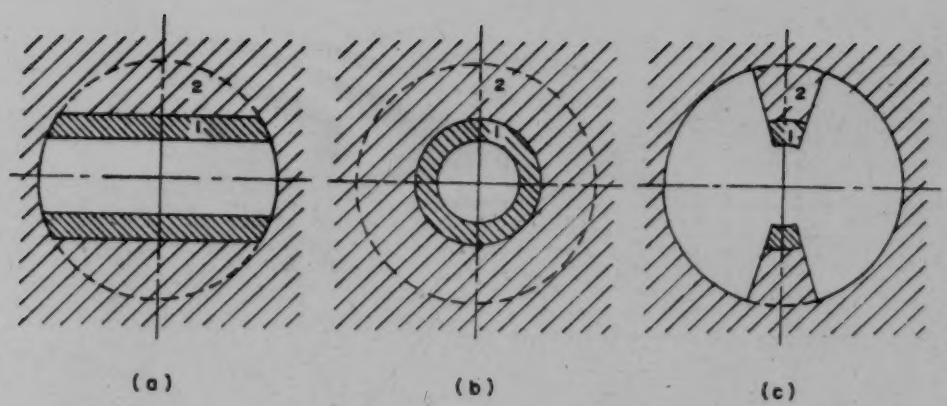

Figure 30. Evaluating monitors: a)Y-component evaluation; b)amplitude evaluation; c)sector-amplitude evaluation.

The equipment used to move the test coil assembly was elaborate; a system normally used for ultrasonic immersion C-scans. Plate 2 shows the overall C-scan system, consisting of (from left to right): 1)a mechanical X-Y scanner assembly supported by an acrylic plastic tank (Techno Scientific Inc.), 2)an X-Y chart recorder (Hewlett Packard, Model 7041A) and 3)power supply/microcomputer controller/X-Y recorder interface (Techno Scientific Inc.).

The X-Y scanner provides 18" (457 mm) of travel along the Y-axis and 16" (406 mm) along the X-axis and is equipped with a scanning head which allows for ±14° of rotation in the Y-Z plane and ±20° in the X-Z plane. The X and Y movements of the scanning head, along a preprogrammed zig-zag pattern, are microcomputer controlled. The scanning speed (up to 0.5"/s or 12.7 mm/s), length of scan and number of scans are set by hexadecimal programming of the controller. Manual control of the scanning head is also possible.

The X-Y recorder interface and X-Y chart recorder provide a means of obtaining C-scans. By adjusting the threshold on the interface, the chart recorder pen is made to either lift or drop if the analog signal input exceeds the preset threshold. The X-Y interface also provides synchronization of the X and Y movements of both the chart recorder and X-Y scanner. By properly adjusting the controls, flaws detected by ultrasonic or eddy current scans are plotted on the X-Y chart recorder in map form. The

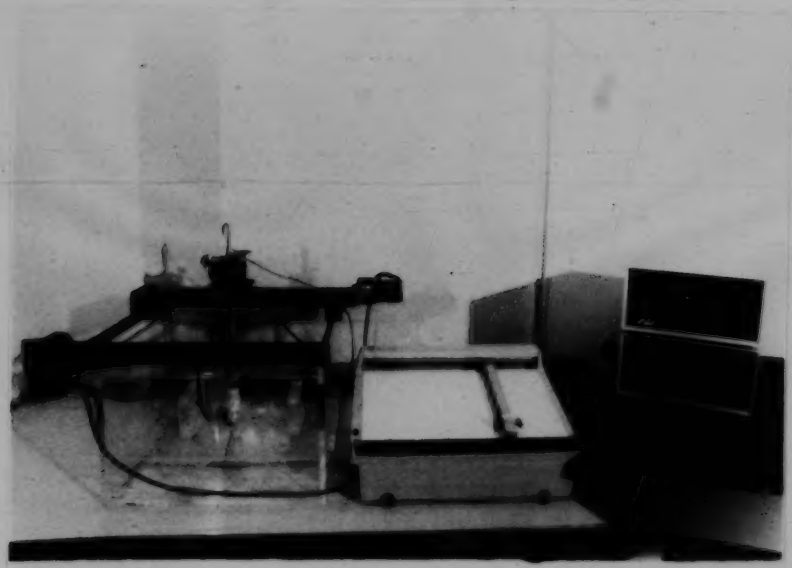

Plate 2. Test coil assembly handling/C-scan equipment.

recorder output is actually an outline of the flaw, by line shading or, alternatively, by the absence of line shading. Such a scan is commonly referred to as a C-scan.

To minimize the possibility of any interferences to the magnetic field produced by the probes, the probes were mounted to the scanning head via an acrylic plastic holder, as shown in Plate 3. The holder allows for 5" (127 mm) separation of the excitation and sensing coils and keeps the coils in constant alignment. Plate 4 shows the probe assembly scanning along the length of a weld bead.

3.4.4 Test Coil Configurations

To complete the eddy current test system, the test coil assembly must be included. The importance of the test coil assembly cannot be overstated. The test coil assembly is the link between the eddy current test instrument and the test object. Its design is a major factor in signal modulation and, ultimately, in the performance of the eddy current test system.

The orientation of the test coil assembly is also important, since it determines, to a large extent, the direction of flow of the eddy currents within the test object. It is essential that the flow of eddy currents be kept perpendicular to the flaw to obtain a maximum response from the flaw. If the flow is parallel to the flaw there will be little or no distortion of the currents; hence, very little response is obtained from the flaw. As a consequence,

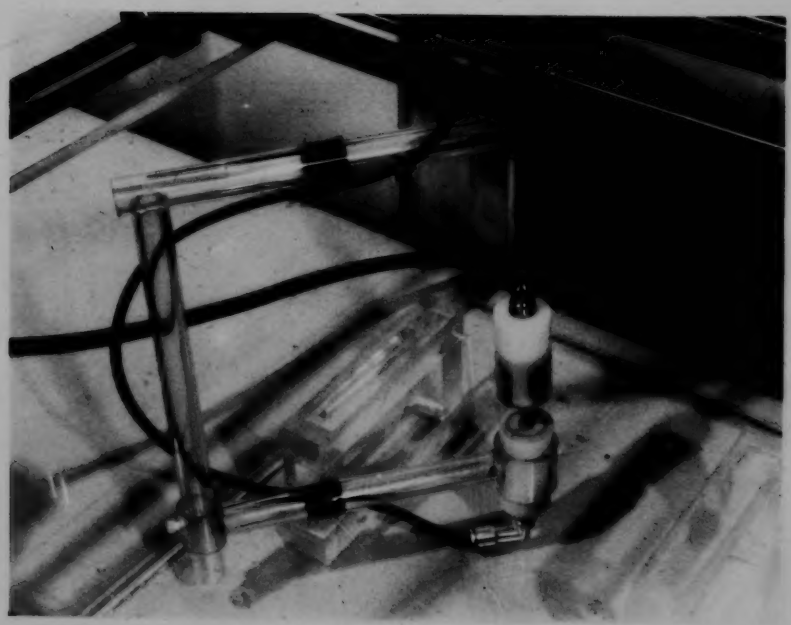

Plate 3. Probe assembly mount.

Plate 4. Horizontal scanning of a weld bead.

a large number of coil configurations are available for a variety of uses.

Among the large variety of testing coils employed in eddy current testing, three main prototypes exist. These are illustrated in Figure 31. Figure 31a illustrates an encircling coil used for testing bars and tubes. Figure 31b illustrates an inside coil used for inspecting the inside of tubes and Figure 31c a probe coil used for inspecting sheet, plate or surfaces of test objects. These coils are represented as single windings; however, it is more common to find double coil configurations, where one winding is used for transmission (i.e., the excitation winding) and the other for reception of the modulated signal (i.e., the sensing winding). Such an arrangment is shown in Figure 32. In this case, the coil monitors the test object without comparison and, therefore, is called an absolute coil. Signals are obtained from the sensing or secondary coil.

Coils may also be wound in a differential arrangement, as shown in Figure 33a. In such a configuration, the test object is compared with a standard specimen or, in the case of Figure 33b, comparison is made between two different sections of the same test object (i.e., a self-comparison type of configuration). The advantage of using a self-comparison differential arrangement is that slowly changing signals will be discriminated against, whereas short localized cracks or other abrupt changes in the specimen may be readily detected. In each case, a flaw or

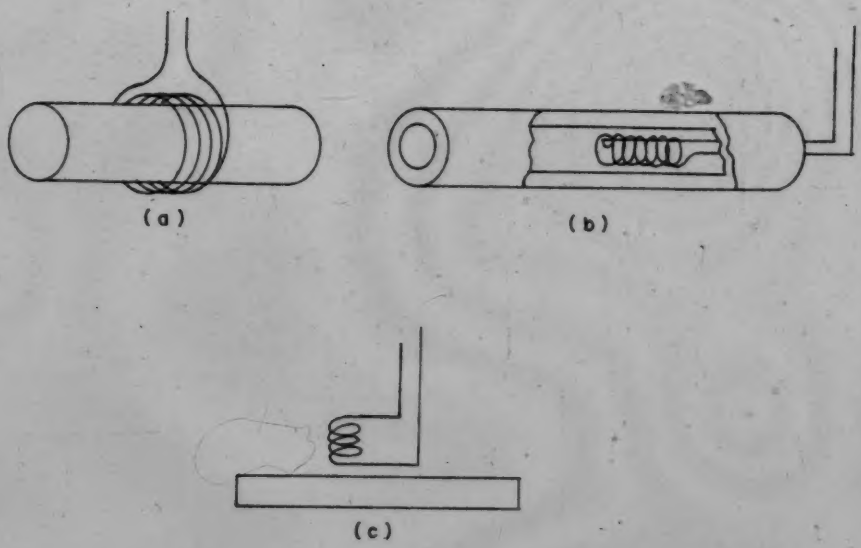

Figure 31. Prototype eddy current coils: a)encircling coil; b)inside coil; c)probe coil.

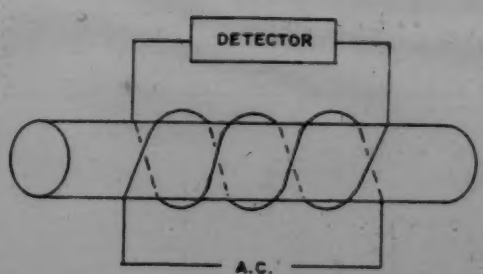

Figure 32. Double coil configuration.

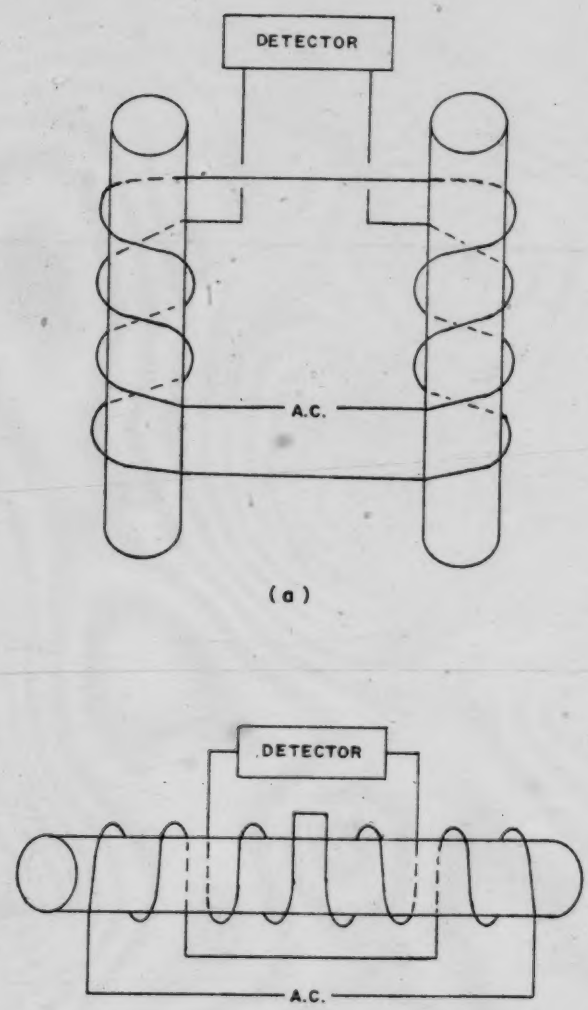

Figure 33. Differential eddy current coils: a)standard-comparison arrangement; b)self-comparison arrangement.

sudden change in conductivity or permeability will cause an imbalance in the bridge circuitry, thus producing an indication on the indicating device.

The test coil assemblies used in this project were a hybrid type of probe configuration. Rather than place the excitation and sensing coils adjacent to each other, the coils were separated from one another so that they could be placed on opposite sides of the aluminum plate (i.e., a through-transmission arrangement). The coils are illustrated in Figures 34-37. Exact coil design details are proprietary'. The illustrations are given for comparison purposes only.

In this study, only one sensing coil was used in conjunction with three different excitation coils. The sensing coil's diameter, as shown in Figure 34, was made small to provide good sensitivity to small flaws (i.e., good resolution). A differential self-comparison arrangement was established within the sensing coil by winding two small coils in opposition and adjacent to one another. In general, the excitation coils were designed to provide maximum penetration. In some cases the coils were wound on special ferrite cores to increase the magnetic flux, thus improve the penetration characteristic of the probe. The shape and size of the ferrite cores were also altered to "shape" the magnetic field, thus improve the sensitivity and resolution

---

'For more information on coil designs, contact Mr. S. DeWalle of *ANDEC*, 18 Canso Road, Rexdale, Ontario, M9W 4L8, ph.: (416)243-3456.

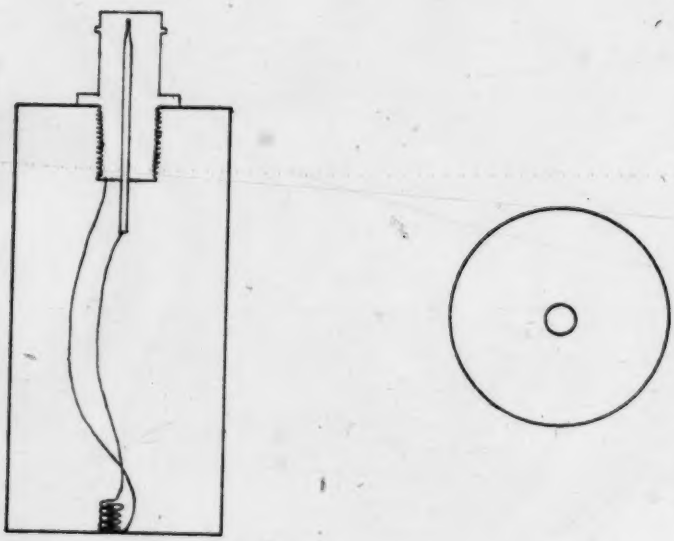

Figure 34. Through-transmission sensing coil.

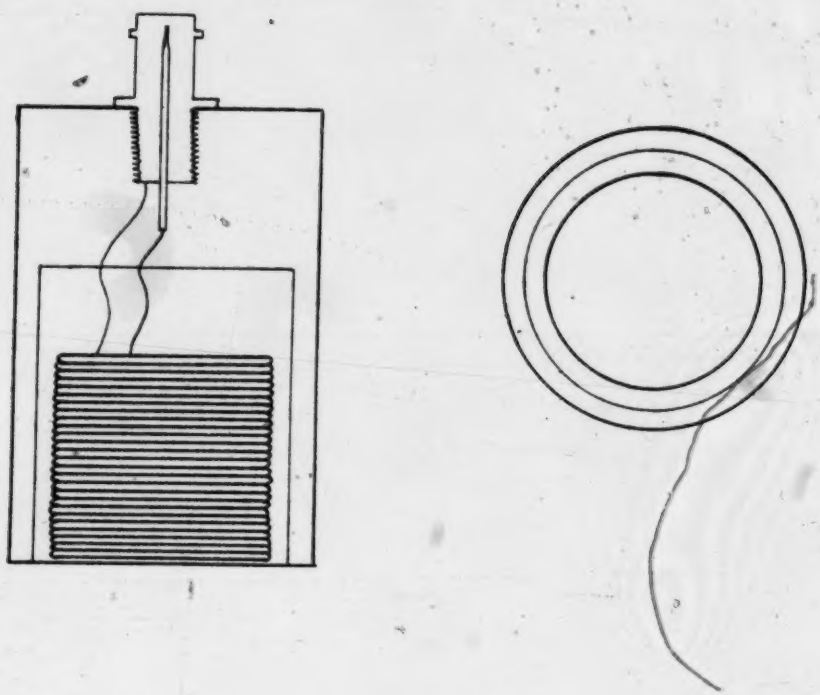

Figure 35. Probe *A* - excitation coil.

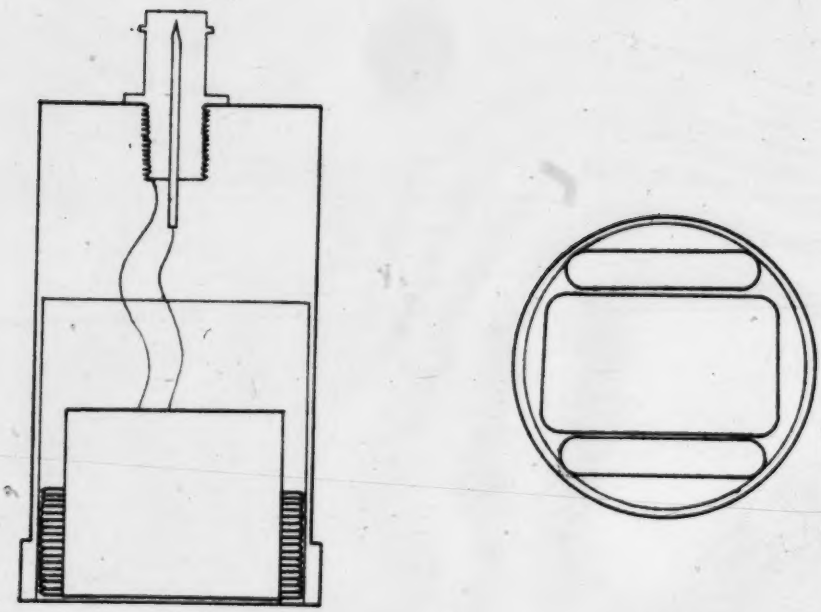

Figure 36. Probe *B* - excitation coil.

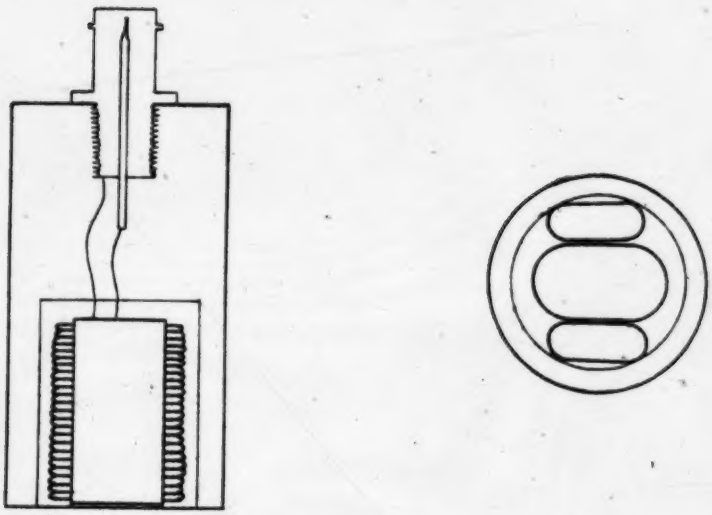

Figure 37. Probe C - excitation coil.

to flaws. Shields were also provided to decrease the noise from stray fields and/or provide increased sensitivity. The cables connecting the probes to the testing instrument were also well shielded to avoid problems with stray fields. Figures 35, 36 and 37 roughly show the shield and ferrite core configurations for probes *A*, *B* and *C*, respectively.

3.5 Test System Operation

3.5.1 Initial Probe Studies

Since the test coils were such an important component of the eddy current test system, tests were performed to evaluate probe performance under fixed conditions. The conditions of the test (i.e., instrument sensitivity, filtering, frequency, etc.) were held constant in order to provide a basis for probe design.

To conduct the initial studies a flat, flawless 1/2" (12.7 mm) thick plate of 6061 aluminum was placed between the excitation probe and sensing probe. Unlike normal through-transmission scanning, the sensing probe was left stationary, 1/4" (6.35 mm) below the surface of the plate and the excitation probes were scanned, one at a time, 1/4" (6.35 mm) above the surface of the plate. The scanning rate was set at 0.2"/s (5.1 mm/s). In this manner, the magnetic field of each excitation probe was monitored as a function of the change in amplitude of the output signal to evaluate the penetration characteristics of the excitation probes.

When performing these scans the frequency was maintained at 100 Hz for each probe. In each case, the test coil level was set at 0 dB, the sensitivity at 65.0 dB and the filter control was positioned at 3 in the low pass mode. The phase control was adjusted to obtain maximum deflection in the Y-axis direction. The phase angle was set at 80° for probe *A*, 70° for probe *B* and 250° for probe *C*. The Y-axis amplitude readings were continuously recorded using the X-Y chart recorder.

To assess each probe's sensitivity to flaws, specimen 1 was scanned using the through-transmission technique. The separation and alignment of the probes was held constant by the acrylic plastic holder. The separation of the probes was adjusted to provide 1/8" (3.2 mm) clearance between the probes and the plate. The scanning rate was fixed at 0.2"/s (5.1 mm/s). Scans were made across the machined surface of the plate using frequencies between 100 and 1900 Hz. The test coil level was set at 0 dB, the sensitivity at 65.0 dB and filter control was positioned at 3 in the low pass mode. The phase control was adjusted to obtain lift-off indications along the horizontal axis for the initial frequency. In the same manner, the unmachined portion of the plate was scanned across the weld bead to investigate lift-off effects. All indications were photographed from the CRT display of the X-Y storage oscilloscope.

3.5.2 Impedance-Plane Analyses

Inspection of the aluminum plates (specimens 2 and 3) was accomplished by the impedance-plane analysis technique. Scanning was performed using the through-transmission scanning technique. The distance between the probe and plate was adjusted to provide enough clearance for the weld bead crowns, where the nominal distance between the weld bead crown and the probes was held at 1/8" (3.2 mm). The weld beads were scanned longitudinally at 0.2"/s (5.1 mm/s). The frequencies used for the analyses ranged between 100 and 1700 Hz. In each case, the test coil level was set at 0 dB, the sensitivity at 65.0 dB and the filter control was positioned at 3 in the low pass mode. In most cases, the phase control was adjusted to obtain lift-off indications along the horizontal axis for the initial frequency. All scans were recorded by photographing the CRT display of the X-Y storage oscilloscope.

4. Test Results and Discussion

4.1 Verification Test Results

Radiographs of specimens 1-3 were obtained to : 1)confirm the presence of the artificially produced flaws,. 2)locate the flaws and 3)determine the width of the flaws. Positive prints of the radiographs are shown, in reduced form, in Plates 5, 6 and 9. True size prints of the flaws in specimens 2 and 3 are shown in Plates 7, 8 and 10.

The incomplete penetration (IP) flaw in specimen 1 (Plate 5) appears as a dim white line along the full length of the weld with only a small amount of gap closure in the central portion of the weld. The IP flaw closed up near the center of the weld due to shrinkage distortion after welding. This portion of the weld was not used for the subsequent eddy current tests. The radiograph distinctly shows the machined and unmachined portions of the plate, as described in section 3.2. The average width of the IP flaw, as estimated from the radiograph, was approximately 0.016" (0.41 mm). The average depth of the IP flaw, as determined by ultrasonic testing, was approximately 0.095" (2.4 mm).

The cluster porosity (CP) in specimen 2 appears on the top half of Plate 6 as a cluster of white dots. The diameter of the CP, as estimated from the true size print (Plate 7), range from 0.055" (1.4 mm) to 0.070" (1.8 mm). The large isolated pores (LIP) appear on the bottom half of Plate 6 as two large white dots. The diameter of the large pores, as

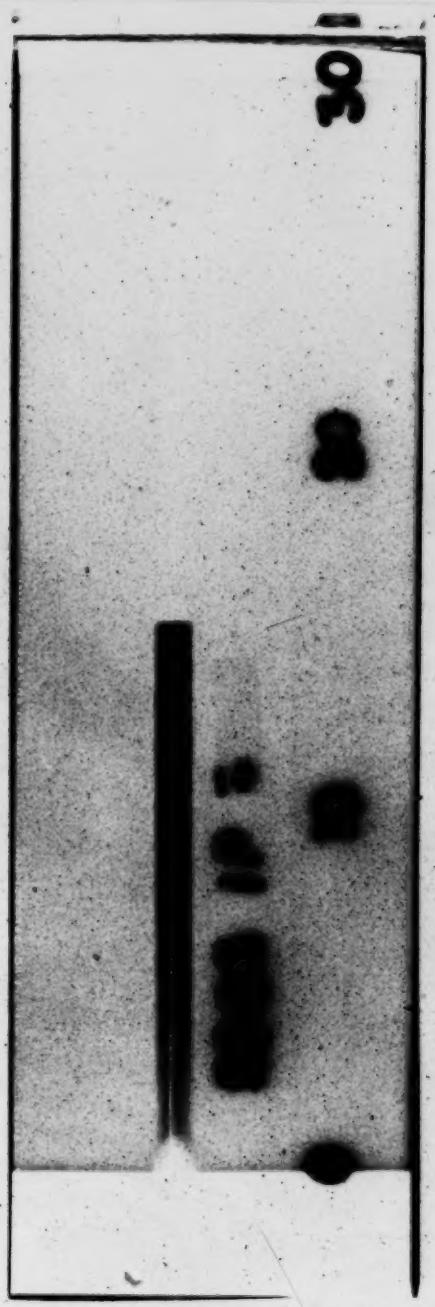

Plate 5. Radiograph of specimen 1 - IP flaw (reduced size).

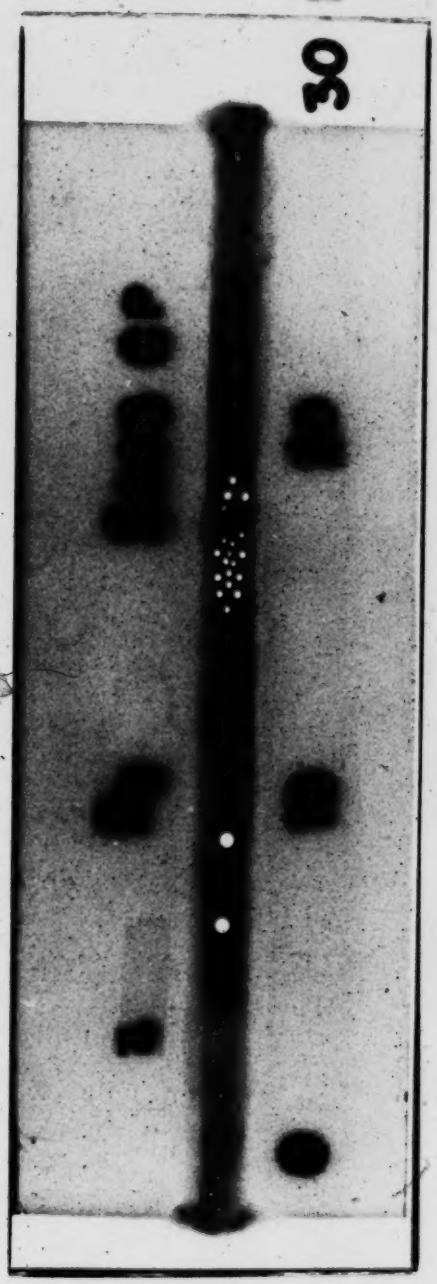

Plate 6. Radiograph of specimen 2 - CP and LIP flaws (reduced size).

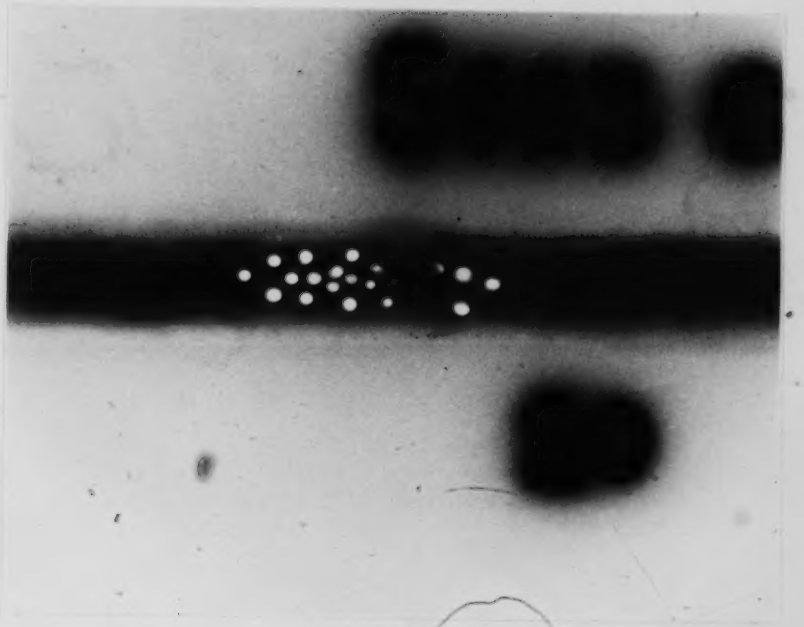

Plate 7. Radiograph of specimen 2 - CP flaw (true size).

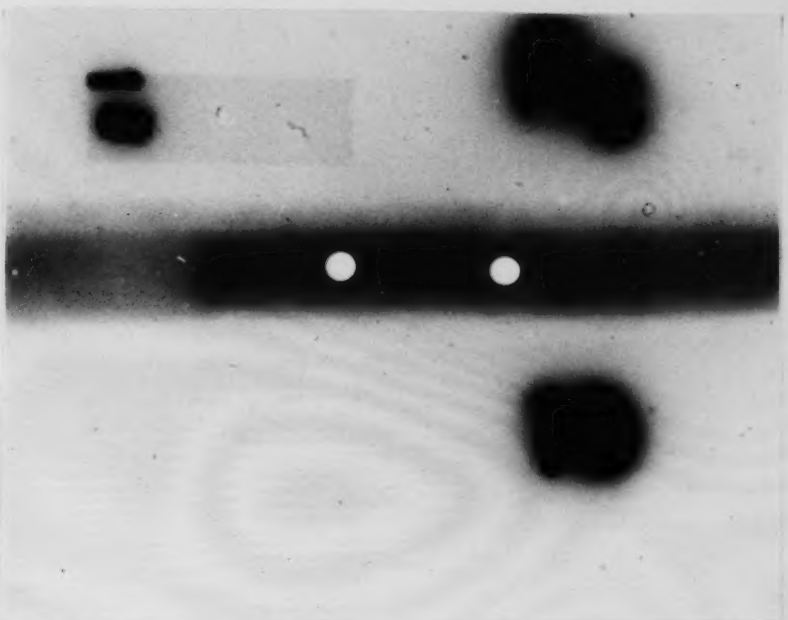

Plate 8. Radiograph of specimen 2 - LIP flaw (true size).

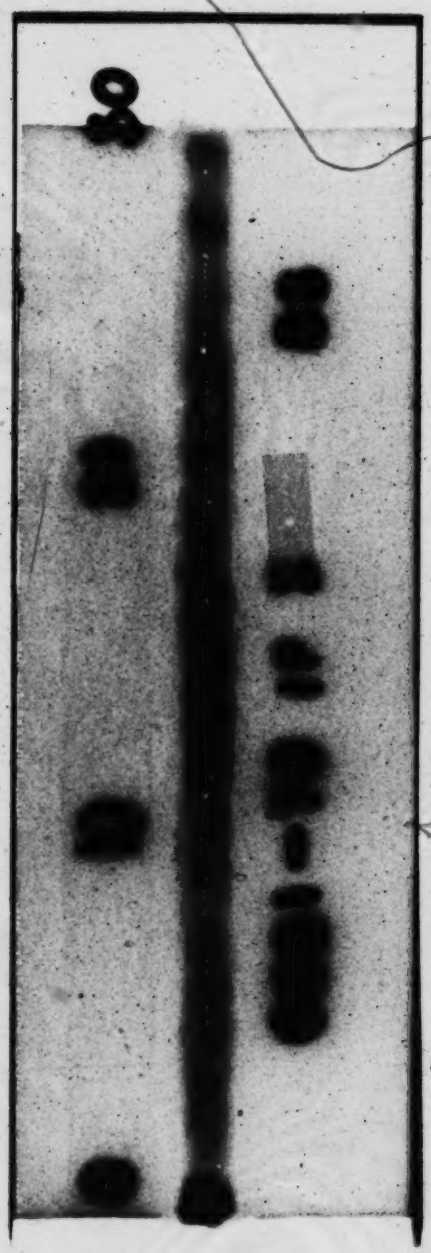

Plate 9. Radiograph of specimen 3 - IP flaw (reduced size).

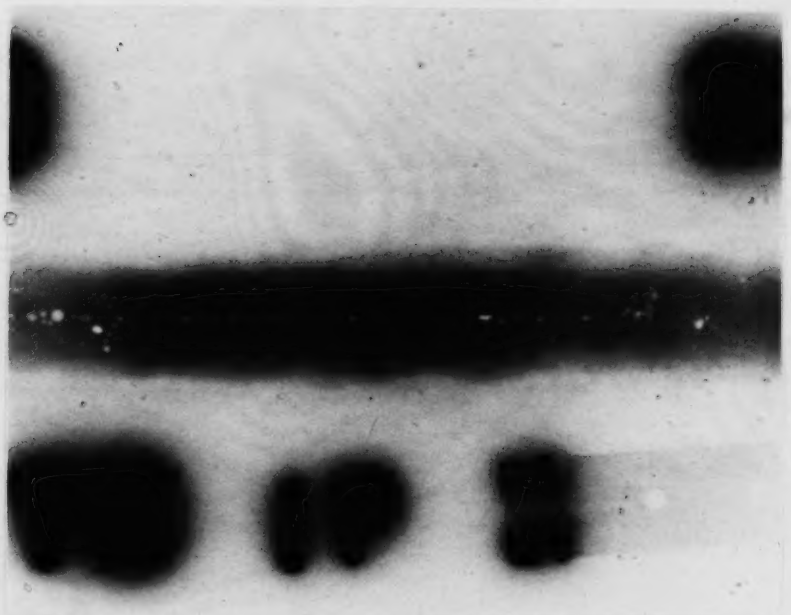

Plate 10. Radiograph of specimen 3 - IP flaw (true size).

estimated from the true size print (Plate 8), was 0.18" (4.6 mm).

The IP flaw in specimen 3 (Plate 9) appears as a dim white line in the central portion of the weld. The average width of the IP flaw, as estimated from the true size print (Plate 10), was 0.023" (0.59 mm). The average depth of the IP flaw, as determined by ultrasonic testing, was approximately 0.098" (2.5 mm).

A comparison of these results with nondestructive tests made of real welding flaws in aluminum, showed that the artificially produced flaws adequately simulate real flaws.

4.2 Initial Probe Studies

4.2.1 Penetration Characteristics

The first objective of this thesis was the development of a suitable probe system for the inspection of welds in thick metal plates. A through-transmission probe arrangement was a logical choice for these studies, since lift-off effects are eliminated if the distance between the two coils is fixed and the driving and detecting circuits have high impedances. The eddy current testing instrument used in this project was equipped with high impedance circuitry. By using the through-transmission arrangement, in conjunction with the eddy current testing instrument, it was believed that changes in the profile of a weld crown would not result in any signal indications due to lift-off effects.

To enable successful through-transmission inspection of thick plates another factor had to be considered; the skin effect had to be overcome. Normally the standard depth of penetration is quite shallow, even for very low frequencies (eg. 1/4" (6.4 mm) at 260 Hz). To enable operation at realistic operating frequencies (i.e., 100 to 2000 Hz) special eddy current probes were designed. The probes were designed to provide a sufficient magnetic flux density to penetrate 1/2" (12.7 mm) thick aluminum plate at these frequencies. Design criteria were based on experimental tests rather than theoretical calculations, since most theoretical calculations are based on ideal coil configurations and the impedance changes caused by localized flaws are usually too complex to treat analytically.

The penetration characteristics of the excitation probes were observed by monitoring the magnetic flux or field penetrating the plate and surrounding the sensing coil. The tests were conducted in the manner described in section 3.5.1. An operating frequency of 100 Hz was chosen, since this was the lowest frequency setting on the signal generator. Since the movement of the test object (i.e., with respect to the magnetic field) induces a voltage within the object, scanning rates were kept constant throughout the test to avoid unwanted changes in the impedance. Y-axis amplitude readings were compiled from a series of X-Y plots for a 4"x4" (102 mm x102 mm) area surrounding the sensing coil. The results are illustrated in Figures 38-43 in the

form of contour plots and perspective block diagrams. The perspective diagrams are presented at two different angles, for each probe, for the purpose of clarity.

The first probe design, probe *A*, was wound as a simple probe without any ferrite core. This probe showed excellent penetration capabilities, with amplitudes exceeding the 1 volt threshold of the eddy current instrument (see Figures 38 and 39). The penetration capability of the probe was excellent by virtue of a large number of turns of wire in the excitation coil. The shape of the magnetic field was uniform because of the circular coil design. The shielding used in this probe was found to be excellent, since very little drift was observed after balancing the bridge circuitry.

The second probe, probe *B*, was designed after probe *A*, but included a ferrite core to shape the magnetic field. The effect of adding the ferrite core is easily observed in the perspective diagrams (Figure 41). The field is much narrower in the direction parallel to the ferrite core. This occurs because the ferrite core tends to redirect the lines of magnetic flux in the direction parallel to the length of the core. It was hoped that the core might also concentrate the magnetic flux in the center of the coil, but the results showed that the penetration capability of this probe was poorer than that observed for probe *A* (cf. Figures 38 and 40). The shielding used in this probe was also found to be effective.

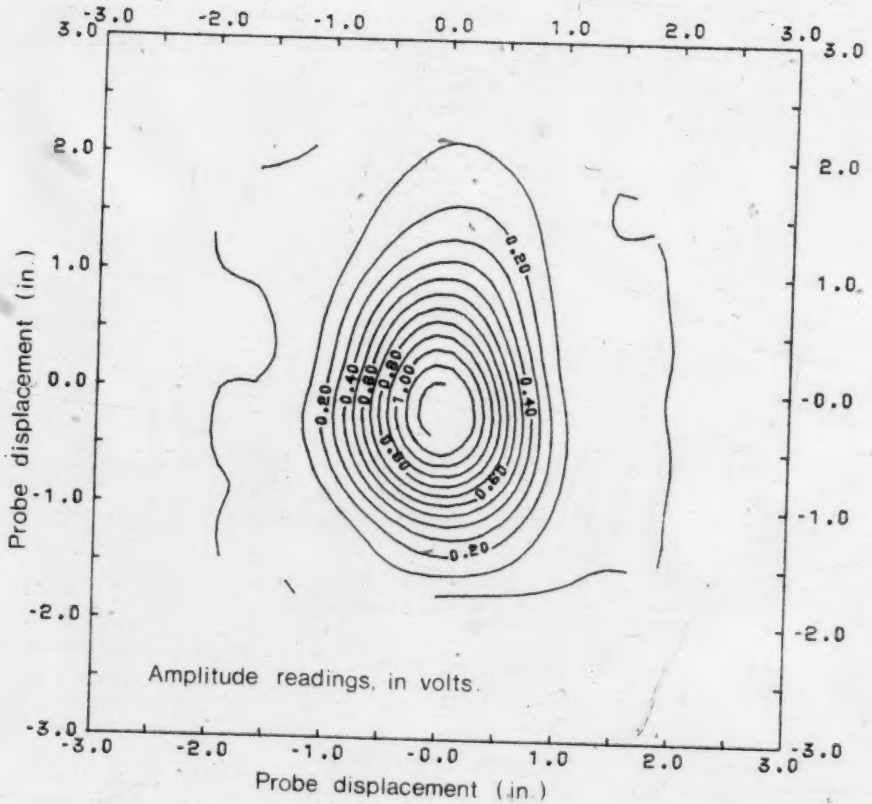

Figure 38. Magnetic field produced by probe *A* (contour plot).

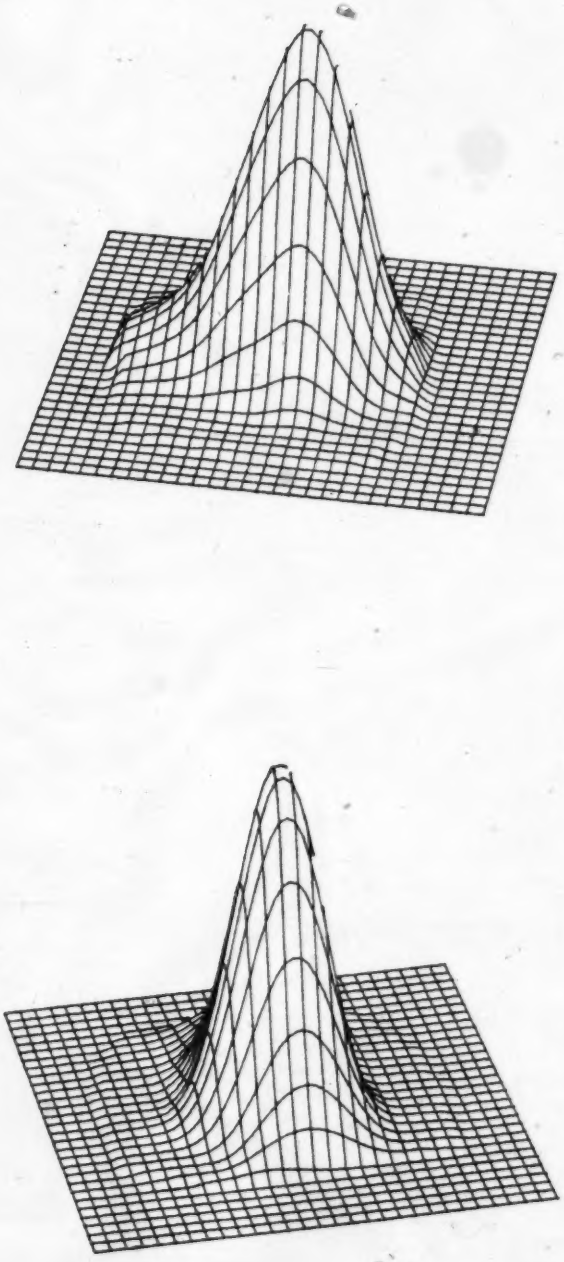

Figure 39. Magnetic field produced by probe *A* (perspective block diagrams).

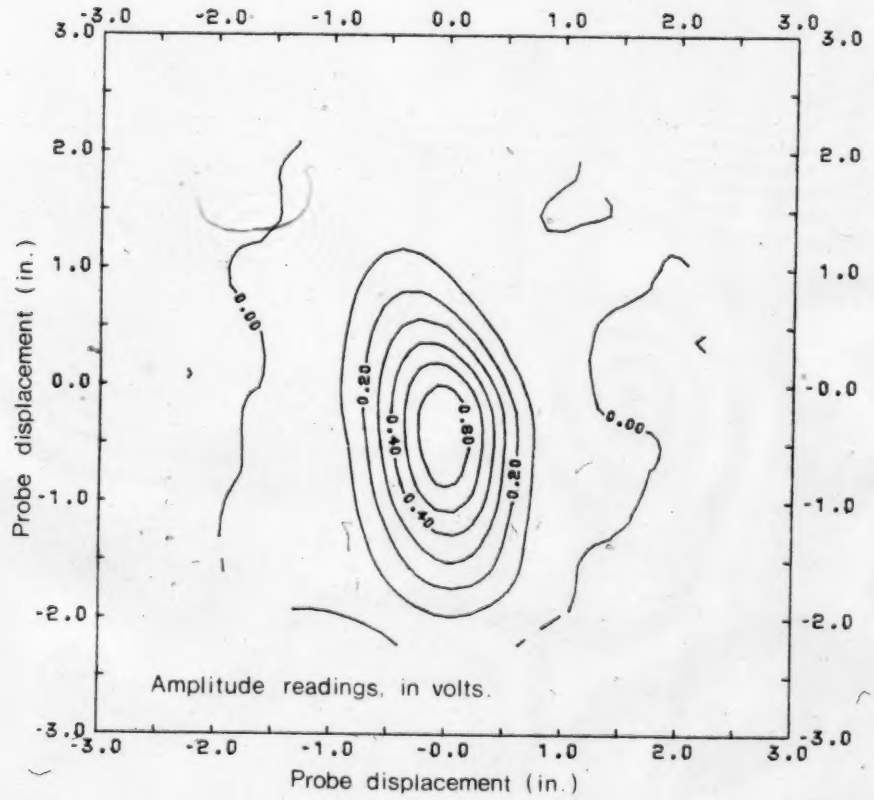

Figure 40. Magnetic field produced by probe *B* (contour plot).

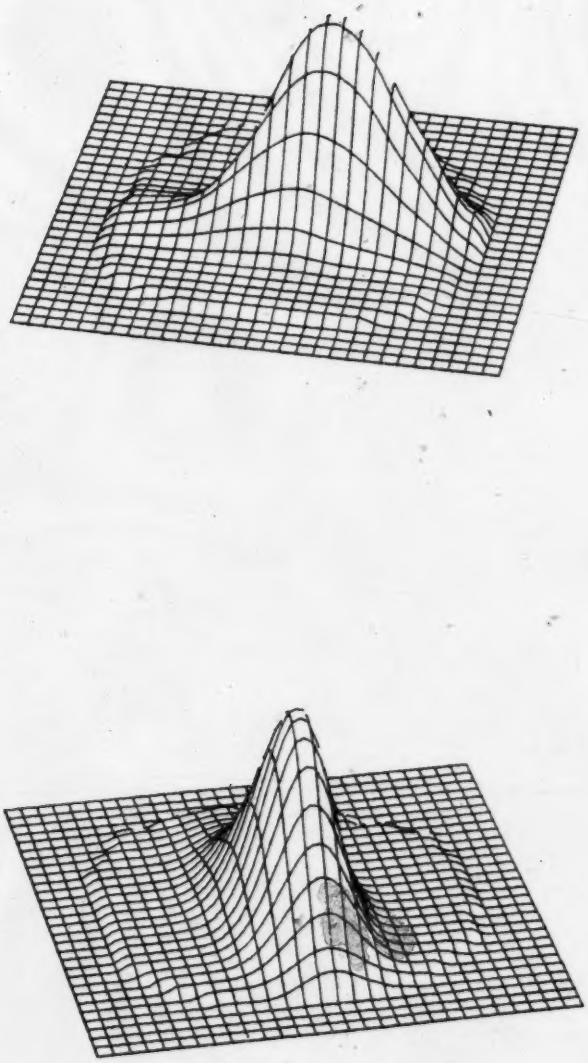

Figure 41. Magnetic field produced by probe *B* (perspective block diagrams).

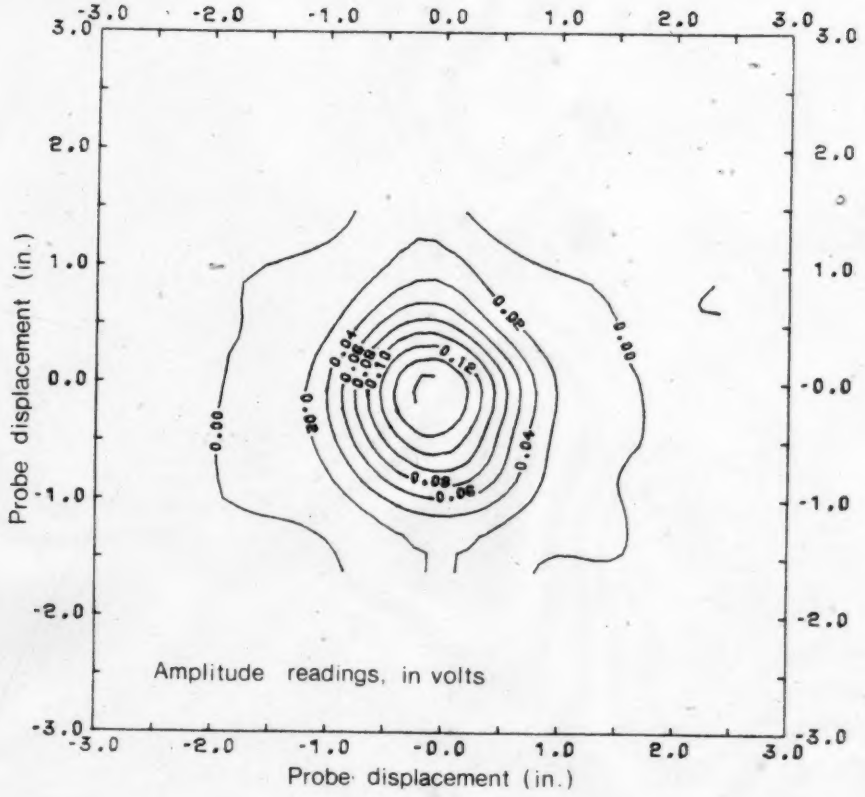

Figure 42. Magnetic field produced by probe *C* (contour plot).

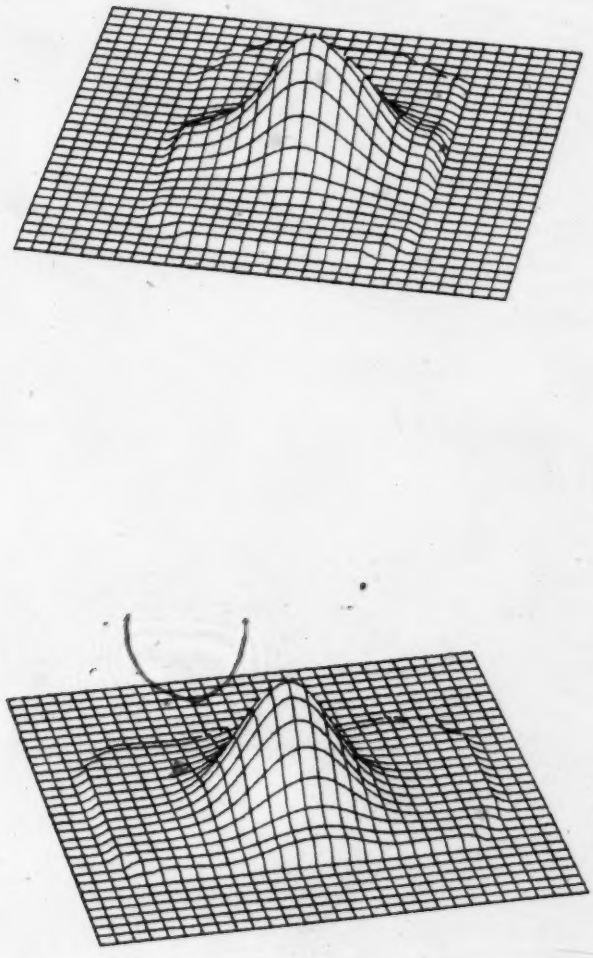

Figure 43. Magnetic field produced by probe *C* (perspective block diagrams).

The third probe, probe *C*, is merely a small version of probe *B*. It has a rectangular shaped magnetic field, similar to that produced by probe *B* (cf. Figures 43 and 41); however, the penetration capability of probe *C* is even worse than probe *B*. Once again, the shielding used in this probe was found to be effective.

4.2.2 Probe Sensitivity

The above results gave some indication of the probes' penetration characteristics, but to fully evaluate the performance of each probe, studies of their sensitivity to real flaws was required. To evaluate the sensitivity of each probe, scans were made across the machined portion of specimen 1, as described in section 3.5.1. The machined portion of the specimen was scanned, rather than the weld, to avoid any possibility of lift-off effects. The incomplete penetration flaw in the plate was detected using the impedance-plane analysis technique. The results of the scans are shown in Plates 11, 12 and 13.

Probe *A* was operated using frequencies between 100 and 1100 Hz in 100 Hz increments. This probe showed excellent sensitivity to the incomplete penetration flaw, with the best sensitivity occurring at 400 Hz (see Plate 11). The indications are typically single loops or double loops depending on the probe configuration used. In this case, a single loop was observed. A loop was formed, since the coil was much larger than the flaw. As the probe was scanned over

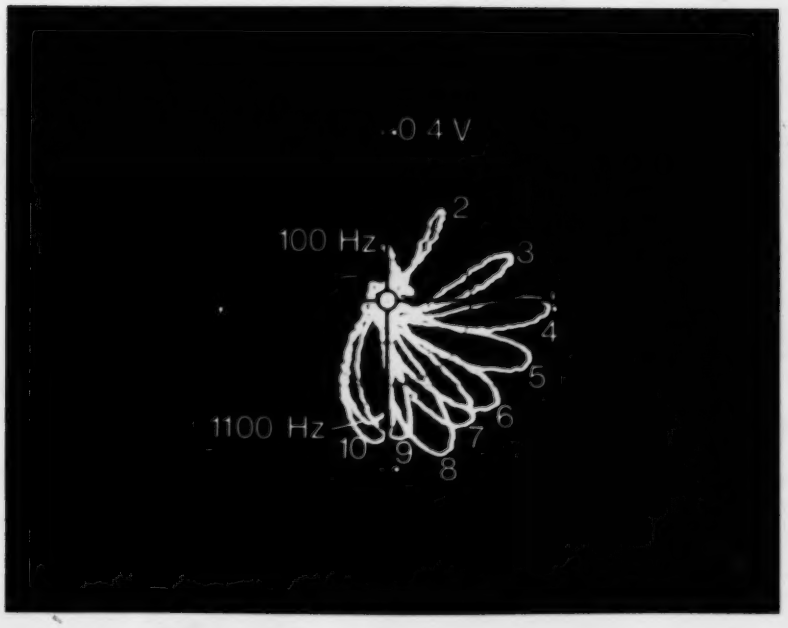

Plate 11. Probe *A* - sensitivity to IP flaw (specimen 1).

the incomplete penetration flaw, half of the loop was formed as the first edge of the coil in the excitation probe moved over the flaw. The other half of the loop was formed as the second edge of the coil moved over the flaw. The resulting indication was a single loop, often referred to as the "signature" of the flaw. The phase angle of these indications change with frequency because the inductive reactance value is a function of inductance and frequency (see section 2.3.2.1). This phenomenon often enables several operating variables to be separated from each other on the impedance plane by selecting a suitable frequency.

Probe *B* was operated using frequencies between 300 and 1700 Hz in 200 Hz increments. The probe showed a similar response to the incomplete penetration flaw, except that the sensitivity was reduced to less than one half the amount achieved by probe *A*. Maximum sensitivity was attained at about 500 Hz and 1100 Hz for probe *B* (see Plate 12). Probe *B* was prone to overheating at frequencies above 500 Hz. This may be attributed to an insufficient number of turns of wire, or insufficient gauge thickness, or a combination of the above.

Probe *C* was operated using frequencies between 300 and 1900 Hz. Probe *C* also showed a similar response to the IP flaw. Unlike probe *B*, the sensitivity was quite high, although still less than that attained by probe *A*. Maximum sensitivity was attained at 1100 Hz (see Plate 13). Although this probe design was merely a small version of probe *B*, no

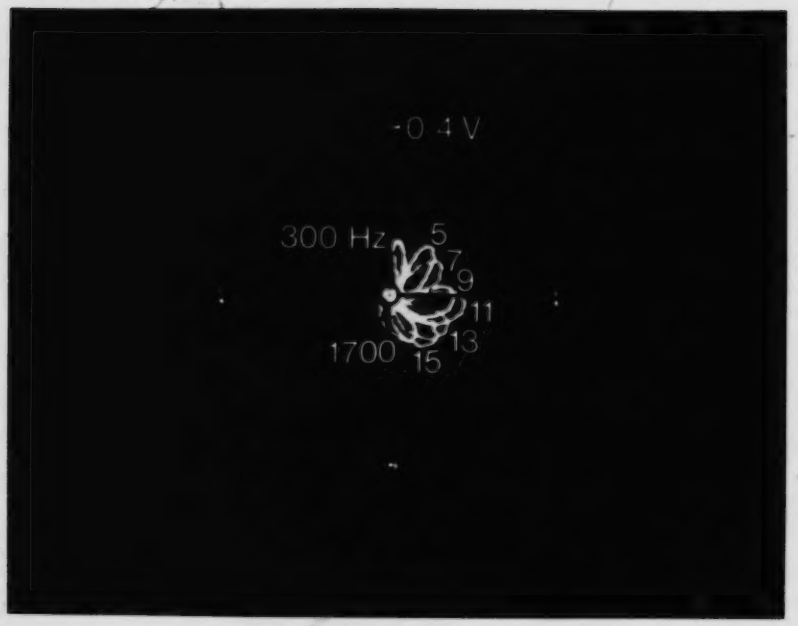

Plate 12. Probe *B* - sensitivity to IP flaw (specimen 1).

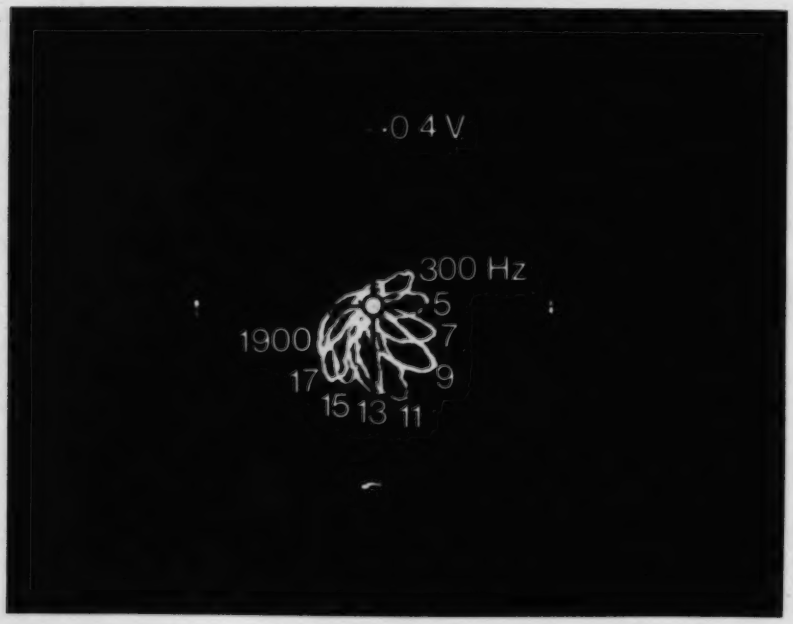

Plate 13. Probe *C* - sensitivity to IP flaw (specimen 1).

overheating was noticed in the range of frequencies used for the scans.

In general, the test probe sensitivity was increased as the frequency was increased, but at the same time penetration was reduced, so the two effects must be considered simultaneously. The sensitivity was increased since high-frequency eddy currents are more easily distorted by imperfections than low-frequency eddy currents. Penetration was reduced due to the skin effect (see section 2.3.2.4).

4.2.3 Lift-off Effects

To evaluate the effects of scanning over a weld bead crown, the unmachined portion of specimen 1 was inspected in the same manner as the machined portion. The results of these scans are shown in Plates 14 and 15. Probe *C* was not included in these scans, since only very small deflections were obtained. The deflections were small because of the increased thickness of metal created between the probes by the crown of the weld. In this case, probe *C* had insufficient penetration power or magnetic flux to penetrate the weld. In addition, a decrease in sensitivity to the incomplete penetration flaw was observed for probe *A* and *B* as a result of this increased thickness. The frequency effects were similar to those encountered in section 4.2.2.

Although these observations were important, the main objective of these tests was to investigate the effect of

Plate 14. Probe *A* - lift-off effects (specimen 1).

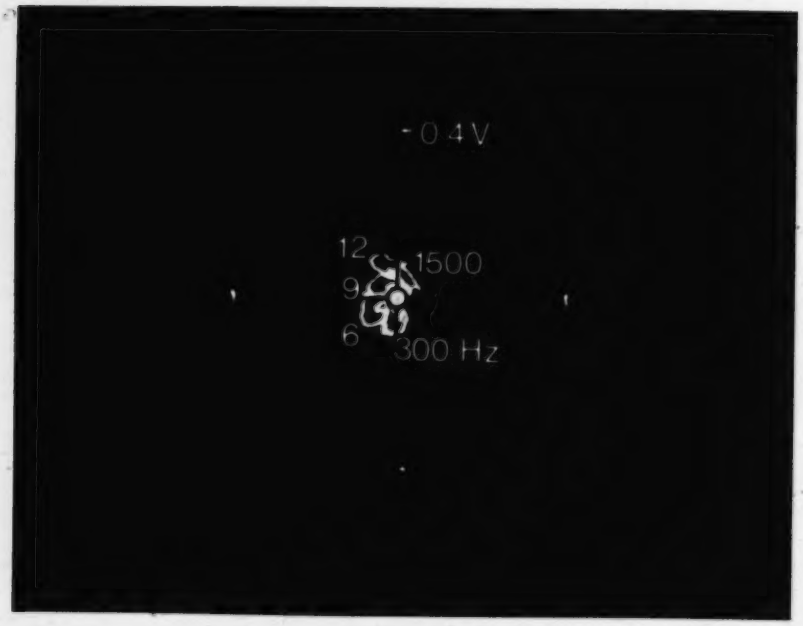

Plate 15. Probe *B* - lift-off effects (specimen 1).

lift-off. The results showed that changes in the thickness of the plate did not have a profound effect on the display output. As the probe moved over the weld, the impedance did not change until the flaw was encountered. This proved that the through-transmission probe arrangement was an effective means of overcoming the lift-off effect, although no formal explanation for the reason why it is effective can be given. Perhaps the combination of low-frequency and differential arrangement compensates for the lift-off. Normally a differential arrangement is used to compensate for minor fluctuations in thickness and conductivity (see section 3.4.4). In addition, low-frequency eddy currents tend to be less affected by lift-off than high-frequency eddy currents.

In general, the probe penetration and sensitivity studies showed that probe designs *A* and *B* were adequate for the inspection of welds in 1/2" (12.7 mm) thick aluminum alloy plate. Further studies were required to evaluate the feasibility of using this low-frequency through-transmission technique for the detection and characterization of flaws in an industrial application. These studies are presented in the following section.

4.3 Impedance-Plane Analyses

4.3.1 Flaw Detection

Detection of a wide variety of flaws is necessary to make this form of eddy current testing a feasible method for

the inspection of welds in aluminum plate. As a consequence, tests were performed to detect a number of flaws common to welds in aluminum plate using probe designs *A* and *B*. The poor penetration characteristics of probe *C* disqualified its use in the detection of flaws in aluminum plate exceeding 1/2" (12.7 mm) thickness. Specimens 2 and 3 were used as the standards for the tests and scans were made in the manner described in section 3.5.2. Rather than center the probe assembly over the weld bead, it was found that off-centered scanning provided better sensitivity. This may be explained by magnetic field variations. Imperfections in the test object are detected by monitoring changes in the impedance or voltage caused by distortions in the flow of eddy currents and, hence, variations in the magnetic field. Eddy currents near the edge of the magnetic field are more easily distorted than eddy currents in the central portion of the field where the flux density is greatest; hence, off-centered scanning is often an effective method of increasing the sensitivity to flaws. The results of the scans are shown in Plates 16-21.

Plates 16 and 17 show the indications obtained by scanning specimen 2 with probe *A*. In each case, deflections caused by lift-off (LO) were also included for the initial frequency chosen (eg. lift-off is at 100 Hz on plate 16). Lift-off did not occur; rather, the deflections were forced by altering the separation between the probes. Edge effect deflections occurred in the same direction, but are not

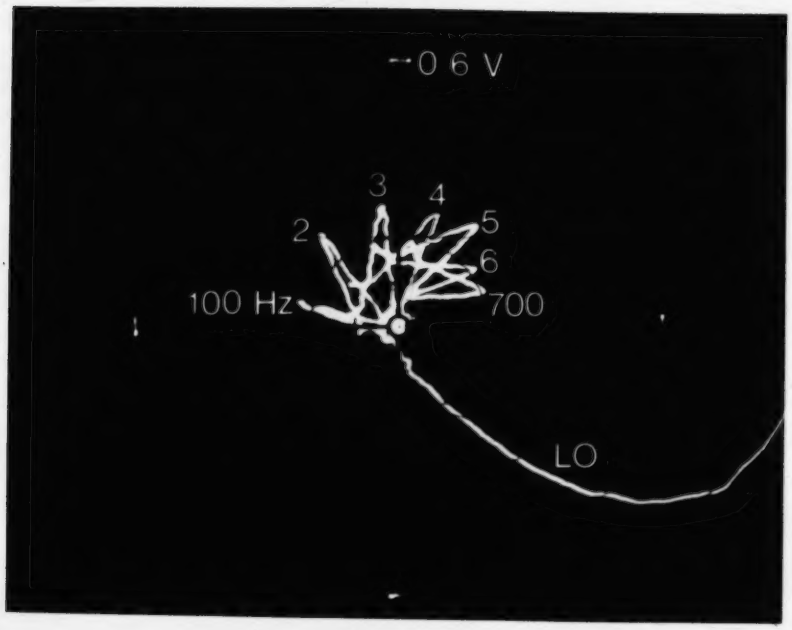

Plate 16. Detection of cluster porosity - probe *A*.

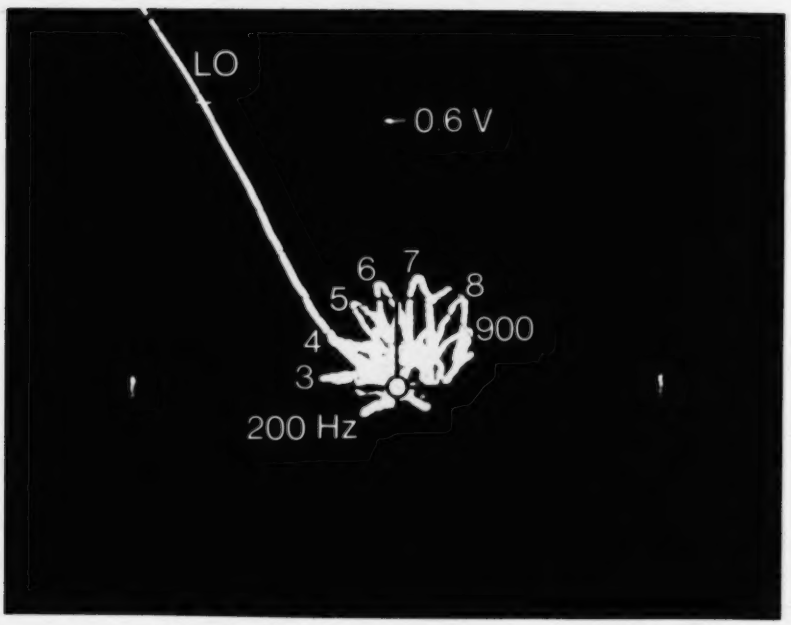

Plate 17. Detection of large isolated pores - probe *A*.

shown on the plates. The sensitivity to cluster porosity was greatest at 300 Hz, while the sensitivity to large isolated pores was greatest at 700 Hz. The indication obtained for the two pores appeared as a single loop, illustrating a lack of sensitivity to closely spaced, small flaws, or lack of resolution. Indications obtained from an incomplete penetration flaw are shown in plate 18. These indications were obtained by scanning specimen 3. Maximum sensitivity was obtained at 400 Hz. In each case, the flaw indications were distinct, without any spurious signals present.

Plates 19 and 20 show the indications obtained by scanning specimen 2 with probe *B*. Again, lift-off indications were included. The sensitivity to cluster porosity was greatest between 300 and 700 Hz. Tests at 500, 700, 900 and 1100 Hz showed little difference in the case of the large isolated pores; however, the indications from each pore showed up as a distinct loop, illustrating the excellent resolution properties of this probe. Plate 21 shows the indications obtained by scanning specimen 3. The sensitivity to the IP flaw was greatest between 500 and 700 Hz. Once again, the flaw indications were distinct, without any spurious signals present. Unlike probe *A*, maximum sensitivity to flaws was obtained over a range of frequencies. As a result, probe *B* offers greater flexibility to the operator. This is necessary if the probe is required for multi-purpose use.

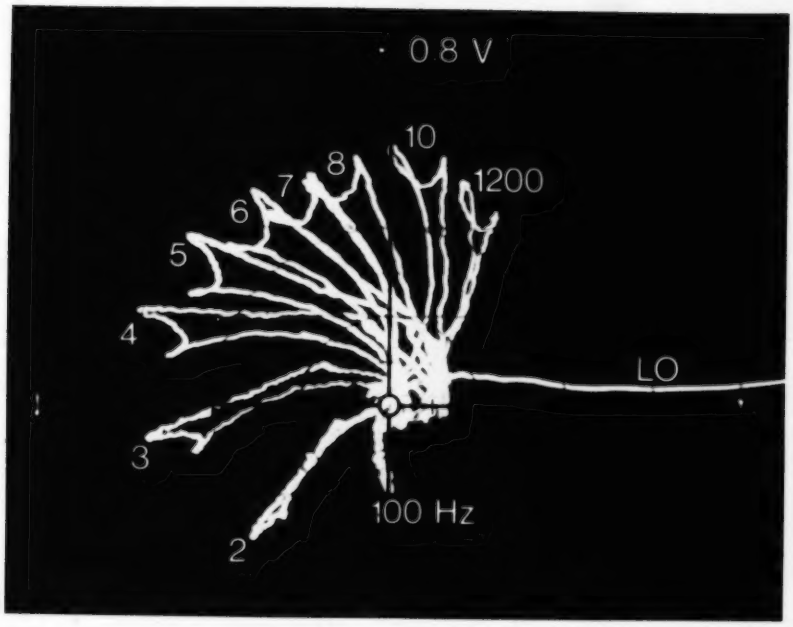

Plate 18. Detection of incomplete penetration - probe *A*.

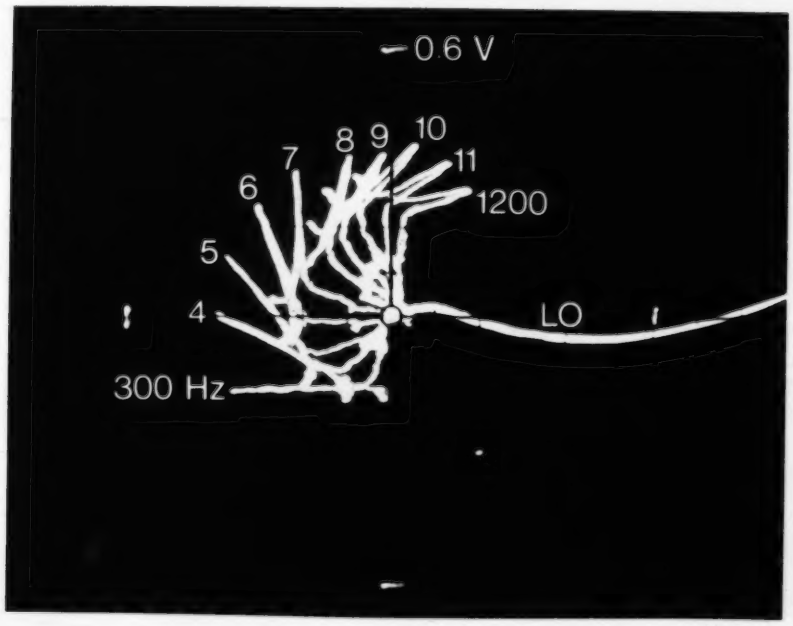

Plate 19. Detection of cluster porosity - probe *B*.

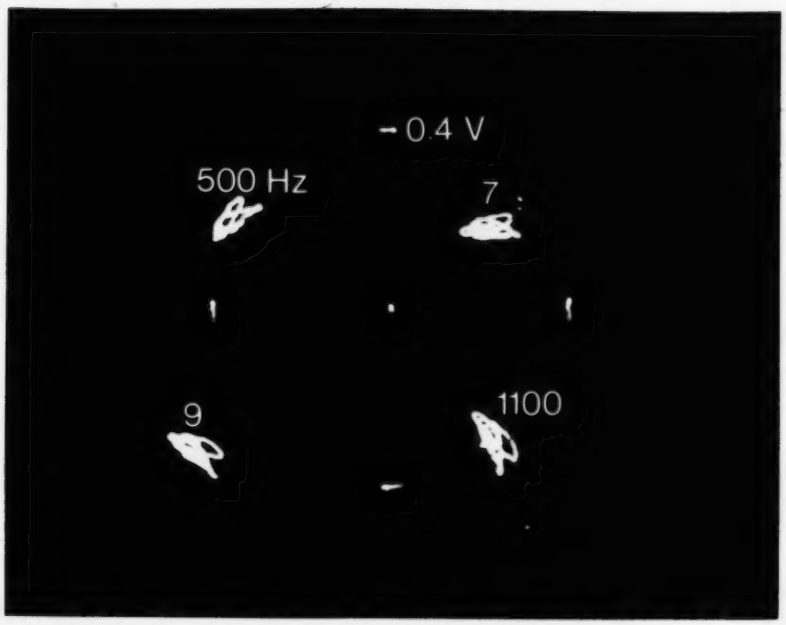

Plate 20. Detection of large isolated pores - probe *B*.

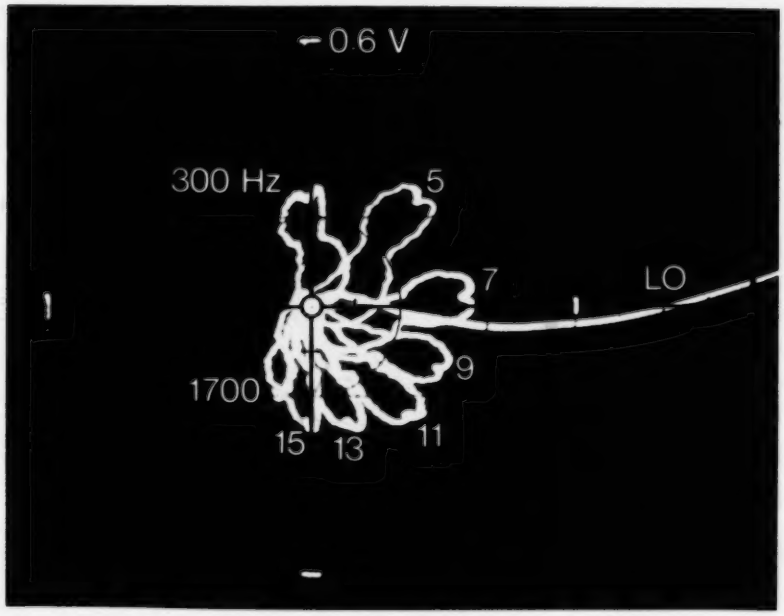

Plate 21. Detection of incomplete penetration - probe *B*.

4.3.2 Characterization of Flaws

The detection of flaws is important; however, it is generally desirable to not only detect flaws, but to identify them. To accomplish this task, the welds in specimens 2 and 3 were scanned at a fixed frequency. Three separate frequencies were selected which covered the optimum range of operating frequencies for probes *A* and *B*.

Welding causes thermal transients in the weld area, which change grain size and the state of work or age hardening in the heat-affected zone. As a result, electrical conductivity, σ, is a variable in this zone and it was necessary to monitor the phase angle of the conductivity changes. In each case, a comparison between flaw-free sections of specimens 2 and 3 was made to determine the phase angle of the conductivity changes. The results of the scans are shown in Plates 22-27. The arrows indicate the direction of decreasing conductivity.

The first frequency used for the scans was 300 Hz. Plate 22 shows the flaw indications for probe *A*. The incomplete penetration flaw indication appeared as a very narrow single loop, whereas the cluster porosity appeared as a wide loop. The large isolated pores, although not as well defined as the cluster porosity, appeared as a single, moderately wide loop. The change in appearance of the loops may be explained by the difference in cross-sectional area of the various flaws. Cracks, lack of fusion and incomplete penetration are generally very long and narrow flaws, as

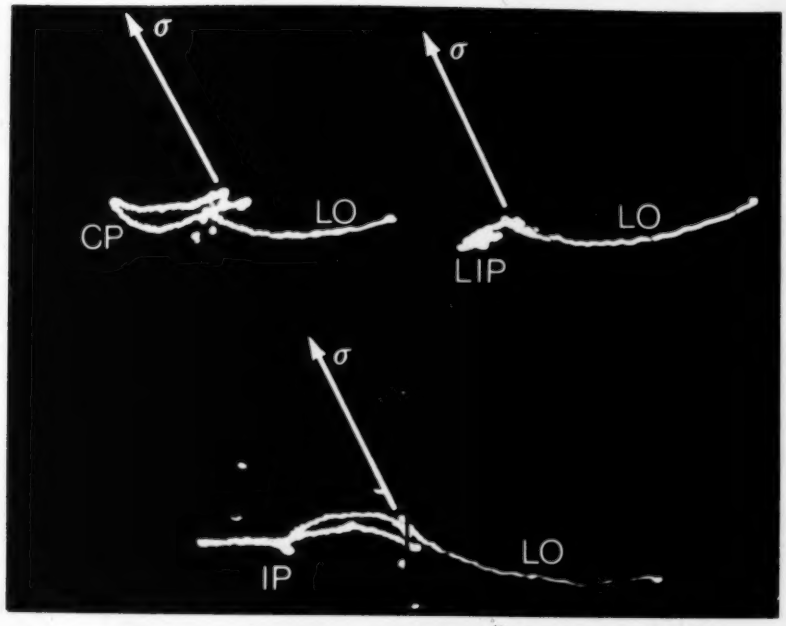

Plate 22. Flaw signatures - probe *A* (300 Hz).

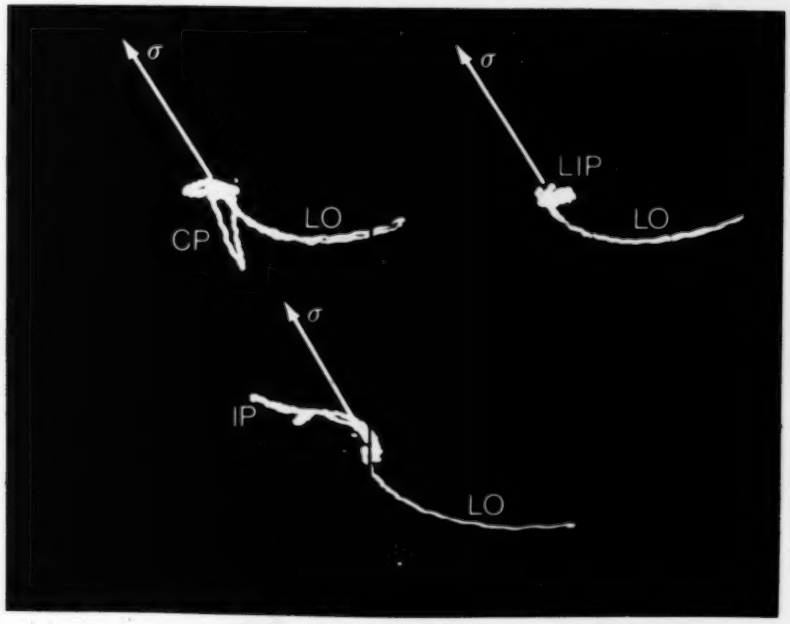

Plate 23. Flaw signatures - probe *B* (300 Hz).

compared to porosity, inclusions and large voids. Since large cross-sectional areas perpendicular to the flow of eddy currents tend to distort the eddy currents more than small cross-sectional areas, the loops formed by scanning over long and narrow flaws tend to be more tight. Although this phenomenon is useful for the characterization of flaws, the phase angle of the deflections is also important. The flaw indications obtained for probe *A* tend to have the same phase angle. This may lead to confusing results if several types of flaws are present in a single weld. Ideally, the flaws should give indications that have both different appearance and phase angle. Fortunately, the conductivity and lift-off changes were separated, in phase, from all other operating variables. As a result, they were clearly distinguished from the other variables.

At 300 Hz the shape of the loops were similar for probes *A* and *B* (cf. Plates 22 and 23). The only noticeable difference was in the phase angle of the indications. Probe *B* provided much better separation of the variables, since the phase angle was different for each flaw indication (i.e., there was almost a 120° phase angle shift between each flaw indication). Probe *B* also provided good separation of the conductivity and lift-off loci.

An increase in the frequency to 500 Hz generally resulted in a marked increase in the sensitivity, as shown in Plates 24 and 25. The shape of the indications obtained by probe *A* were similar to those obtained at 300 Hz. The

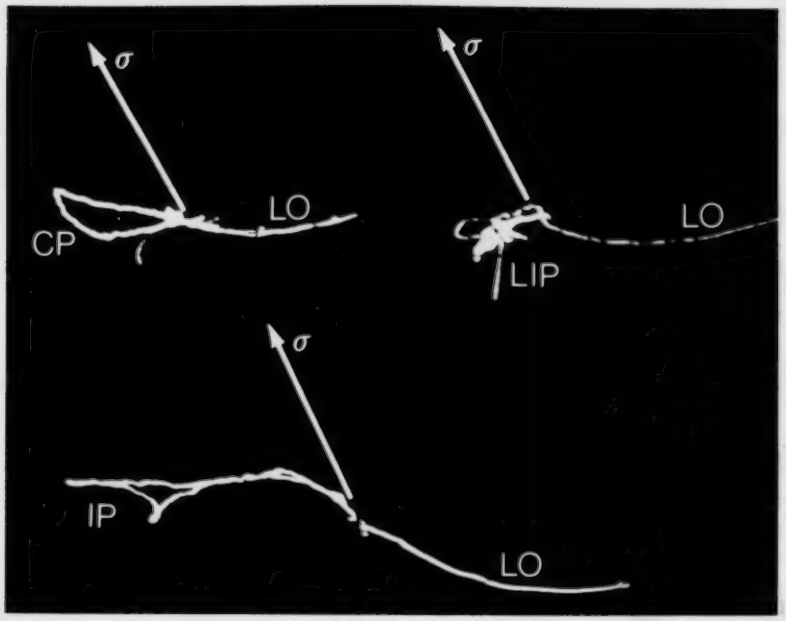

Plate 24. Flaw signatures - probe *A* (500 Hz).

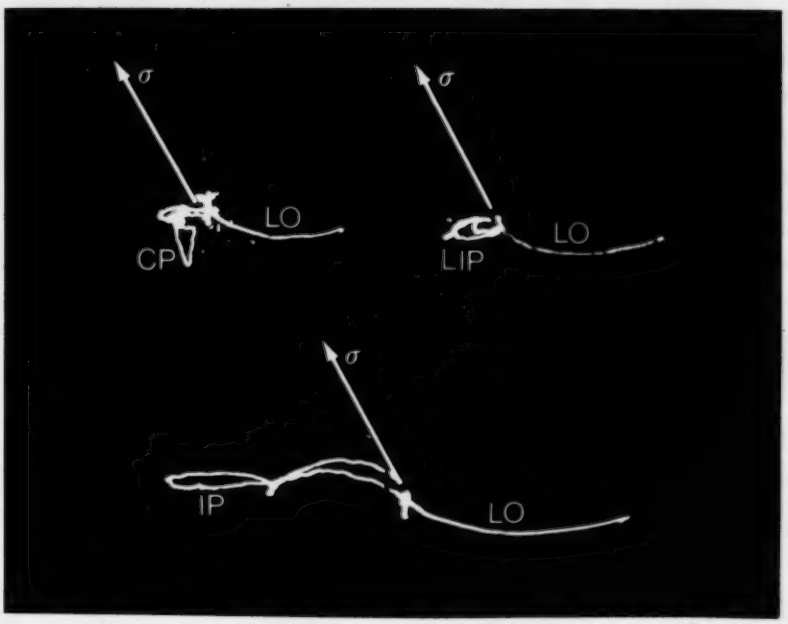

Plate 25. Flaw signatures - probe *B* (500 Hz).

large isolated pores were more pronounced at this frequency, but the phase angles of the indications were still the same. Probe *B*, on the other hand, showed two distinct loops for the large isolated pores, the sensitivity to the cluster porosity was only slightly reduced and the phase angles of each indication remained fairly distinct. In each case, the phase angle separation between the conductivity and lift-off indications was large, allowing for good separation of these variables.

An increase in the frequency to 700 Hz resulted in increased sensitivity to the cluster porosity and large isolated pores for probe *A* (see Plate 26). The shapes of the indications remained the same; however, the phase angles shifted toward the conductivity locus. In this case, the flaws could only be identified by the shape of their loops. The scans at 700 Hz with probe *B* showed decreased sensitivity to incomplete penetration and cluster porosity, and increased sensitivity to large isolated pores (see Plate 27). Indications caused by the large isolated pores were very distinct (i.e., the resolution was excellent). In addition, the separation of the phase angles for each variable was very good.

In general, the flaws were easily characterized using probe *B* between the frequencies of 300 and 700 Hz. The phase angles and signatures (i.e., loop shapes) were unique, resulting in the rapid indentification of the flaws. Overheating was the only problem associated with probe *B*.

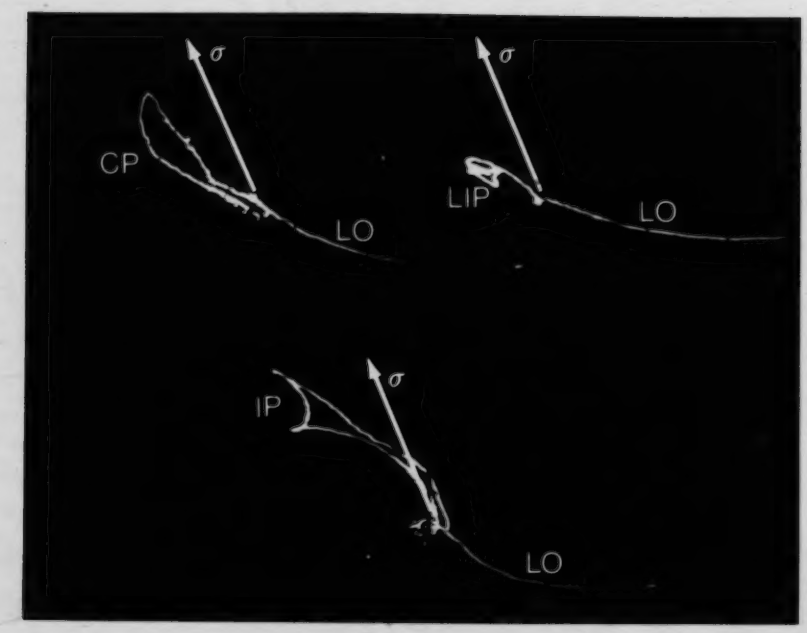

Plate 26. Flaw signatures - probe *A* (700 Hz).

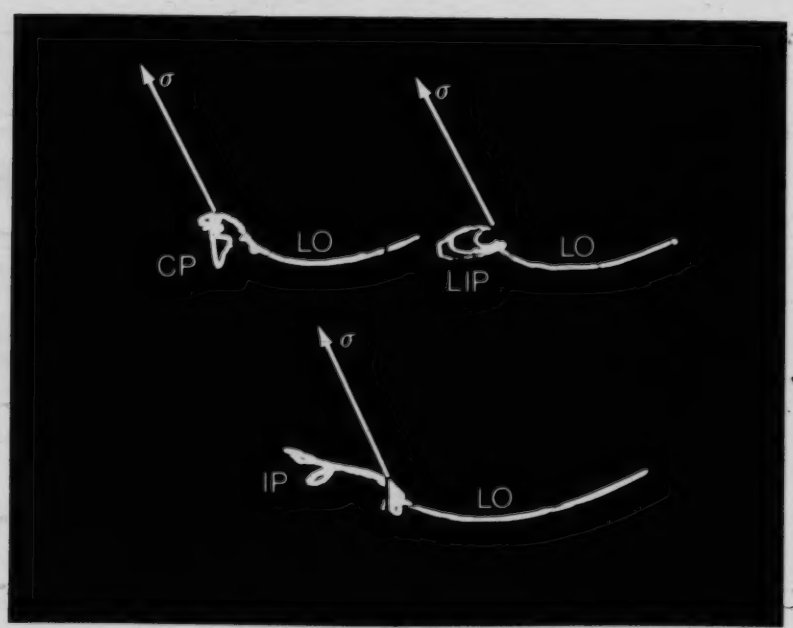

Plate 27. Flaw signatures - probe *B* (700 Hz).

Probe *A* did not have a problem of overheating, but the phase angles of the flaw indications were not distinct at any frequency. This did not present a problem in this project, since the loop shapes were so distinct that the flaws were easily identified by shape alone. Probe *A* generally had a greater sensitivity to the artificial flaws at a given frequency, but less resolution than probe *B*. Also, it was observed that scans made over real flaws produced similar signatures on the impedance plane.

The separation in phase between the conductivity, lift-off and flaw indications was excellent for both probes. Conductivity and lift-off changes are often an important consideration in the inspection of weld beads. The conductivity changes associated with the welds occur mainly in the transverse direction and are dependent on the thermal histories of the base plate, heat-affected zone (HAZ) and weld metal. Conductivity changes along the length of the weld are only slight and, as a consequence, were of little concern in this project. In addition, lift-off effects were not a problem because of the through-transmission probe arrangement. If, in fact, conductivity and lift-off changes did occur, the phase selective circuitry would allow for simple, quick discrimination of these variables, since the phase angle separation between these variables was good. Edge effect indications can be discriminated against in the same manner.

Probe design was a very important factor in the development of this eddy current inspection technique. The probes were designed to provide a sufficient degree of penetration to inspect thick sections of metal, yet maintain a suitable degree of sensitivity to flaws. The design of the probes may be altered to adapt to different test conditions (i.e., thicker sections, cylindrical shapes, ferrous materials, etc.). In all cases, the main features of the probes are the ferrite core and conducting metal shield. Without a ferrite core the sensitivity to flaws would be diminished and resolution would be poor. Poor ferrite core design also results in diminished sensitivity and resolution, as well as poor penetration characteristics. A conducting metal shield is essential in all probes to guard against noise from stray fields surrounding the probe which may cause an imbalance in the balance circuits. Proper coil design is the key to successful characterization of the flaws and separation of the operating variables.

4.4 Industrial Applications

The through-transmission probe arrangement used in this project offers little flexibility in an industrial application. To make low-frequency eddy current testing a feasible nondestructive testing technique for the inspection of welds in pipes, for example, the excitation and sensing coils would have to be wound as a single unit and scanned over the outside surface of the pipe. A drawback to such a

configuration is lift-off. Lift-off indications were not observed using the through-transmission probe arrangement, since the distance between the sensing and excitation coils was held constant while scanning over the weld. If the coils are wound as a unit, lift-off indications become pronounced when scanning over irregular surfaces. Fortunately, phase selective circuitry allows the operator to separate lift-off indications, flaw indications and conductivity changes on the impedance plane, provided a suitable testing frequency is selected.

An attempt should be made to design a probe assembly which combines both the sensing and excitation coils in a single housing. The probe's performance should be evaluated using a phase selective or amplitude-phase detector system in the same manner as outlined in the experimental section of this thesis. With a suitable selection of probe design and operating frequency, flaws associated with welds in aluminum and other metals may be detected and characterized in the same manner as illustrated in this thesis.

In a practical application, modulation analysis is often preferred over the impedance-plane analysis technique, since a hard copy of the flaw indications is obtained directly from the strip chart recorder. Recent developments in the field of electronics has made it possible to record the results of an impedance-plane analysis directly onto magnetic tape. The tape may be stored and then played back on an X-Y storage oscilloscope display as a reference. As a

result, impedance-plane analyses should be chosen over modulation analyses, since flaw indications are more easily interpreted and separated from unwanted signals using the impedance-plane analysis technique. Cathode ray tubes also provide a faster response to output signals than strip chart recorders. In some cases, the operating variables of the eddy current test are difficult to separate, despite the use of impedance-plane analyses. In such cases, a multifrequency or multiparameter method may be used. Libby[20,22,25] describes this method of eddy current testing in great detail in several of his papers.

Although eddy current nondestructive testing has been used extensively in the aircraft industry for surface and subsurface inspection, the use of low-frequency techniques and other specialized techniques have allowed for increased use of subsurface inspection in other industries, such as tubular goods manufacturing. The results obtained in this project have shown that testing can be done to even greater depths using special probes and a low-frequency a.c. signal generator. This allowed for through-transmission inspection of weld beads in 1/2" (12.7 mm) thick aluminum alloy plate to locate flaws, as well as identify each flaw, by distinguishing the characteristic display outputs. Although inspection was limited to aluminum alloys in this project, the system may be easily adapted for the inspection of other metals. Development of modified probe designs may allow for low-frequency inspection of pipes and thick aircraft

structural members.

5. Conclusions

The results obtained in this project show that low-frequency eddy current testing is an effective means of inspecting welds in aluminum alloy plates up to 1/2" (12.7 mm) thick. By using special through-transmission probes and a low-frequency a.c. signal generator, welding flaws such as IP, CP, and LIP can be located, as well as identified, by distinguishing the characteristic display outputs. Phase selective circuitry permits flaw signatures, conductivity changes and lift-off indications to be separated on the impedance plane. In particular, the results show that:

1. Flaw characterization and phase angle separation of the operating variables is mainly dependent on the frequency and coil design.

2. Flaw signature shape is determined by the cross-sectional area of the flaw perpendicular to the flow of eddy currents.

3. Off-centered scanning provides for increased sensitivity to flaws due to increased distortion of the eddy currents near the edge of the magnetic field.

4. Probe *A* provides excellent penetration and sensitivity characteristics, with maximum performance at 500 Hz; however, the resolution of this probe is only fair. Flaw characterization is only possible by distinguishing the signatures or loops formed on the CRT, where planar flaws, such as cracks, lack of sidewall fusion and incomplete penetration, produce tightly closed loops and volumetric flaws, such as porosity, produce wide, open loops. The phase angle separation of the flaws is poor for probe *A*, but the phase angle separation of the conductivity and lift-off loci from the flaw indications is good.

5. The addition of a ferrite core gives probe *B* excellent resolution characteristics, allowing for the detection of very small flaws. Flaw characterization is possible over a wide frequency range (i.e., 300 to 700 Hz) for this probe. The characterization of flaws is excellent, since the phase angles and signatures are unique for each flaw. The signatures produced by planar flaws are typically tightly closed loops and the signatures produced by volumetric flaws are typically wide, open loops. The phase angle separation of the conductivity and lift-off loci from the flaw indications is also excellent.

6. Probe *C* does not provide enough penetration for the inspection of welds in 1/2" (12.7 mm) thick aluminum alloy plate.

7. Sizing of flaws is possible to some extent. The length of a planar flaw may be determined by monitoring the probe displacement while the signature is formed on the impedance plane. Accurate results may only be obtained if the probes are calibrated to a known flaw length or standard. Determination of the depth of flaws is difficult, since the magnetic field intensity is nearly uniform throughout the specimen; therefore, the position of the flaw does not affect the test response.

8. Although inspection was done at only 0.2"/s (5.1 mm/s) in this thesis, inspection up to about 8'/s (2500 mm/s) is possible for industrial applications, since no physical contact is required between the testing probe and test object.

9. Low-frequency eddy current testing allows for the identification of a wide variety of physical, electrical, structural and metallurgical conditions in metals, including: electrical conductivity, magnetic

permeability, physical dimensions, cracks, voids, laps and inclusions.

6. Recommendations for Future Work

6.1 General Recommendations

It was important, from a practical point of view, to use qualitative analyses to observe the influence of various flaws on the impedance-plane diagram and, hence, evaluate the performance of the excitation probes used in this project. The analyses allow for preliminary determination of suitable coil dimensions, ferrite core shapes and sizes, and signal generator operating frequencies. These variables may be improved, in future works, by applying numerical calculations when possible, or by adequate experimental tests.

As described in section 4.4, an attempt should be made to design a probe assembly which combines both the sensing and excitation coils in a single housing. An attempt should also be made to develop a probe capable of inspecting welds in steel plate. Existing probe designs may be used. In this case, a saturation coil should be included to minimize the magnetic effects encountered when testing ferrous materials. The saturation coil should surround the sensing and excitation coils. A sufficient amount of direct current is applied to the saturation coil in order to raise the magnetic flux of the material adjacent to the coil to a maximum. This condition is known as magnetic saturation. In such a manner, small variations in permeability will be eliminated; hence, reduce the possibility of false readings

or indications.

6.2 Thermal Stability

A characteristic often overlooked when designing coil systems is thermal stability. The excitation current causes I^2R losses which heat the coil, and eddy currents flowing within the test object heat the object. Dimensional changes caused by the thermal expansion of the coil may cause small changes in the inductance of the coil. If multiple coils are used in a single probe, temperature changes may cause a variation in the coupling between the coils, as a result of the expansion of the coil supports. All of these factors should be taken into account in the development of new eddy current probes.

6.3 Standards

The development of standards for use in eddy current nondestructive testing has proceeded at a much slower rate than for the other major nondestructive test methods. There is a need for a more quantitative approach in eddy current testing, thus a need for establishing standard calibration and operating procedures and specifications for reference test specimens.

Artificially produced flaws were used as a means of evaluating probe performance in this project. Artificial flaws were chosen over milled notches or drill holes, since they were more representative of naturally occurring flaws

in welds. Unfortunately, artificially produced flaws cannot be easily duplicated, thus ruling out the possibility of using them in a performance standard. Small drilled holes and milled notches have been used in performance standards for ultrasonic testing equipment and conventional eddy current testing equipment calibrations. They are easily reproduced and, in most cases, simulate naturally occurring flaws.

Existing standards for use in eddy current testing, as described by Hochschild[39,40], are designed for surface and subsurface inspection. At present, ASTM standards do not extend below 1000 Hz for eddy current testing. As a consequence, these standards are not suitable for use in low-frequency eddy current testing of thick sections. If the low-frequency testing method described in this thesis is to be used in a practical application, a standard will have to be developed to reliably qualify and calibrate the eddy current testing system.

Crowe[41] describes a method of calibrating an eddy current test system using simulated signals or "signal injection". In this case, preprogrammed signals which simulate real flaw indications on the impedance plane are injected into the eddy current test instrument from an electronic device. This method may prove to be a useful alternative to the conventional standards used in eddy current testing.

References

1. Oersted, H.C., Experiments on the Effect of Electricity on the Magnetic Needle. *Ann. Phil.*, 16:273-276 (1820).
2. Hatchett, On the Electromagnetic Experiments of Oersted and Ampére. *Phil. Mag.*, 56:308 (1820), 57:40-47 (1821).
3. Memoires de l'Institut, IV, *Theorie des phenomenes electro-dyamique*, 1823.
4. Abraham-Becker, *The Classical Theory of Electricity and Magnetism*, Blackie and Son, Ltd., Glasgow, 1932.
5. Faraday, M., *Faraday's Diary*, Vol. 1, Bell and Sons, Ltd., London, pp. 367-397, 1932.
6. Faraday, M., *Experimental Researches in Electricity*, Vol. 1, Dover Publications, Inc., New York, pp. 1-16, 1965.
7. Stine, W.M., *The Contributions of H.F.E. Lenz to Electromagnetism*, The Acorn Press, Philadelphia, 1923.
8. Ohm, G.S., *Die Galvanische Kette Mathematisch Bearbeitet*, Berlin, 1827.
9. Maxwell, J.C., *Scientific Papers of James Clerk Maxwell*, Dover, New York, pp. 526-597, (not dated).
10. Gillmor, C.S., *Coulomb and the Evolution of Physics and Engineering in Eighteenth Century France*, Princeton University Press, New Jersey, 1971.
11. Panofsky, W.K. and Phillips, M., *Classical Electricity and Magnetism*, 2nd ed., Addison-Wesley, London, 1962.
12. Vigness, I., Dinger, J.E. and Gunn, R., Eddy Current

Type Flaw Detectors for Nonmagnetic Metals. *J. Appl. Phys.*, 13:377-383 (1942).

13. Farrow, C., Nondestructive Electrical Testing of Metals. *U.S. Patent No. 2,415,789*, issued Feb. 11, 1943.
14. Zuschlag, T., Electromagnetic Inspection. *U.S. Patent No. 2,329,811*, issued Sept. 21, 1943.
15. Förster, F., et. al., Grundlagen der zerstörungsfreien Werkstoffprüfung. *Z. Metallk.*, 43:I., pp. 163-171; II., pp. 172-180 (1952).
16. Förster, F., et. al., Grundlagen der zerstörungsfreien Werkstoffprüfung. *Z. Metallk.*, 45:III., pp. 166-179; IV., pp. 180-187; V., pp. 188-193; VI., pp. 197-199; VII., pp. 221-226 (1954).
17. McMaster, R.C.(ed.), *Nondestructive Testing Handbook*, Vol. 2, Ronald, New York, pp. 40-1 to 40-48, 1959.
18. McMaster, R.C. and Wenk, S., in *Symposium on the Role of Nondestructive Testing in the Economics of Production*. ASTM Spec. Tech. Pub. No. 112, pp. 11-37, 1950.
19. Libby, H.L., Nondestructive Eddy Current Subsurface Testing Device Providing Compensation for Variation in Probe-to-Specimen Spacing and Surface Irregularities, *U.S. Patent No. 3,197,693*, issued July 27, 1965.
20. Libby, H.L., Eddy Current Nondestructive Testing Device for Measuring Multiple Parameter Variables of a Metal Sample, *U.S. Patent No. 3,229,198*, issued Jan. 11,

1966.

21. Libby, H.L. and Wandling, C.R., Eddy Current Nondestructive Testing Device using an Oscilloscope to Identify and Locate Irregularities in a Test Piece, *U.S. Patent No. 3,302,105*, issued Jan. 31, 1967.

22. Libby, H.L., Multiparameter Eddy Current Concepts. *Research Techniques in NDT*, Vol. I, Academic Press, London, pp. 345-382, 1970.

23. Libby, H.L., Eddy Current Test for Tubing Flaws in Support Regions. *Research Techniques in NDT*, Vol. II, Academic Press, London, pp. 151-184, 1973.

24. Libby, H.L., Basic Principles and Techniques of Eddy Current Testing. *Nondestructive Testing*, 27:12-18 (1956).

25. Libby, H.L., *Introduction to Electromagnetic Nondestructive Test Methods*, Wiley-Interscience, New York, 1971.

26. Hochschild, R., The Theory of Eddy Current Testing in One (Not-So-Easy) Lesson. *Nondestructive Testing*, 12:31-40 (1954).

27. Hochschild, R., Eddy Current Testing by Impedance Analysis. *Nondestructive Testing*, 12:35-44 (1954).

28. Hagemaier, D.J., Eddy Current Impedance Plane Analysis. *Materials Evaluation*, 2:211-218 (1983).

29. Mattis, D.C., *The Theory of Magnetism*, Harper and Row, New York, 1965.

30. Duckworth, H.E., *Electricity and Magnetism*, Macmillan,

Toronto, 1960.

31. Plonsey, R. and Collin, R.E., *Principles of Applications of Electromagnetic Fields*, McGraw-Hill, New York, 1961.

32. Tyndall, J., *Faraday as a Discoverer*, Crowell, New York, pp. 108-111, 1961.

33. Hagemaier, D.J. and Steinberg, A.P., Low-frequency Eddy Current Inspection of Aircraft Structure. *Materials Evaluation*, 2:206-210 (1982).

34. Smith, J.H. and Dodd, C.V., Optimization of Eddy Current Measurements of Coil-to-Conductor Spacing. *Materials Evaluation*, 12:279-283,292 (1975).

35. Dodd, C.V., Deeds, W.E. and Spoeri, W.G., Optimizing Defect Detection in Eddy Current Testing. *Materials Evaluation*, 3:59-63 (1971).

36. Dodd, C.V., Deeds, W.E., Analytical Solutions to Eddy Current Probe Coil Problems. *Nucl. Sci. Abstr.*, 22:2271 (1967).

37. Dodd, C.V., Deeds, W.E. and Luquire, J.W., Integral Solutions to Some Eddy Current Problems. *Physics and Nondestructive Testing* (ed. McGonnagle, W.J.), vol. 2, pp. 233-292, 1971.

38. Luquire, J.W., Deeds, W.E., Dodd, C.V. and Spoeri, W.G., Computer Programs for Some Eddy Current Problems. *Nucl. Sci. Abstr.*, 23:40960 (1969).

39. Hochschild, R., Electromagnetic Testing of Tubing: Standardization of Specifications and Test Methods,

Part 1. *Nondestructive Testing*, 16:495-499 (1958).

40. Hochschild, R., Specifications and Standards for Eddy Current Flaw Detection in Tubing. *Nondestructive Testing*, 18:403-407 (1960).

41. Crowe, J.C., Calibration of Eddy Current Systems with Simulated Signals. *Materials Evaluation*, 9:59-64 (1977).